BINDING KINETICS INVESTIGATION OF A PEPTIDE FRAGMENT OF THE PSYCHIATRIC RISK PROTEIN, DISC1, TO THE KINASE GSK3β

A Thesis Submitted to the

College of Graduate and Postdoctoral Studies

In Partial Fulfilment of the Requirements

For The Degree of Masters

In the Department of Veterinary Biomedical Sciences

University of Saskatchewan

Saskatoon

By

STEPHANIE SAUNDH

Permission to Use

In presenting this thesis in partial fulfillment of the requirements for a Postgraduate degree from the University of Saskatchewan, I agree that the Libraries of this University may make it freely available for inspection. I further agree that permission for copying of this thesis in any manner, in whole or in part, for scholarly purposes may be granted by the professor who supervised my thesis work or, in their absence, by the Head of the Department or the Dean of the College in which my thesis work was done. It is understood that any copying or publication or use of this thesis or parts thereof for financial gain shall not be allowed without my written permission. It is also understood that due recognition shall be given to me and to the University of Saskatchewan in any scholarly use which may be made of any material in my thesis.

Requests for permission to copy or to make other uses of materials in this thesis in whole or part should be addressed to:

Head of the Department of Veterinary Biomedical Sciences

52 Campus Drive,

University of Saskatchewan

Saskatoon, Saskatchewan S7N 5B4

Canada

Or:

Dean College of Graduate and Postdoctoral Studies

University of Saskatchewan

116 Thorvaldson Building, 110 Science Place

Saskatoon, Saskatchewan S7N 5C9

Canada

Abstract

GSK3β is a multipurpose serine-threonine kinase which plays a role in many signaling pathways. Abnormal Glycogen Synthase Kinase 3β (GSK3β) function has been implicated in many diverse disease states including mental illness. Its part in neurological disease stems from its abnormal activity within the WNT/β-catenin signaling pathway. One of the binding partners of GSK3β within the WNT pathway that is linked to psychiatric disease is Disrupted in Schizophrenia 1 (DISC1). DISC1 has been suspected to play a role in individuals presenting with mental illness. Research in this area is lacking in the amount of information known about how GSK3β and DISC1 interact together. In the presence of a WNT signal, DISC1 is thought to participate in the binding complex that inhibits GSK3β activity. This thesis aims to identify a potential binding site for a small fragment of the DISC1 protein. Studies were conducted using Surface Plasmon Resonance and kinetic enzyme assays. The ability to determine the location of DISC1 binding is essential to better understanding the mechanism behind DISC1's ability to inhibit GSK3β. Most of the work is centered around the production of a His-tagged GSK3β eukaryotic construct using a bacterial overexpression system and its subsequent isolation utilizing a series of affinity and ion exchange liquid chromatography columns. This process was optimized to obtain GSK3β with a purity level of 80% to use in subsequent studies. Binding interaction studies using surface plasmon resonance technology were conducted to determine the suspected binding site of a short 44mer fragment of DISC1 on GSK3β. The binding interaction studies utilized competitive binding methods between the 44mer fragment and a small peptide fragment of the GSK3β binding protein FRAT (FRATtide). FRATtide is a peptide with a known binding location on GSK3β. The work developed a likely model representing how the DISC1 fragment binds GSK3β in the presence of FRATtide.

Acknowledgements

I would like to give a special acknowledgement and a heartfelt thank you to my supervisor Dr. Adelaine Leung for hosting me in her laboratory and providing countless hours of guidance and encouragement. Her efforts were instrumental in the development of my knowledge base, skill set and scientific abilities.

I would like to acknowledge the efforts of Dr. Steve Gagné and all the work he contributed to the project prior to my arrival in the lab. His work set the foundation for the project and acted as a catapult for my thesis.

Many thanks go out to former and present members of Leung Lab (Narsimha Pujari, Robert Bigsby and Sean Lipsit) for helping me, acting as a sounding board and contributing to the project along the way.

I would like to thank the members of my Advisory Committee; Dr. David Sanders and Dr. Ali Honaramooz for their continued guidance, positive encouragement and support throughout the process of completing this thesis.

I am thankful for the opportunity to study at the University of Saskatchewan within the Department of Veterinary Biomedical Sciences hosted by the Western College of Veterinary Medicine. I would have been lost if it were not for the help and support of all the departmental staff (Cindy Pollard, Cheryl Hack, Susan Cook) who care for, remind, inspire and guide all of the graduate students.

Dedication

This thesis is dedicated to my children, Dakota and Tristan, who have been the driving force pushing me to work harder, achieve more and never give up.

My sun and stars. My heart and soul. My love and life.

Table of Contents

List of Tables

List of Figures

List of Abbreviations

ADP-GLO – Adenosine Di Phosphate Glow

ADP – Adenosine Di Phosphate

AKT - RAC-alpha serine/threonine-protein kinase

APC - Adenomatous polyposis coli

ATF5 – Cyclic AMP-dependent transcription factor

CK1α – Casein Kinase 1 α

Contaminant10 – 10 kDa Contaminant

Contaminant25 – 25 kDa Contaminant

Contaminant60 – 60 kDa Contaminant

Contaminant70 – 70 kDa Contaminant

DB1 - Dilution Buffer 1

DISC1 – Disrupted in Schizophrenia 1

DISC1-44mer – Disrupted in Schizophrenia 1 44mer peptide fragment

DIX Domain – Domain on Dsh containing five β-strands and one α helix

Dsh - Dishevelled

FRAT2 - Frequently Rearranged in Advanced T Cell Lymphoma 2

FRATide – 23 mer fragment of FRAT2

FRAT – Frequently Rearranged in Advanced T Cell Lymphoma

Fzd - Frizzled

GBP – GSK3β Binding Protein

GF – Gel Filtration

Grb2 – Growth Factor Receptor Bound Protein 2

GroEL - Growth Factor Protein Extra Large

GroES - Growth Factor Protein Extra Small

GS1 - Glycogen Synthase 1

GSK3β – Glycogen Synthase Kinase 3 Beta

Hsp90 – Heat Shock Protein 90

Ind1 – Induction protocol 1

Ind2 – Induction protocol 2

K_a – Kinetic Association Constant

KB1 - Kinase Buffer 1

K_d – Kinetic Dissociation Constant

KD – Measure of Binding Affinity

L803-mts - GSK3β Selective Inhibitor (Ligand 803)

LB – Lysogeny Broth

LRP5/6 – Low Density Lipoprotein Receptor-Related Protein 5/6

lsGF1 – Large Scale Gel Filtration Buffer 1

lsGS2 – Large Scale Gel Filtration Buffer 2

lsGS3 – Large Scale Gel Filtration Buffer 3

lsL1 – Large Scale Lysis Buffer 1

lsL2 - Large Scale Lysis Buffer 2

lsL3 - Large Scale Lysis Buffer 3

lsL4 - Large Scale Lysis Buffer 4

lsL5 - Large Scale Lysis Buffer 5

lsNA1 – Large Scale NiNTA Wash Buffer 1

lsNA2 - Large Scale NiNTA Wash Buffer 2

lsNB1 -Large Scale NiNTA Elution Buffer 1

lsSPA1 – Large Scale SP Wash Buffer 1

lsSPA2 – Large Scale SP Wash Buffer 2

mDISC1 – Mouse Disrupted In Schizophrenia 1

mGSK3β – Mouse Glycogen Synthase Kinase 3β

NDEL1 – Nuclear Distribution Protein nude-like 1

NiNTA – Nickel Nitrilotriacetic Acid

NUDEL – Nuclear Distribution Protein Nude-like1

PDE4 – cAMP Specific 3',5'-cAMP Phosphodiesterase 4

PDZ domain – Common structural domain found in signalling proteins

PI3K – Phosphatidylinositol 3 Kinase

PP2A – Serine/Threonine Protein Phosphatase

PuriA – Purification Protocol A

PuriB – Purification Protocol B

RB1 - Running Buffer 1

RGB - Regeneration Buffer

R_{max} – Maximum Response

RU – Response Units

SB - Stripping Buffer

SP-FF – SP Sepharose Fast Flow Cation Column

SP-HP – SP Sepharose High Performance Cation Column

SP-XL – SP Sepharose Extra Large Cation Column

SPR – Surface Plasmon Resonance

ssL1 – Small Scale Lysis Buffer 1

ssNA1 – Small Scale NiNTA Wash Buffer 1

ssNA2 – Small Scale NiNTA Wash Buffer 2

ssNB1 – Small Scale NiNTA Elution Buffer 1

TB – Terrific Broth Medium

TCF/LEF – Transcription Factor / Lymphoid Enhancer Binding Factor

TEV – Tobacco Etch Virus

TNIK – TRAF2 and NCK Interacting Protein Kinase

UVR – UVR ABC System Binding Domain

WNT - Wingless/Integrated

βME – β Mercaptoethanol

1.0 Introduction

1.1 General Topic & Significance

There exists a biological link between the way in which disease is experienced by an individual and the molecular functioning of the protein subunits within that individuals' cells. For many disease states, including mental illness, the presentation of the disease is the result of one or more malfunctioning proteins at the cellular level. An example of this was noted in a large Scottish family where a specific chromosomal translocation resulted in a truncated protein responsible for members of the family who presented with schizophrenia, bipolar disorder or depression (Millar et al., 2000). Genes such as these, often interact with environmental factors to produce the manifestation of disease. Particularly in the case of mental illness, there is a substantial connection between mental health and the molecular functioning of neural progenitor cells. Neural progenitor cells are essentially neural stem cells produced in the subventricular zone and the olfactory bulb of the adult human brain (Piatti et al., 2013; Snyder et al., 1992; Temple, 1989). These neural progenitor cells can migrate throughout the brain and differentiate into necessary cell types (Magavi et al., 2000). Neural progenitor cells have been hypothesised to aid in the typical brain functioning, memory and in response to injury (Kim et al., 2012; Magavi et al., 2000). Irregularities within these neural stem cells may lead to the development or presentation of specific mental illness. These irregularities can occur in genes coding for enzymes or structural proteins which is why it becomes essential to understand the relationship between proteins at a molecular level. Gaining insight into the complexity and intricacies of protein-protein interactions is a critical fundamental building block to understanding disease states as a whole. This thesis focuses on the relationship between an enzyme, Glycogen Synthase Kinase 3β (GSK3β), and a scaffold-like protein, Disrupted in Schizophrenia 1 (DISC1), both of which have been implicated in psychiatric disease (Chen et al., 2015). Both proteins have been identified within neural stem cells and have been linked to the presentation of psychiatric disease states in animal models (Mao et al., 2009)

Of specific interest within the scope of this thesis, is the role DISC1 plays in regulating GSK3β activity within the canonical Wingless/Integrated (WNT) signaling pathway

1.2 GSK3β Structure and Function

GSK3β is a serine/threonine kinase that has a broad spectrum of potential substrates and influences many different signalling pathways. Its structure consists of a typical kinase fold comprising of two main domains (Figure 1-1). The β strand domain resides from residues 25 to 138 in the N terminal end of the protein (Dajani et al.; Haar et al., 2001). This β strand domain has

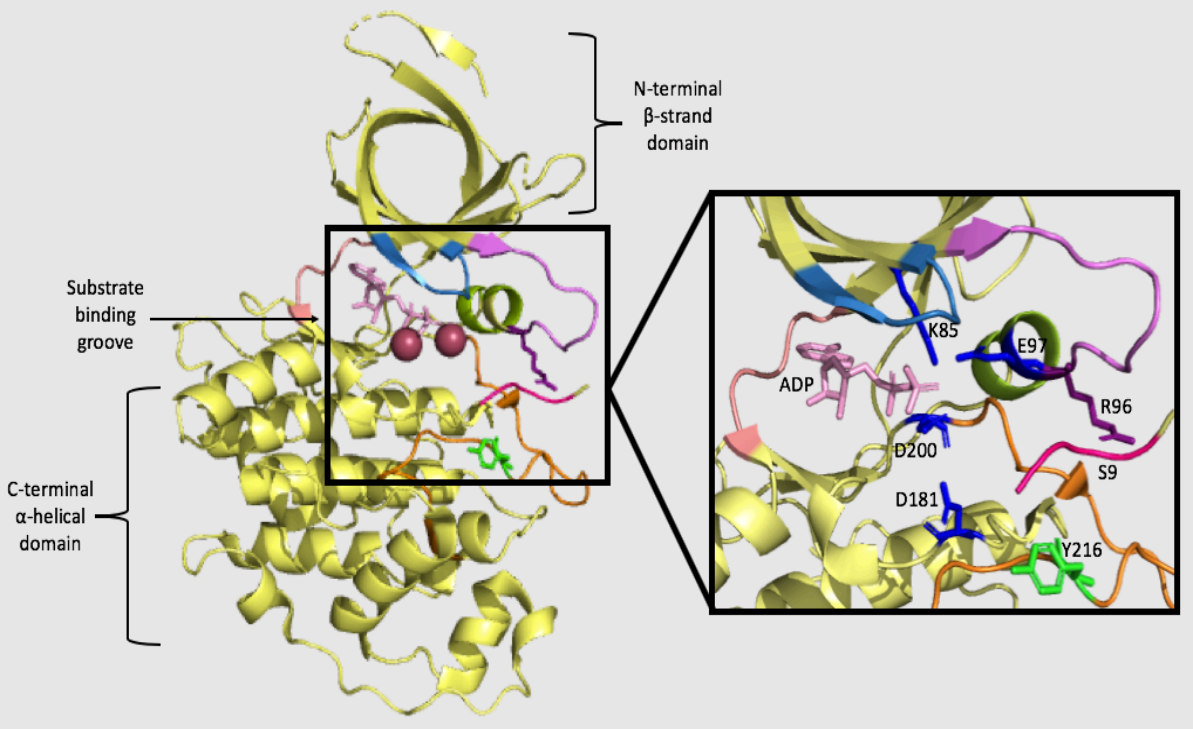

Figure 1- 1: Protein structure of GSK3β.

Enzyme active site (boxed) sandwiched between an N terminal - barrel domain and a C terminal α-helix domain by a functional hinge (salmon pink). ADP (light pink) and two Mg^{2+} molecules (raspberry) bound in the substrate binding groove. Short α helix in the N terminal domain (lime green) followed by the C loop (violet). A glycine-rich loop (sky blue), activation loop (orange) and C loop (violet) all play a role in the active site. Tyr216 (lime green) is auto-phosphorylated for enzyme activity. Phosphorylated peptide Ser9 (bright pink) interacts with Arg96 (purple sticks) in the region where phosphorylated Ser9 is predicted to bind for enzyme inhibition. The active site consisting of Asp181, Asp200, Lys85, and Glu97 (dark blue sticks) is required for substrate binding (PDB file 4NM3).

seven antiparallel β strands where the 4th and 5th strand are separated by a short α helix (Dajani et al.; Haar et al., 2001) (Figure 1-1 Lime green helix). This helix is typical of the functionality of catalytic activity in kinases. The C terminal domain resides from residues 139 to 343 and is made up of α helices (Dajani et al.; Haar et al., 2001). The ATP binding site is at the interface of the two domains and is accompanied by a glycine-rich loop (Figure 1-1 sky blue) and a functional hinge (Haar et al., 2001) (Figure 1-1 salmon). The activation loop of the enzyme is located from residues 200 to 226 and outlines the substrate binding groove (Figure 1-1 orange). The far ends of the N terminus (preceding Lys35) and C terminus (following Ser386) are disordered in nature and can be challenging to visualize within the crystal structure (Dajani et al.). The C loop (Figure 1-1 violet) is involved in enzyme inhibition mechanism as it undergoes a conformational change when an inhibitor peptide is bound as a pseudo-substrate (Stamos et al., 2014). This C loop moves towards the C terminal lobe of the kinase and sits down on top of the inhibitory peptides in a clamp-like fashion (Stamos et al., 2014). GSK3β contains a short segment which acts as a nuclear localization signal (NLS) located in the N terminus (Residues 85-103) which is required for nuclear shuttling, but despite its presence, GSK3β remains primarily localized in the cytosol (Meares and Jope, 2007).

GSK3β is a constitutively active Ser/Thr kinase which is unique in that phosphorylation acts to inhibit the enzyme instead of activating it. GSK3β is predominantly a Ser/Thr kinase but can phosphorylate its own Tyrosine residues in an autophosphorylation event (Tong et al., 2018). This autophosphorylation occurs via the aid of heat shock protein (Hsp90) at Tyr216 (Figure 1-1 bright green stick) during a transitory intermediate phase that occurs after translation and during protein folding (Lochhead et al., 2006). The autophosphorylation of Tyr216 is required for GSK3β activity as it allows for a conformational change which opens up the binding site for substrates (Cole et al., 2004; Hughes et al., 1993; Tong et al., 2018). This phosphorylation appears to be hidden or protected from dephosphorylation, and thus inhibition of GSK3β is not achieved through removal of this phosphate group (Lochhead et al., 2006). Instead, inhibition is achieved through phosphorylation of a separate amino acid residue, specifically Ser9 (Cross et al., 1995; Shaw et al., 1997) (Figure 1-1 Inhibitory Phosphorylated S9 bright pink). Ser9 is located in the disordered N terminus of the protein and as such is not easily viewed in crystal structures (Stamos et al., 2014). This characteristic leads many groups use versions of the construct that lack the end

terminal disordered region altogether. Stamos and colleagues (2014) successfully crystallized a full-length GSK3β construct which contained a phosphorylated Ser9 residue. The resulting structure showed the phosphorylated Ser9 bound to GSK3β near the active site while the remainder of the N terminal residues (residues 1-5 and 11-25) are mostly disordered and unable to be viewed clearly in the crystal structure (Figure 1-1). Stamos and colleges (2014) simultaneously conducted enzymatic studies of GSK3β activity in the presence of a phosphorylated Ser9 and demonstrated that Ser9-P was able to inhibit GSK3β. It is hypothesized that Ser9 bends around and interact with Arg96 (Frame et al., 2001) (Figure 1-1 purple stick) since it is located in the flexible N terminal region of the protein. Arg96 is the same residue within the binding site that would regularly interact with the primed phosphate on GSK3β substrates (Frame et al., 2001). The function of this phosphorylated Ser9 is to act as a physical obstruction against primed substrates for access to the active site (Beurel et al., 2015; Stamos et al., 2014). The active site for GSK3β involves the residues Asp181 (D181), Asp200 (D200), Lys85 (K85), and Glu97 (E97) (Dajani et al.) (Figure 1-1 dark blue sticks). The priming phosphate region refers to GSK3β's preference to phosphorylate substrates that have already been pre-phosphorylated at a Ser or Thr four residues in the C-terminal direction from GSK3β's phosphorylation site (P+4) (Beurel et al., 2015). The specific sequence motif recognized in this phosphorylation event is S/T-X-X-X-S(P)/T(P). Some substrates contain multiple sequential motifs such that another enzyme phosphorylates the first S/T but once GSK3β recognizes the first S/T it acts as the pre-phosphorylated site for the next phosphorylation event 4 additional residues in the N terminal direction (Beurel et al., 2015; Frame et al., 2001; Stamos et al., 2014).

GSK3β is highly conserved across plants, fungi, worms, flies, sea squirts and vertebrates (Woodgett JR, 1991) and ubiquitously expressed in all types of cells and tissues including the brain (Doble, 2003; Krishnankutty et al., 2017). GSK3β is involved in a diverse set of cell signaling pathways including those responsible for cell proliferation, cell architecture and neural development (Patel and Woodgett, 2017). As a result of being so diverse, it has been implicated in playing a role in the development of some cancers, diabetes, neurodegenerative and psychiatric disease (Krishnankutty et al., 2017). Its malfunction has also been implicated in neurological conditions including Alzheimer's disease where it is predicted to influence hyperphosphorylation of the Tau protein, the subsequent detachment of microtubules and the phosphorylation of amyloid

precursors leading to aggregation of αβ plaques (Maqbool et al., 2016; Martin et al., 2018). Abnormal GSK3β function has been hypothesized as playing a major role in mental illness including schizophrenia, bipolar disorder and major depressive disorder (Chen et al., 2015; Karege et al., 2012; Muneer, 2017). GSK3β's role in these types of psychological conditions is thought to be attributed to GSK3β's function in active neurogenesis. During neurogenesis, GSK3β is prominent in the canonical WNT pathway and ultimately controls the amount of free β-catenin which functions to push the cell through the stages of differentiation (Hur and Zhou, 2010). In addition to neurological conditions, GSK3β has also been implicated in diabetes for its role in the P13K/Akt pathway and its function in the insulin signaling pathway regarding glycogen synthesis (Kleinridders et al., 2014; Saltiel and Kahn, 2001). The many functions of GSK3β further solidifies its diversity in both application and substrate specificity. This diversity becomes important when identifying or designing enzyme inhibitors that will not serve to inhibit GSK3β in every signaling pathway, but rather, in specific pathways. In order to better appreciate GSK3β's role and activity, a closer look at the WNT/β-catenin signalling pathway and participants is necessary.

1.3 The WNT/β-Catenin Pathway

The WNT/β-catenin canonical pathway is complex and made up of many key players. The pathway itself serves to regulate the expression of genes involved in cell proliferation, differentiation and fate specification (Eastman and Grosschedl, 1999). Cells can accomplish this regulation by moderating the amount of available β-catenin in the cytoplasm (Figure 1-2). The pathway is initiated by extracellular WNT signals which bind to membrane spanning receptors (Logan and Nusse, 2004). WNTs are a group of 19-24 different cysteine-rich proteins that are secreted or presented on cells and function as signaling molecules (MacDonald et al., 2009; Miller et al., 1999). An extracellular WNT molecule will simultaneously bind two central receptors, Frizzled (Fzd) and LRP5/6 (He, 2004; Logan and Nusse, 2004) (Figure 1-2). Both Fzd and LRP5/6 interact with WNT extracellularly and interact with the β-catenin destruction complex intracellularly (Wu and Pan, 2010). The β-catenin destruction complex consists of six known protein components; Disheveled (Dsh), Axin, GSK3β, Casein kinase one α (CK1α), Adenomatous polyposis coli (APC) and β-Trcp (Logan and Nusse, 2004; MacDonald et al., 2009) (Figure 1-2). Dsh is a necessary component of this complex and acts as the initial instigator in response to a

WNT signal (Mannava and Tolwinski, 2015). Dsh is recruited by Fzd via its PDZ domain and can bind and phosphorylate the LRP5/6 receptor which acts to recruit Axin to the membrane via its DIX domain (Gao and Chen, 2010). Both Axin and Dsh contain DIX domains allowing them to form heterodimers which keep the destruction complex at or near the membrane in response to WNT (MacDonald et al., 2009). Axin is a scaffolding protein which can simultaneously bind GSK3β, CK1α, and β-catenin (Liu et al., 2002; Wu and Pan, 2010). When WNT activates the receptors, all of the participants in the β-catenin destruction complex are held in a conformation which inhibits GSK3β's enzymatic activity (McManus et al., 2005). The manner in which GSK3β is inhibited within the complex is not yet well understood, although it is noted that GSK3β inhibition within the complex does not involve phosphorylation on Ser9 or Ser21 (Ding et al., 2000; McManus et al., 2005) suggesting that enzyme inhibition occurs via other means possibly involving steric hinderance mechanisms. When GSK3β is inhibited, β-catenin accumulates in the cytoplasm and can translocate to the nucleus where it acts on transcription factors TCF/LEF (Logan and Nusse, 2004). TCF/LEF are upstream of genes which participate in cell proliferation and differentiation (Eastman and Grosschedl, 1999).

When WNT signals are absent, Fzd and Dsh are not bound and subsequently, the β-catenin destruction complex, complete with GSK3β, remains active in the cytoplasm (Figure 1-2). Since Axin acts as the proverbial anchor by holding the main players near each other (Liu et al., 2002; Wu and Pan, 2010) it can associate β-catenin with CK1α and GSK3β. CK1α is a kinase which phosphorylates β-catenin at its Ser45 thereby priming it for hyperphosphorylation by GSK3β (Wu and Pan, 2010). After β-catenin has been primed, GSK3β will phosphorylate β-catenin at Thr41, Ser37, and Ser33 (MacDonald et al., 2009; Wu and Pan, 2010). The phosphorylated Ser33 and Ser37 is a docking site for β-Trcp, a ubiquitin ligase, and

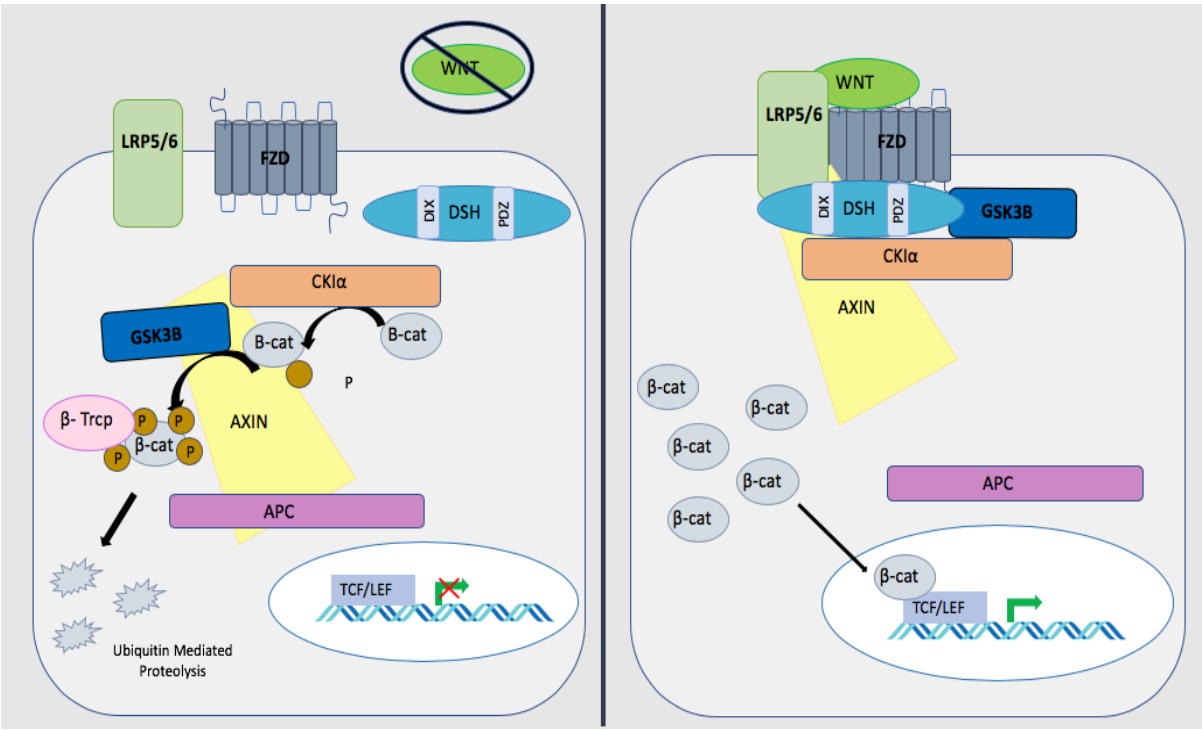

Figure 1- 2: Canonical WNT/β-catenin signaling pathway.

Left: When there is no external WNT signal present Axin binds CKIα, GSK3B, β-catenin, and APC. CKIα phosphorylates β-catenin priming it for GSK3β hyper-phosphorylation. Once hyper-phosphorylated β-Trcp binds β-catenin it can transport it to the proteasome for degradation. Right: When external WNT signals are present they bind to receptors LRP5/6 and FZD. Cellular protein DSH binds to both these receptors and also sequesters the Axin, CKIα, GSK3β complex to the membrane. This interaction inhibits GSK3β activity towards β-catenin decreasing its rate of degradation and allowing it to accumulate in the cytoplasm. β-catenin can then translocate to the nucleus and interact with promoters TCF/LEF and increase the transcription of genes involved in cellular proliferation.

will transport phosphorylated β-catenin to the proteasome for degradation (Logan and Nusse, 2004). APC within the complex has been theorized to release β-catenin from Axin by competing for the same binding site and essentially freeing up Axin to bind more β-catenin (MacDonald et al., 2009). Axin appears to be the rate-limiting component as it is present in the cell in a limited amount (Fraser et al., 2002). Therefore, APCs role as a ratchet becomes paramount to continuing the process of hyper-phosphorylating β-catenin. All these individual players work together to maintain the levels of β-catenin present in the cell. The feedback loops are intricately designed and as such can create disruptions at many different points within the pathway causing the feedback loops to deviate from their designated outcomes. The protein players described above are only the known components and the pathway and can potentially include other proteins that have yet to be described. Of particular interest to researchers is the ability to inhibit this pathway without

inhibiting GSK3β functioning in other pathways. One such protein discovered which acts in this manner is FRAT.

1.4 FRAT Function and Role in WNT Signalling

Frequently Rearranged in Advanced T Cell Lymphoma (FRAT) is a GSK3β binding protein that was initially identified as an ortholog of the GSK Binding Protein (GBP) present in Xenopus (Yost et al., 1998). Both FRAT and GBP were found to inhibit GSK3β leading to the accumulation of β-catenin within the cell (Hagen et al., 2006). FRAT is expressed in all tissue types with low detectable levels in the brain (Freemantle et al., 2002). Within the cell, FRAT is primarily located in the nucleus and contains a vital N terminal region responsible for its ability to shuttle to the cytosol (Freemantle et al., 2002). FRAT appears to have a role within the GSK3β/Axin/β-Catenin destruction complex as a result of WNT signaling and actively acts to transport GSK3β from the nucleus into the cytoplasm (Bechard et al., 2012). Under normal WNT signaling, Dsh interacts with Axin and forms a bridge between Dsh-Axin-GSK3β□(Li, 1999) (Figure 1-2) which is thought to bring the entire complex to the cellular membrane. However, FRAT has been shown to form a stable complex with GSK3β but cannot form a bridge with Dsh (Li, 1999). This observation suggests that FRAT does not bind to the β-catenin destruction complex and inhibit GSK3β by an interaction with Dsh. This was further confirmed by assays which showed that FRAT has the unique ability to inhibit GSK3β activity towards β-catenin without inhibiting GSK3β activity towards other substrates such as Glycogen Synthase 1 (GS1) (Culbert et al., 2001; Hedgepeth et al., 1999; Thomas et al., 1999) (Figure 1-4). This specificity is achieved through the manner in which FRAT1 inhibits GSK3β. FRAT1 and Axin were predicted to have overlapping or identical binding sites on GSK3β and thus act in a competitive manner for binding (Bax et al.; Dajani et al.; Hagen et al., 2006). Also, FRAT shows an elevated affinity for GSK3β in response to PI3K/AKT signaling apart from the WNT pathway (Bechard et al., 2012).

FRATtide is a 25 mer fragment derived from the GSK3β binding domain of the FRAT2 homolog (174-196). FRATtide binds to GSK3β in the C terminal region in the channel between the helix and the extended loop where a hydrophobic helix-helix ridge groove is located (Bax et al.; Dajani et al.) (Figure 1-3). The GSK3β residues located within this hydrophobic groove (Figure

1-3 pink sticks) forms Van der Waals interactions with the hydrophobic residues on the binding face of FRATtide (Bax et al.) (Figure 1-3 green sticks). Dajani et al. (2003) and Bax et al. (2001) were able to show the unique binding modes of FRATtide and a peptide fragment of Axin on GSK3β (Figure 1-3). Despite the similarities, the binding sites for FRATtide and Axin are not identical and instead are overlapping (Figure 1-3). The FRAT peptide binds in a bent formation creating two separate alpha helical segments compared to the Axin peptide which binds in a single alpha helical segment. The competition for binding sites on GSK3β between Axin

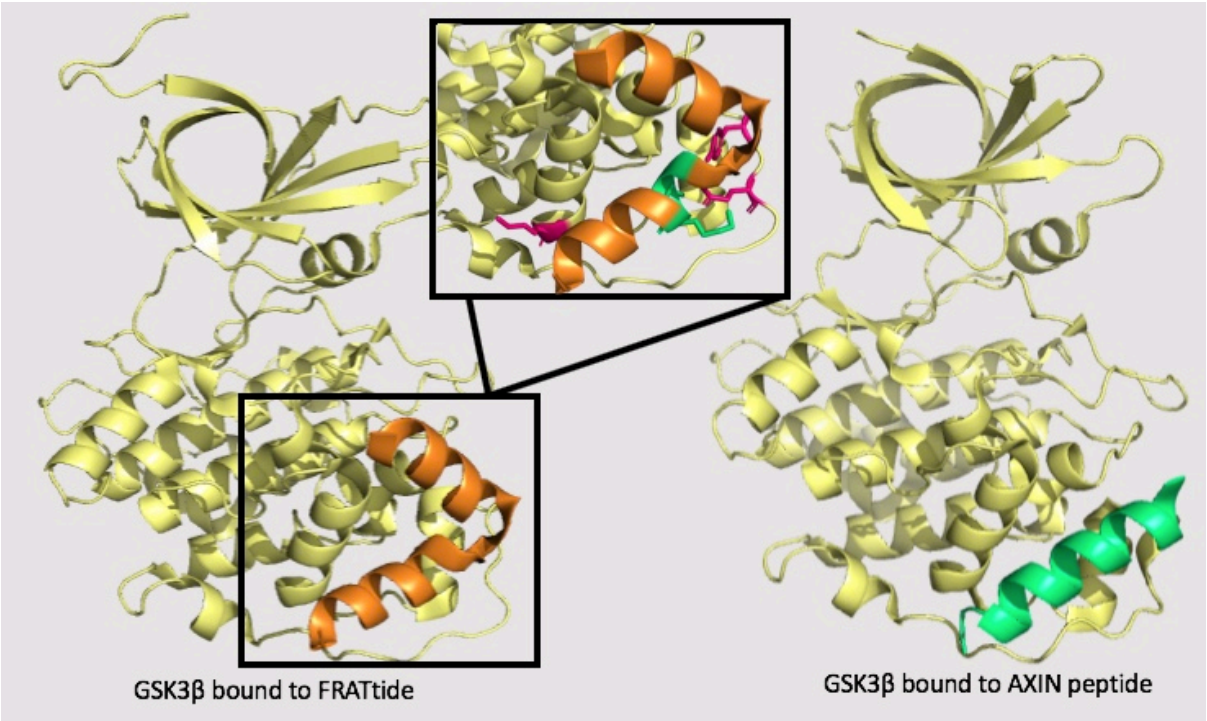

Figure 1- 3: Comparing the binding sites of FRATtide (orange) and a peptide fragment of Axin (lime green) to GSK3β.

Left: GSK3β (Yellow / PDB 1GNG) bound to FRATtide (Orange). Boxed region shows the hydrophobic residues of GSK3β (Pink) interacting with the corresponding hydrophobic residues on FRATtide (Green). Right: GSK3β (Yellow / PDB 3ZDI) bound to a peptide fragment of Axin (Green). The binding sites for FRATtide and Axin are overlapping but not identical. The crystal structures demonstrate how FRATtide acts to prevent Axin binding.

peptide and FRATtide is surprising considering that the two peptides share minimal sequence identity except for a Leu-Ile sequence within a helix forming region (Bax et al., 2001). The discovery of this overlapping of binding sites helped to explain past observations which showed

that FRATide was able to block the specific interaction between GSK3β and Axin (Hagen et al., 2006; Thomas et al., 1999).

The interaction between FRAT, Axin, and GSK3β is significant because of its ability to act in a targeted substrate specific fashion (Figure 1-4). As described above, Axin acts as a docking site for GSK3β, β-catenin, and CKIα (Dajani et al.; Liu et al., 2002). Axin also interacts with Dsh (Li, 1999) and phosphatase PP2A (Hsu et al., 1999). In the absence of an external WNT signal, β-catenin is hyperphosphorylated by GSK3β, both of which bind to Axin (MacDonald et al., 2009). This robust scaffolding protein has a pivotal role in the β-catenin destruction complex by acting as a magnet to bring all the players into close proximity with one another. Axin itself contains many phosphorylation sites and has a higher affinity for β-catenin when it is phosphorylated (Willert et al., 1999) adding an additional level of regulation to the complex formation. When FRAT/FRATtide is present, it competes for GSK3β binding with Axin so that GSK3β bound to FRAT

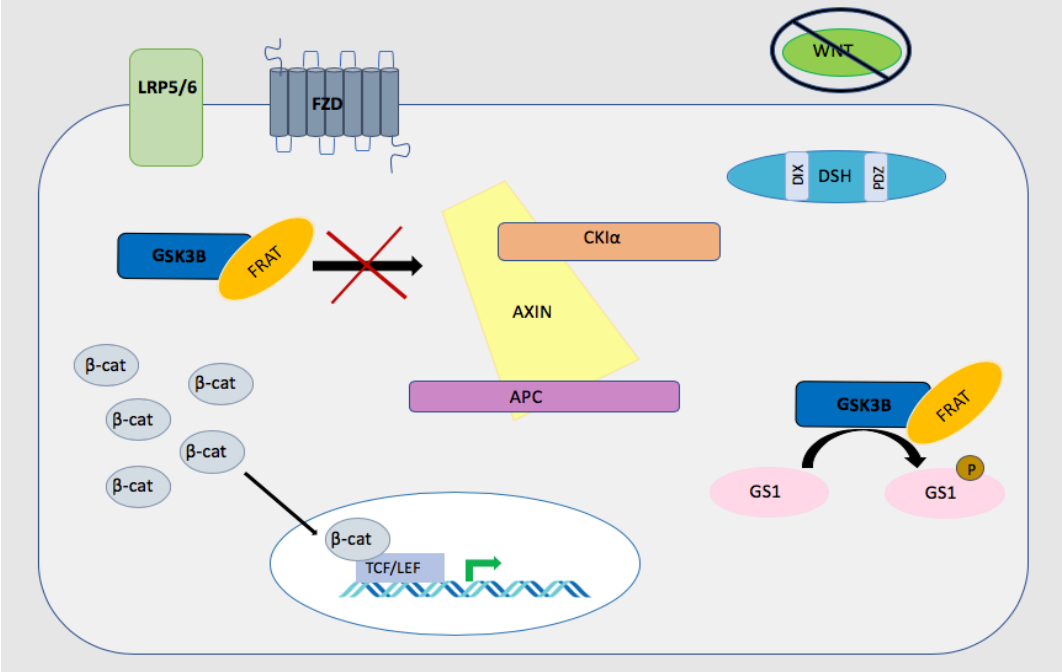

Figure 1- 4: FRATs interaction with GSK3β and the WNT signalling pathway.

Figure illustrates the targeted fashion of how FRATtide can inhibit GSK3β activity towards β-catenin without influencing GSK3β activity towards other substrates such as GS1. Even in the absence of an external WNT, β-catenin can still act on promoters TCF/LEF because FRAT prevents GSK3β from associating with Axin/CKIα/APC complex.

cannot simultaneously be bound to Axin. If FRAT bound GSK3β cannot bind to Axin then it cannot congregate in the β-catenin destruction complex (Thomas et al., 1999). As a result, FRAT bound GSK3β is not in close enough proximity with primed phosphorylated β-catenin to initiate the hyperphosphorylation process (Figure 1-4). This is how FRAT can cause inhibition of GSK3β towards β-catenin without causing inhibition of GSK3β towards other substrates. Considering GSK3β's multiple roles in many different pathways throughout the body, this directed inhibition becomes increasingly valuable as a potential interaction to exploit. The next logical step is to investigate if other scaffold or scaffold-like proteins, such as DISC1, behave similarly.

1.5 DISC1 Function and Role in GSK3β/WNT Signalling

DISC1 is a structural scaffold-like protein 854 amino acids long (93.6kDa). It was first discovered as segregating with psychiatric illness in a large Scottish family (Blackwood et al., 2001; Millar et al., 2000). Certain individuals within this family were found to have a genetic translocation between chromosomes 1 and 11 creating a truncated version of the DISC1 protein (Blackwood et al., 2001). Persons carrying the truncated gene had a higher chance of presenting with some form of mental illness (Blackwood et al., 2001). As a result of this original observation, DISC1 became the focus of investigation concerning its role in specific psychiatric disorders. DISC1 is currently known as a psychiatric risk protein that has been shown to associate with schizophrenia, schizoaffective disorder, major depressive disorder, bipolar disorder, and autism spectrum disorder (Hikida et al., 2007; Hodgkinson et al., 2004; Johnstone et al., 2011; Kilpinen et al., 2008). Its expression is found in a variety of tissue types (Ma et al., 2002) but is predominantly found within the brain. The regions of the brain where DISC1 is most prominent include; hippocampus, cortical, cerebellar and olfactory neurons of which both the hippocampal and olfactory neurons are capable of producing neural progenitor cells (Lipska et al., 2006; Miyoshi et al., 2003). DISC1 primarily functions in neuronal mechanisms including neuronal migration (Kamiya et al., 2005), integration of adult neurons into the neural network (Duan et al., 2007), canonical WNT signaling pathway (Mao et al., 2009) and the development of dopaminergic, NMDA and GABA neurotransmission (Hayashi-Takagi et al., 2010; Kim et al., 2012; Niwa et al., 2010). Despite the primary presence of DISC1 in neuronal type mechanisms, its function within each of these pathways is different, and it has been shown to associate with a variety of un-related binding partners including NUDEL, α-actinin2, ATF5, GSK3β, and more

(Morris, 2003). Due to the vast variety of interacting partners, DISC1 was hypothesized to act similarly to a scaffold protein. In general terms, scaffold proteins act to bind many participants of a single signaling pathway and bring them into proximity creating multi-protein complexes. This often places catalytic components of a signaling pathway near one another to increase access or activity. Scaffold proteins do not become consumed by these reactions and instead act primarily as a docking site. In this context, DISC1 can be considered a scaffold protein in that it interacts with many enzymes of which it is not the substrate including Kal-7, GSK3β, PDE4, Grb2 TNIK and NDEL1 (Yerabham et al., 2013).

Interestingly, DISC1 does not show any sequence similarity to other scaffold proteins logged in the protein database (Soares et al., 2011). Its crystal structure has yet to be determined but is predicted to contain a distinct and disordered N terminal domain spanning amino acids 1-350 and a mostly ordered C terminal domain spanning amino acids 350-854 (Miyoshi et al., 2003; Soares et al., 2011) (Figure 1-5). The N terminal domain does not share sequence identity to any known protein fold and contains a nuclear localization signal (Ma et al., 2002) (Figure 1-5, NLS green) and a serine-phenylalanine rich motif (Taylor et al., 2003) (Figure 1-5, SF red). It is predicted that these disordered regions give DISC1 its ability to bind to a wide variety of proteins (Fink, 2005). However, it is also the disordered regions which makes overexpression and purification of recombinant versions of the DISC1 protein difficult (Ma et al., 2002). The C terminus is predicted to consist of coiled-coil or helical domains with two UVR domains (Miyoshi et al., 2003) (Figure 1-5). DISC1 is predicted to have more than 40 different splice variants with the most highly expressed variant being the full-length 93kDa version (Nakata et al., 2009). DISC1 levels are regulated within the cell by the ubiquitin-proteasome degradation system (Yalla et al., 2018). It is hypothesized that GSK3β plays a role in DISC1's rate of turn over by phosphorylating the priming sites for the initial binding of ubiquitin E3 ligase enzymes (Yalla et al., 2018). Little is currently known concerning the mechanism DISC1 uses to cause inhibition of enzymes, specifically of relevance to this thesis is how DISC1 acts to inhibit GSK3β within the WNT signaling pathway.

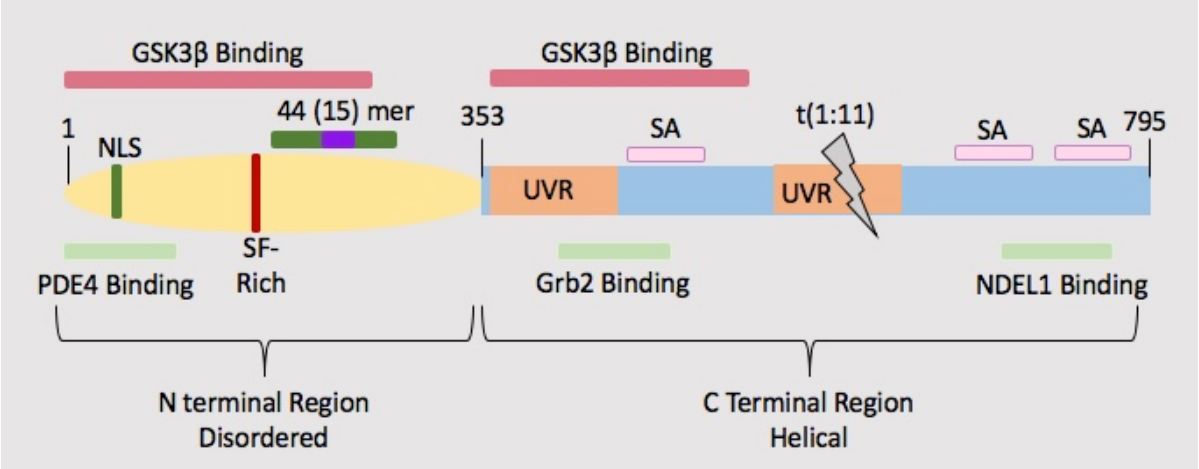

Figure 1- 5: Schematic showing the hypothesized structure of DISC1.

The N terminal region (yellow) is mostly disordered with a nuclear localization signal (NLS) and a GSK3β binding domain (red). The generalized location of the DISC1-44mer is depicted (dark green) with the 15-mer GSK3β binding domain highlighted (purple). The C terminal region (blue) is helical in structure and contains two UVR domains (orange). The C terminal region also contains three self-association domains (SA-pink) allowing the protein to form oligomers. The t(1:11) truncation occurs in the middle of the second UVR domain (grey). Binding domains for various other proteins are present throughout the protein. Three of the many regions are depicted in light green.

Mao and colleges in 2009 first characterized DISC1's involvement in the WNT signaling pathway. Their studies involved the investigation of mouse construct of DISC1 (mDISC1) with purified human GSK3β. They initially realized that mDISC1 was expressed in the dentate gyrus and olfactory bulb of mice brains, both areas are known for producing new neurons from neural stem cells. When they knocked down mDISC1 in utero, they noticed a significant reduction in neural progenitor proliferation which hinted at a potential role for mDISC1 in the process of proliferation and thus in the WNT signaling pathway. The role of mDISC1 in this pathway was confirmed by a series of knockdown experiments linked to luciferase reporter constructs for the transcription factors LEF/TCF. Furthermore, by testing the effect of mDISC1 knockdown in the presence of wild-type β-catenin and a degradation-resistant form of β-catenin, Mao and colleagues (2009) were able to determine that mDISC1 acts upstream of β-catenin. This observation, combined with the knowledge of GSK3β's role in phosphorylating β-catenin during WNT signaling, lead them to investigate mDISC1's role with mouse GSK3β (mGSK3β). mGSK3β can be inhibited by phosphorylation at Ser9 (Cross et al., 1995; Emamian et al., 2004; Park et al., 2013) as described above in Figure 1-1, but Mao and colleges (2009) found that overexpression of mDISC1 did not influence GSK3β's phosphorylation at Ser9.

Conversely, Mao and colleges (2009) saw that mDISC1 overexpression reduced GSK3β phosphorylation at Tyr216 (Figure 1-1) which is GSK3β autophosphorylation site required for enzyme activity (Cole et al., 2004; Lochhead et al., 2006). They went on to perform *in vitro* association assays to determine if GSK3β and mDISC1 had a direct interaction with each other, the results of their experiments determined that two regions of mDISC1 (1-220 and 356-595) bound directly to GSK3β (Figure 1-5, GSK3β binding light red). Of these two mDISC1 regions, the segment containing residues 1-220 was able to inhibit GSK3β activity towards β-catenin and Axin at 0.5 μM whereas the 221-595 regions were only able to cause inhibition at concentrations higher than 2 μM. These mDISC1 fragments were not able to inhibit AKT which works against the suggestion that mDISC1 may act as a general kinase inhibitor. Mao and colleges (2009) further broke down the mDISC1 peptides to obtain a narrower range and found that a 44 amino acid region (195-238) was able to inhibit GSK3β with more potency than the commonly known GSK3β inhibitor L803-mts (Figure 1-5, 44mer green and purple).

Additionally, Mao and colleges (2009) used the biophysical assay technology of Surface Plasmon Resonance (SPR) to determine that this 44 amino acid region of mDISC1 binds directly to human GSK3β. To further narrow down the region responsible for binding they created overlapping 15 mer fragments and found that one fragment from region 211-225 was the only one which bound to GSK3β via SPR (Figure 1-5, 15 amino acid segment in purple). When they tested this short 15mer fragment with GSK3β in a kinase assay, Mao and colleges were able to determine that the 15 amino acid region did not inhibit GSK3β. As a result of these experiments, they concluded that the 44 mer (195-238) was able to bind and inhibit GSK3β but only a short 15 amino acid region of that peptide (211-224), was required solely for binding. This suggested that the inhibitor effect of GSK3β lies in the regions outside of the 15 amino acid segment. They further confirmed these findings by studying the effects of mDISC1 knockdown complimented with GSK3β loss of function and found that cell proliferation was restored further confirming mDISC1's role in inhibiting GSK3β. Lastly, Mao and colleagues finished off their study of mDISC1 loss of function by observing mice behaviors and found that mice lacking mDISC1 exhibited behaviors which approximate to human behaviors characteristic of schizophrenia and depression. The study acts as a significant anchor for DISC1 research as it was the first of its kind

to determine a direct role for DISC1 in the WNT pathway by determining that DISC1 inhibits GSK3β activity. However, the Mao study lacks any attempts to address a mechanism of inhibition leaving a niche in the research that this thesis will attempt to explore.

1.6 Project Outline and Research Objectives

The nice in the field involves the mechanism of how DISC1 can inhibit GSK3β, therefore, gaining insight into this mechanism is a crucial undertone for this thesis. In order to address this, the work mainly focuses on comparing FRATtide and DISC1-44mer binding in an attempt to identify any possible similarities between their binding sites. Preliminary studies from a group of collaborators in Boston utilized enzyme kinetic data to show that DISC1-44mer inhibits GSK3β in a manner that was non-competitive for ATP and substrate binding (unpublished). This observation shows that DISC1-44mer is not likely binding GSK3β in a fashion that occupies the substrate/ATP binding pocket. Since DISC1 is theorized to act in a scaffold-like manner, one valid prediction is that DISC1 may interfere with Axin binding similar to FRAT inhibition (Bax et al., 2001; Dajani et al., 2003). If DISC1-44mer inhibited GSK3β by blocking Axins access then it would mean that DISC1-44mer could also be targeted to cause inhibition of GSK3β only within the WNT pathway and not towards other potential GSK3β substrates. Better understanding the similarities and differences between DISC1 and FRAT inhibition of GSK3β could potentially lead to the design of a therapeutic drug modeled after DISC1-44mer that could be targeted to cells undergoing neurogenesis. The overall goal of this thesis is to increase our understanding behind the kinetic and physical mechanisms with which the DISC1-44mer can inhibit GSK3β.

1.6.1 Hypothesis

A short 44-mer fragment of DISC1 binds and inhibits GSK3β in a region which overlaps the FRATtide binding site and is distinctly separate from the substrate and ATP binding pocket.

1.6.2 Objective 1: Optimization of Heterologous Overexpression of Human GSK3β in Bacteria

Expression of GSK3β through the use of bacterial plasmid vectors continuously yielded a low amount of protein. Due to this, optimization of the overexpression protocol was necessary to create a reproducible method that would give a high rate of expression for the construct.

1.6.3 Objective 2: Optimization of Purification of Human GSK3β

GSK3β tends to purify along with various contaminating proteins and other impurities. The presence of these impurities can potentially cause problems for downsteam studies or assays. Due to this, optimization of a purification protocol which utilizes affinity chromatography in order to reproducibly achieve a protein product with a level of purity at or above 80% was necessary.

1.6.4 Objective 3: Investigation of the Inhibition Mechanism of DISC1-44mer Against GSK3β using Biochemical and Biophysical Approaches

Biochemical and biophysical assays are an essential part of understanding the binding efficiency and binding kinetics of GSK3β with DISC1-44mer. Surface plasmon resonance (SPR) allows the ability to determine the binding capability and efficiency of DISC1-44mer to GSK3β. SPR also provided the opportunity to analyze possible details regarding the binding location in relation to FRATtide. Kinase activity assays such as ADP-GLO allowed for the determination of the overall inhibition effect of DISC1-44mer on GSK3β.

2.0 Materials and Methods

2.1 Constructs

2.1.1 Plasmid Vector: pST50Trc1-HisNDHFR

Plasmid vector contains a 6 Histidine tag following a T7 promoter with a TEV cleavage site separating the tag from the sequence of interest insertion site. The plasmid contains ampicillin resistance gene for ease of selection.

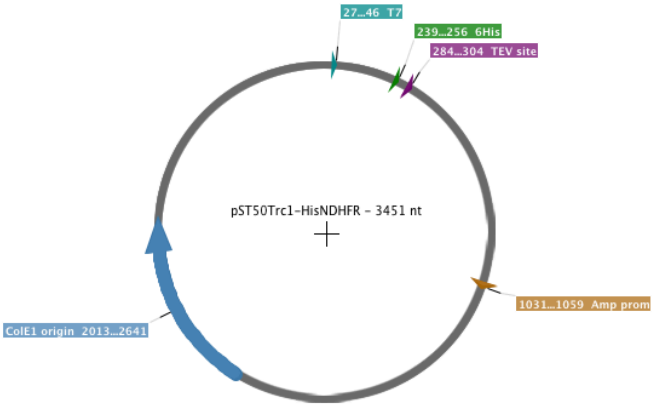

2.1.2 FRATtide

174 196

DPHRLLQQLV LSGNLIKEAV RRLHS

- Total Amino Acids: 25
- Molecular Weight: 2.89 kDa
- Isoelectric point: 10.74

2.1.3 DISC1-44mer

193 236

PEVPPTPPGS HSAFTSSFSF IRLSLGSAGE RGEAEGCPPS REAE

- Total Amino Acids: 44
- Molecular Weight: 4.53 kDa
- Isoelectric point: 4.75

2.1.4 6xHis-TEV-GSK3β

```
        10         20         30         40         50         60
MGSSHHHHHH SSGSGGGGGE NLYFQGSMSG RPRTTSFAES CKPVQQPSAF GSMKVSRDKD

        70         80         90        100        110        120
GSKVTTVVAT PGQGPDRPQE VSYTDTKVIG NGSFGVVYQA KLCDSGELVA IKKVLQDKRF

       130        140        150        160        170        180
KNRELQIMRK LDHCNIVRLR YFFYSSGEKK DEVYLNLVLD YVPETVYRVA RHYSRAKQTL

       190        200        210        220        230        240
PVIYVKLYMY QLFRSLAYIH SFGICHRDIK PQNLLLDPDT AVLKLCDFGS AKQLVRGEPN

       250        260        270        280        290        300
VSYICSRYYR APELIFGATD YTSSIDVWSA GCVLAELLLG QPIFPGDSGV DQLVEIIKVL

       310        320        330        340        350        360
GTPTREQIRE MNPNYTEFKF PQIKAHPWTK VFRPRTPPEA IALCSRLLEY TPTARLTPLE

       370        380        390        400        410        420
ACAHSFFDEL RDPNVKLPNG RDTPALFNFT TQELSSNPPL ATILIPPHAR IQAAASTPTN

       430        440
ATAASDANTG DRGQTNNAAS ASASNST
```

- Total Amino Acids: 447
- Molecular weight: 49.47 kDa
- Isoelectric point: 8.89

2.2 Reagents

See Appendix A for reagent list

2.3 Overexpression

Overexpression was conducted using BL21 DE3 Star Competent E. *coli* cells. Competent cells were transformed into one of two main types of growth media; 2xYT (Bacto-Tryptone 16 g/L, Yeast Extract 10 g/L, NaCl 5 g/L, 0.1 mg/mL Ampicillin pH 7.0) or TB (Yeast Extract 24 g/L, Tryptone 20 g/L, Glycerol 4 mL/L, 0.017 M KH_2PO_4, 0.072 M K_2HPO_4, 0.1 mg/mL Ampicillin). LB media (Bacto-Tryptone 10 g/L, Yeast Extract 5 g/L, NaCl 10 g/L, 0.1 mg/mL Ampicillin pH 7.5) and LB agar plates (Bacto-Agar 15 g/L, Bacto-Tryptone 10 g/L, Yeast Extract 5 g/L, NaCl 10 g/L, 0.1 mg/mL Ampicillin) were used to initiate growth cultures or for plating bacterial colonies. The cultures were then induced using Ind1 (Induce with 0.15 mM IPTG when OD is between 0.6-0.9 shake at 220 RPM for 16-18 hours at 16-17°C) or Ind2 (Induce with 0.15 mM IPTG when OD reading is between 0.1-0.2 shake at 220 RPM for 35-40 hours at 16-17°C). Following induction and growth, cells were spun down and harvested either in 2L bottles (Nalgene 2L PPCO Bio Bottle with Sealing Closure (Thermo Fisher # 3120-2006) in H-12000 Rotor at 4700 RPM for 20 minutes at 4°C) or 1L bottles (Beckman 1L Polycarbonate Centrifuge Bottles (VWR #BKA98812) in JLA8.1 Rotor at 5000 RPM for 20 minutes at 4°C). Cell pellets produced from this overexpression process were flash frozen using liquid nitrogen and stored at -80°C.

2.4 Protein Purification

2.4.1 Cell Preparation

Frozen cell pellets were weighed and resuspended in lysis buffer at varying ratios of pellet weight to lysis buffer (Table 2-1 or Table 2-2) volume. The pellets were brought into a homogenous state by constant stirring over an ice bath. Following resuspension, cells were lysed either by sonication (S3000, ¼" diameter, sonication times, rates, and duty cycles were varied based on optimization experimental protocol) or cell disruption (Constant Systems LTD 0.75KW with 2-3 run throughs at 25-35 PSI). Lysed cells were pelleted to remove whole cells, nuclei, cytoskeleton, and other large unwanted cellular debris. After cell lysis, all preparations were spun at 40,000 RPM using an ultracentrifuge (Sorvall WX Ultra Series Ultra Centrifuge, Rotor type70Ti) for 60 minutes.

2.4.2 Purification

Protein purification was either completed for a small-scale test of protein expression using Ni Sepharose excel histidine-tagged protein purification resin (GE Healthcare #17371201) by batch or large-scale test of protein expressing using prepacked columns from GE Healthcare (HiTrap SP HP 1mL #17115101, HiTrap SP HP 5 mL #17115201, HiTrap SP XL 1mL #17516001, HiTrap SP FF 1mL #17505404, HiTrap SP FF #17515701, HITrap Q HP 1mL #29051325, HisTrap HP 1mL #17524701, HisTrap HP 5 mL #17524801, Superdex 200 Increase 100/300 GL # 28990944). Buffers and resins were varied to account for what scale and level of purification occurred.

Table 2- 1: Buffer list for small scale purifications describing abbreviations and components.

Buffer	Components
Lysis Buffer (ssL1)	50 mM Hepes pH 7.2, 300 mM NaCl, 20 mM Imidazole, 5% Glycerol, Pierce Protease Inhibitor
Wash Buffer 1 (ssNA1)	50 mM Hepes pH 7.2, 300 mM NaCl, 20 mM Imidazole, 5% Glycerol
Wash Buffer 2 (ssNA2)	50 mM Hepes pH 7.2, 50 mM NaCl, 20 mM Imidazole, 5% Glycerol
Elution Buffer 1 (ssNB1)	50 mM Hepes pH 7.2, 300 mM NaCl, 250 mM Imidazole, 5% Glycerol

Small-scale purification usually required a 0.5 g sample of the frozen cell pellet resuspended in 3-4 mL of lysis buffer followed by cell lysis and spinning as described in the cell preparation subsection. Loose resin and batch method were always used for small-scale experiments. The buffer compositions for small scale experiments were not varied regularly and can be found in Table 2-1. Large-scale purification used anywhere from 10-80 g of frozen cell pellet resuspended in a volume of lysis buffer at 3 or 4 times the amount of cell pellet. Large-scale purifications follow cell lysis and pelleting described in the cell preparation subsection. Pre-packed columns were always used for large-scale experiments. The columns were attached to the ÄKTA Pure 25 L (GE Healthcare #29018224) in an order and protocol outlined as PuriA (Lysate was applied to SP cation exchange column, elutions were pooled and applied to affinity Ni-NTA column) or PuriB (Lysate was applied to NiNTA affinity column, elutions were pooled and diluted 10:1 with SPA1 then applied to SP cation exchange column). A variety of buffers were utilized

for the different experiments and different columns are detailed in Table 2-2. After purification, the protein product was incubated with TEV protease in dialysis tubing and dialysis buffer (lsDB: 50 mM Hepes pH 7.2, 500 mM NaCl, 5 mM BME) at 4°C for 10-16 hours to remove the Histidine tag.

Table 2- 2: Buffer list for large-scale purification describing abbreviations and buffer components.

Buffer	Components
Lysis Buffer 1 (lsL1)	50 mM Hepes pH 7.2, 300 mM NaCl, 20 mM Imidazole, 5% Glycerol, Pierce Protease Inhibitor
Lysis Buffer 2 (lsL2)	50 mM Hepes pH 7.2, Pierce Protease Inhibitor
Lysis Buffer 3 (lsL3)	50 mM Hepes pH 7.2, 300 mM NaCl, 5% Glycerol, Pierce Protease Inhibitor
Lysis Buffer 4 (lsL4)	50 mM Hepes pH 7.2, 100 mM NaCl, 5% Glycerol, Pierce Protease Inhibitor
Lysis Buffer 5 (lsL5)	50 mM Hepes pH 7.2, 300 mM NaCl, 5 mM $MgCl_2$, 1% Glycerol
NiNTA Wash Buffer 1 (lsNA1)	50 mM Hepes pH 7.2, 300 mM NaCl, 20 mM Imidazole
NiNTA Wash Buffer 2 (lsNA2)	50 mM Hepes pH 7.2, 50 mM NaCl, 20 mM Imidazole
NiNTA Elution Buffer (lsNB1)	50 mM Hepes pH 7.2, 300 mM NaCl, 250 mM Imidazole
SP Wash Buffer 1 (lsSPA1)	50 mM Hepes pH 7.2
SP Wash Buffer 2 (lsSPA2)	50 mM Hepes pH 7.2, 50 mM NaCl
SP Elution Buffer (lsSPB1)	50 mM Hepes pH 7.2, 1M NaCl
Gel Filtration Buffer 1 (lsGF1)	50 mM Hepes pH 7.4, 500 mM NaCl, 2 mM $MgCl_2$, 1 mM TCEP
Gel Filtration Buffer 2 (lsGS2)	50 mM MES pH 6.5, 175 mM NaCl, 1 mM $MgCl_2$, 10 mM DTT, 5% Glycerol

2.5 SPR Assay

SPR studies were conducted using the Reichert 2 channel single flow cell (Model: 2SPR). The Nickel Nitrilotriacetic Acid (NiNTA) Sensor Chip (Reichert CA# 13206065) was first prepared by flowing a $NiSO_4$ solution overtop to capture the Ni^+ ions and primed it for protein

capture. SPR assay was conducted using the buffers detailed in Table 2-3. Initially GSK3β was diluted in RB1 and captured onto the Ni-coated surface. After GSK3β was captured, the buffer was run over the surface of the chip until the amount of protein dislodged by the flow of buffer (drift) fell below 5 RU/min. Blanks were injected using RB1 to establish a baseline for background binding. Then the synthesized 25 Amino Acid fragment of FRAT (FRATtide) from GenScript (Lot #: 93874160001/PE1490) or the synthesized 44 Amino acid fragment of DISC1 (DISC1-44mer) from NEO BioLabs (P12485D hd1-44mer, catalog No 249346 with purity rating of 96.5%) were injected and flown over the top. DISC1-44mer was dissolved in KB1, then diluted with DB1 and brought to final volume with RB1. FRATtide was dissolved in RB1. Results were analyzed using TraceDraw software. Chip surface was regenerated with SB and RGB and a 0.5 M NaOH solution.

Table 2- 3: Buffer abbreviations and components used for SPR studies.

Buffer	Components
Running Buffer (RB1)	50 mM Tris pH 7.5, 150 mM NaCl, 5 mM $MgCl_2$, 0.01% Tween 20, 1 mM TCEP
Kinase Buffer (KB1)	50 mM Tris pH 7.5, 5 mM MgCl2, 0.01% Tween20, 1 mM TCEP
Dilution buffer (DB1)	50 mM Tris pH 7.5, 5 mM MgCl2, 300 mM NaCl, 0.01% Tween20, 1 mM TCEP
Stripping Buffer (SB)	20 mM Na-Phos pH 8.5, 300 mM NaCl, 50 mM EDTA
Regeneration Buffer (RGB)	50 mM Hepes pH 7.2, 300 mM NaCl, 250 mM Imidazole

2.6 ADP-GLO

ADP-GLO analysis was conducted with the ADP-GLO kit and reagents from Promega (CA # V6930). Pre-Mix buffer (150uM ATP, 25nM GSK3β, 1X RxnB1) was prepared with ATP and GSK3β. Varying reaction mixtures in reaction buffer (RxnB1: 50 mM Tris pH 7.5, 5 mM $MgCl_2$, 0.01% Tween 20, 3 mM DTT) were set up in a 96 well plate with the synthetic GSK3β substrate GSP2 from SignalChem (Catalogue #: G50-58, Lot #: 01059-3, MW: 3029.13 Da. Purity: 95.85% by HPLC) alone or with the synthetic substrate inhibitor DISC1-44mer from NEO BioLabs (P12485D hd1-44mer, catalog No 249346 with purity rating of 96.5%). The pre-mix buffer was added to the reaction mixture in the 96 well plate and incubated for a set amount of time depending on the parameter being measured. The incubation time allowed for the reaction to occur. To stop the reaction at a set point, 5 µL of ADP-GLO reagent and 5 µL of the reaction were

mixed an allowed to incubate for 60 minutes. The ADP-GLO reagent stops the reaction and simultaneously remove any unused ATP. Detection followed the stop reaction set by adding 10 μL of the ADP-GLO Detection Reagent into the mixture and allowing to incubate for 30 minutes. The ADP-GLO Detection reagent stoped the ATP depletion reaction and converted the ADP in solution to ATP which is further converted to light by luciferase. The luciferase activity is quantified by a luminescence plate reader (SynergyHT Luminescence Plate Reader).

3.0 Objective 1: Optimization of Heterologous Overexpression of Human GSK3β in Bacteria

This chapter focuses on detailing the efforts made to improve the overall amount of protein produced at the stage of overexpression. Overexpression, in the context of this thesis, refers to the act of using an IPTG inducible plasmid containing a copy of His-GSK3β in competent *E. coli* cells. The GSK3β protein used is a eukaryotic protein which tends to be toxic and thus challenging to overexpress in bacterial systems. Also, the protein contains some hydrophobic regions making aggregation a potential issue. This chapter outlines the experiments conducted in an attempt to alleviate some of these issues and increase the overall amount of protein produced at this level.

3.1 Results

3.1.1 Comparison of Ind1 and Ind2

The main differences between Ind1 and Ind2 involve the induction point and the growth duration. Ind1 induces between 0.6 to 0.9 OD then allows the cells to grow over a period of 16-18 hours. Ind1 is compared to Ind2 which induces between 0.1 and 0.2 OD then allows the cells to grow over a period of 35-40 hours (Table 3-1). Both induction conditions were adapted from previously established protocols and compared herein to determine which procedure is better suited for the growth of cells containing a GSK3β expressing plasmid. The two induction conditions were compared between two common media types; 2xYT and TB. In general, media compositions were generated to support bacterial growth through the logarithmic growth phase. Both 2xYT and TB media contained Tryptone and Yeast Extract which act as a source of carbon, nitrogen, vitamins, minerals and amino acids (Kram and Finkel, 2015). The main difference between the two media types is the buffering component in TB media. The potassium phosphate buffer in TB media, acts to prevent cell death and increase plasmid yield by extending the exponential phase of *E. coli* while simultaneously resisting the increase in pH which occurs as a

result of metabolism of amino acids (Kram and Finkel, 2015). Higher points of induction occurring within mid to late log phase (OD_{600} 0.6-0.9) were hypothesized to be optimal as that is the time in which bacterial cellular growth is highest, ensuring that protein production will be at its peak. However, the use of lower induction points in the early log phase (OD_{600} 0.1-0.2) was theorized to be beneficial overall as it allowed for protein production to occur during a time when the cellular growth rate would be slower which may give sufficient time for translated proteins to fold.

Table 3- 1: Summary of the main differences between Ind1 and Ind2.

	Induction OD	[IPTG]	Temperature	Duration
Ind1	0.6-0.9	0.15 mM	16-17°C	16-18 hours
Ind2	0.1-0.2	0.15 mM	16-17°C	35-40 hours

Results show GSK3β present in each of the four test conditions. ImageJ analysis determined that TB media has the propensity to produce GSK3β at a slightly higher amount (~30%) when compared to 2xYT (Figure 3-2). However, TB also appears to produce a higher level of contaminants compared to 2xYT (~15%). The comparisons between Ind1 and Ind2 concerning the amount of GSK3β produced shows that Ind2 can produce more GSK3β but the overall difference in intensity is minimal. When considering the best use of time and materials Ind1 is the more effective method. When considering the downstream effects of overexpression on purification the proportion of contaminants needs to be considered. For these reasons, 2xYT with Ind1 was determined to be the most efficient of the four methods investigated.

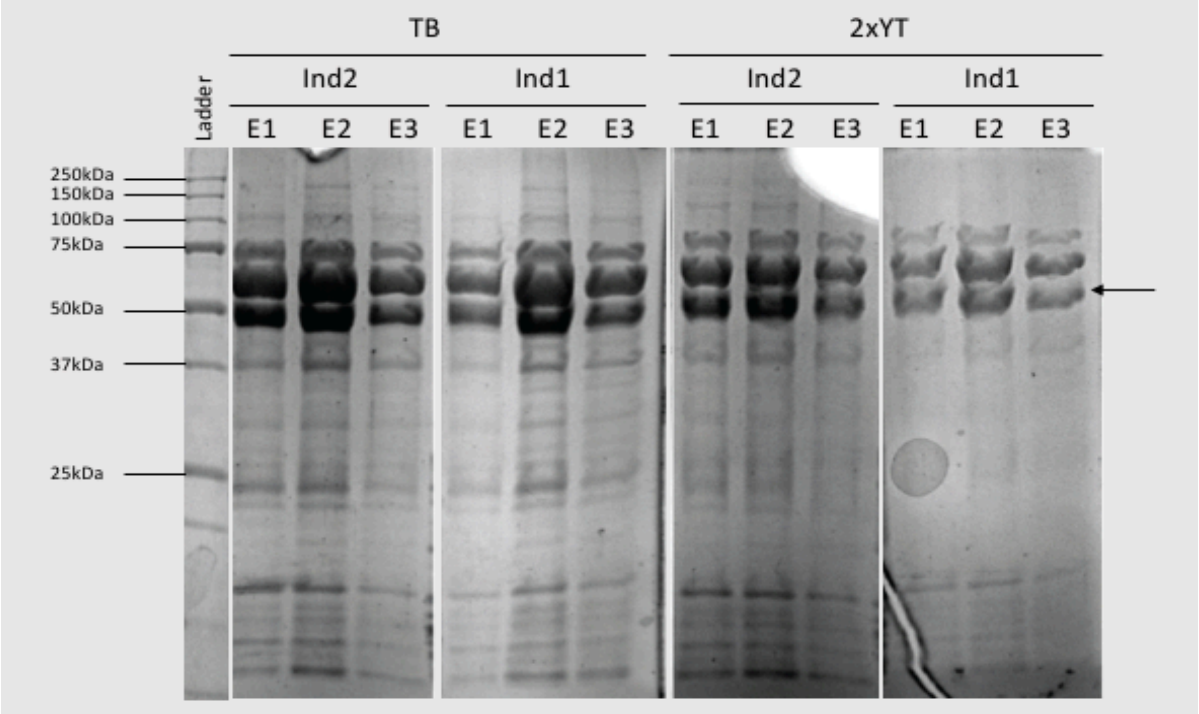

Figure 3- 1: 12% SDS gel showing GSK3β among the four conditions tested comparing Ind1 and Ind2

Each elution fraction (E1-E3) is the result of a 1L preparation of cells resuspended in 15 mL of ssL1 and lysed via sonication (microtip, 3x3 minute sets at 50% duty cycle). Lysed cells were spun down at 14,000 RPM for 40' then bound via batch method to 100 µL of NiNTA resin and allowed to incubate for 40 minutes at 4°C. The resin was washed with 1.5 mL of ssNA1 and eluted with 300 µL ssNB1. ImageJ analysis of the GSK3β band for each elution fraction was added together for each condition. Overall intensity was normalized using the intensity of the 75 kDa band in the ladder and compared to draw conclusions. GSK3β is indicated in the figure by the arrow.

3.1.2 Comparison of Growth Vessels

The design of growth vessels can affect protein overexpression. Ultra Yield Flasks™ are designed with notches in the base to increase aeration for optimal bacterial growth. To test whether these flasks help with GSK3β production by *E. coli* cells, a series of experiments was designed to investigate if the level of protein expression varies between cultures grown in standard Erlenmeyer glass flasks and cultures grown in Ultra Yield Flasks™. ImageJ analysis of band intensity demonstrated that cell cultures grown in the aerator flasks produced 1.5X more GSK3β than cell cultures grown in the glass Erlenmeyer flasks (Figure 3-1). It was suggested that one single batch of 1L cell pellets grown in the Ultra Yield Flasks™ should contain a relatively similar amount of GSK3β protein as one single batch of 2L cell pellets grown in the standard Erlenmeyer flasks. Considering the minimal difference, the practice of using 4L Erlenmeyer flasks to grow 2L of cell culture was continued.

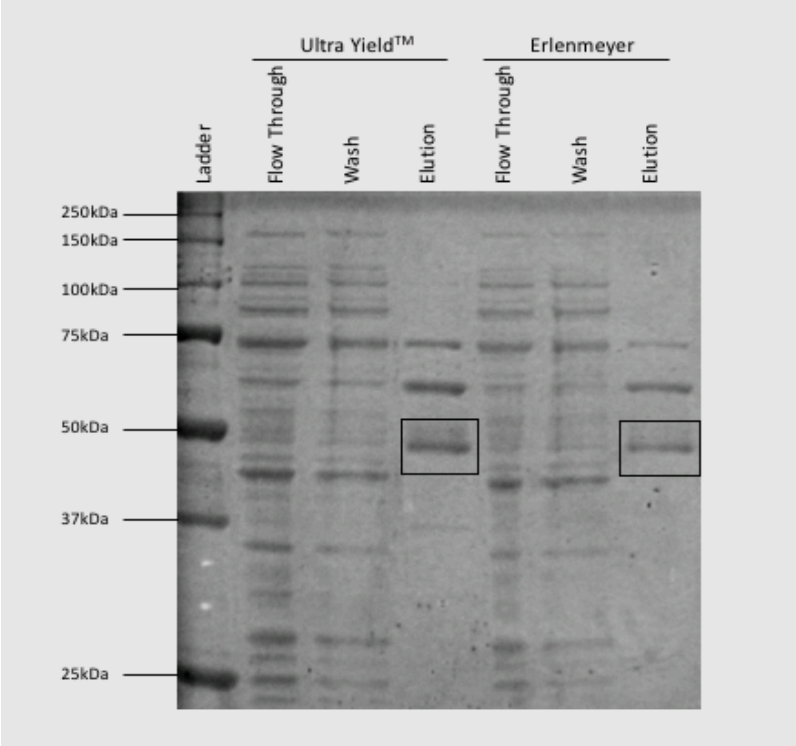

Figure 3- 2: 12% SDS gel comparing protein expression between cultures grown different growth vessels.

Both preparations consisted of 1L of 2xYT media prepared using Ind1. Each fraction depicted in the gel is the result of 0.5 g of cell pellet resuspended in 1 mL of ssL1 and lysed with the addition of lysozyme and incubation at 37°C for 30 minutes. Lysed cells were spun down at 15,000 RPM for 40 minutes then bound via batch method to 25 µL of NiNTA resin and allowed to incubate for 40 minutes at 4°C. The resin was washed with 3 mL of ssNA1 and eluted with 100 µL of ssNB1. Flow-through fractions consist of a sample of lysate that did not bind to the NiNTA resin. The wash fractions consist of a sample after the resin was washed with ssNA1. Elution fractions consist of a sample after the resin was eluted with ssNB1. ImageJ analysis of the GSK3β band in the elution fractions was conducted. GSK3β is highlighted in the figure with rectangular boxes.

3.1.3 Reduce GSK3β Toxicity to Bacteria

In some instances, certain proteins can be toxic to the bacterial host. Toxicity of eukaryotic proteins is one of the many possible explanations for low gene expression (Gubellini et al., 2011). Toxicity, in this context, is a term used to explain low expression levels of recombinant genes when the proteins encoded by those genes are eukaryotic kinases. To further investigate the possibility that the kinase activity of GSK3β is the cause of its toxic effect on BL21 cells, overexpression was conducted with varying concentrations of Lithium Chloride. Lithium chloride (LiCl) is a known inhibitor of GSK3β (Beaulieu, 2007). Since expression levels of GSK3β in BL21 are lower than desired and considering that GSK3β is a eukaryotic kinase, it was hypothesized that GSK3β is having a toxic effect on the bacteria. Given this, it was postulated that

the addition of LiCl to the growth media will increase the overall protein yield by inhibiting the function of GSK3β and thereby limiting its toxic effect.

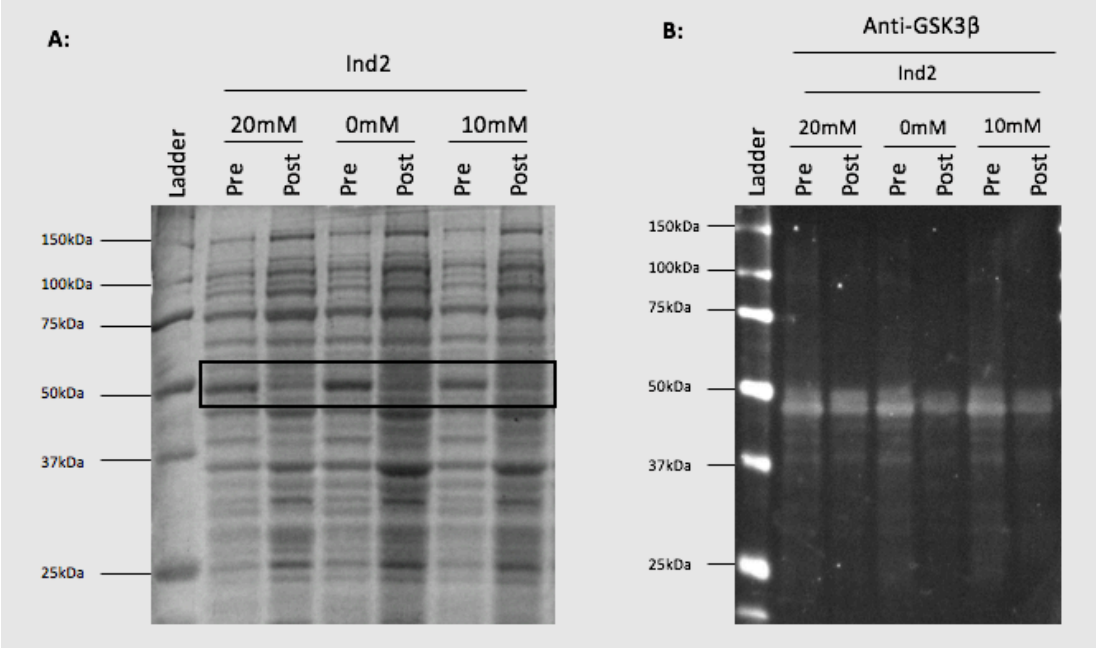

Figure 3- 3: 12% SDS gel and western blot analysis of pre- and post-induction samples taken from 100 mL cultures grown with LiCl.

The experiment was conducted under the induction conditions of Ind2. Samples were taken from the Post-induction condition after the dedicated growth duration. Samples taken from the Post-induction condition were corrected for volume using OD measurements to be representative of having the same number of cells as the sample taken from the pre-induction condition for adequate comparison. Cells were not lysed and instead run directly on an SDS gel after being heated with SDS loading buffer. The GSK3β band is indicated by the rectangular box. B: Western Blot analysis of the same samples depicted in A. Samples were incubated with antibodies against anti-GSK3β (amino acid 1-160 Dilution 1:6000) and visualized with secondary antibody (Anti-mouse dylight 680 in Dilution 1:10000) than detected with G-Box UV imaging.

The results showed a visible GSK3β band that appeared in all the test conditions (Figure 3-3 - A). GSK3β presence was further confirmed by western blot analysis using antibodies against the protein GSK3β itself (Figure 3-3 - B). ImageJ analysis of the Coomassie-stained gel showed that LiCl in the media produced little effect on overall expression as all the conditions appeared to produce a relatively similar amount of GSK3β. Western blot analysis was also unable to distinguish a difference in levels of GSK3β expression among the different test conditions. The conclusion from this series of experiments was that the addition of LiCl up to and including concentrations of 20 mM to cell culture media is not overly helpful in increasing the overexpression levels of this specific GSK3β construct.

3.2 Discussion

3.2.1 Growth Components and Protocols

3.2.1.1 Comparison of Ind1 and Ind2

When only considering the amount of GSK3β alone, TB media with Ind2 appeared to be the best condition. However, extra considerations needed to be addressed concerning time restraints and chaperone levels. The longer cells remain in long-term stationary growth phase, the more likely they are to undergo mutation as a result of oxidative stress (Kram and Finkel, 2015). Mutations of this variety are unpredictable and have the potential to result in lower levels of protein expression. Factoring this information into the comparison between Ind1 and Ind2 it can be argued that since both induction conditions produce protein in relatively similar amounts, Ind1 would be preferable given that the period cells spend in long-term stationary phase is lower. In addition to overall time, deliberations needed to be made for the level of contaminants present. TB media has the unique ability to extend the exponential growth phase of *E. coli* (Kram and Finkel, 2015) which allows for increased protein expression. However, it can be suggested that along with this increased growth phase there is an inherent increase in the expression of native *E. coli* proteins including folding chaperones. Although these chaperones do not play a direct role in the overexpression mechanism, they are noteworthy when observing the project as a whole as they will need to be eventually removed in subsequent purification steps. Ideally, more chaperones would be beneficial to help with folding and lessen any potential aggregation. However, further investigation into purification steps has shown that these chaperones have a higher tendency to stick to GSK3β and can be difficult to remove. The best scenario for overexpression would be a condition where the chaperones are expressed well to aid with folding but not overexpressed at a comparable rate to overexpressed protein. When comparing the ratio of GSK3β to Contaminant60, TB/Ind2 was the highest overall. 2xYT/Ind1 had the second highest ratio. 2xYT/Ind1 and TB/Ind2 were similar. Collective analysis of all the points suggests that 2xYT/Ind1 is the most useful condition to produce an acceptable amount of GSK3β without overloading the system with cellular proteins and chaperones.

3.2.1.2 Comparison of Growth Vessels

The Ultra Yield Flasks™ were more efficient at increasing protein expression per liter of cell media prepared. This is the case because the design of the Ultra Yield Flasks™ creates an environment with greater air exchange for the bacterial cells. The shaking of cultures within these flasks creates an equal distribution of nutrients to the contained cells as well as an increase infusion of oxygen. If oxygen levels are not evenly distributed to all cells then the result for aerobic bacteria such as *E. coli* is cell death ultimately lowering the overall yield of protein production (Kram and Finkel, 2014). This explains why the amount of expression from cells grown in the Ultra Yield Flasks™ flasks (2.5 L) is more comparable to expression from cells grown in a 4L flask than from cells grown in a 2L flask. The ratio of air to media also plays a role in the amount of air exchange occurring (Kram and Finkel, 2014). Ideally the best conditions for bacterial growth, and subsequent protein expression, would be to use the notched design of the Ultra Yield Flasks™ with a high air to media ratio.

3.2.2 Toxicity and Leaky Expression

3.2.2.1 Lithium Chloride

The results from this experiment suggest that LiCl in the media is unable to increase GSK3β expression levels since expression of GSK3β was consistent across the different concentrations of LiCl. The concentrations used were based on values of LiCl adapted from a study which showed that 20 mM of LiCl was sufficient to entirely suppress GSK3β activity (Klein and Melton, 1996). However, it is important to note that the study used GSK3β in solution, not GSK3β contained within the cellular membranes of a bacterial host. It is possible that in order to see any changes in expression as a result of inhibition, a concentration greater than 20 mM of LiCl is necessary. Given that each cell contains multiple copies of the offending protein and a single unit of media solution is dense with cells it can be assumed that the overall concentration of GSK3β within the growing culture is much higher than the amount of GSK3β used for the assay in the Klein *et al*. study (Klein and Melton, 1996). Therefore, 20 mM of LiCl may not have been sufficient to effectively inhibit enough enzyme units to influence any effect on toxicity. It is also possible that LiCl is unable to cross the cell membrane and act directly on GSK3β. Further activity studies of proteins purified after being grown in media containing LiCl will further clarify if the

LiCl actively inhibits the enzyme units within the cells in the media. These further studies would allow for proper conclusions to be drawn regarding GSK3βs activity and its influence on expression levels. At the current stage, the only conclusion that can be drawn from the data is that the addition of LiCl to the media does not positively increase GSK3β expression.

Although LiCl was ineffective under the conditions in which it was used, there are still other ways to potentially reduce recombinant protein toxicity to *E. coli* cells. The addition of ethanol at 1%-4% v/v at the time of induction has been shown to be effective at increasing toxic protein yield in some cases (Chhetri et al., 2015). Alternative methods of decreasing recombinant protein toxicity to *E. coli* include manipulations to the gene sequence. One group has successfully shown abundant overexpression of a toxic eukaryotic protein in *E. coli* by including a leader sequence that correlated to the S-loop of the bacterial chaperone GroES. This leader sequence is known to interact with bacterial chaperone GroEL and increases the recombinant proteins affinity for GroEL. Thereby increasing the rate at which the recombinant protein will undergo proper folding and in doing so, decrease the toxic consequence of the protein (Donnelly et al., 2001). Given GSK3β's low expression levels, it is possible that the use of a leader sequence with affinity to GroES may help increase the overall yield in a similar fashion. Additionally, alternative cell lines are available that specialize in expressing toxic proteins including C41(DE3) or C43(DE3). The strains claim to be useful in expressing toxic and membrane proteins from all classes including eukaryotes. The cell line contains a mutation that prevents cell death in the presence of toxic recombinant proteins. These constructs could potentially decrease the toxic effect GSK3β has on the bacterial expression system.

3.2.3 Leaky Expression

Leaky expression of the induction system was witnessed in previous experiments (Figure 3-3). Leaky expression is problematic as it can act as an initiator of aggregation. The proteins expressed earlier on are likely in an aggregated form and this aggregation can trigger more aggregation of newly synthesized proteins. One potential suggestion for further optimization to reduce leaky expression includes attempting overexpression in bacterial cell lines other than BL21(DE3). For instance, BL21(DE3)pLysS includes the pLysS plasmid which contains a T7 lysozyme. This lysozyme aims to reduce basal levels of gene expression before IPTG induction.

Additionally, the addition of glucose to the growth media may also prove effective at reducing leaky expression. Leaky expression can occasionally be attributed to the lack of a carbohydrate source in the media which increases the presence of activator proteins involved in alleviating lac operon repression (Grossman et al., 1998). Addition of glucose at a rate of 1% to the growth media has been shown to eliminate this form of leaky expression for the IPTG inducible Lac operon system (Grossman et al., 1998). Both methods are worth investigating to analyze their potential for increasing protein yield levels.

3.2.4 Summary

The work conducted within the confines of this thesis served to investigate specific issues involved with overexpression such as media preference, growth vessel preference, toxicity, and leaky expression. While the thesis was able to bring the protocol to a workable point, more optimization will be necessary in order to get the construct to express at a level required for crystallization protocols. If none of the suggestions discussed above proves to be effective in increasing GSK3β yield, future research may have to investigate using Baculovirus/Insect Cell lines or plant-based platforms in place of bacterial cell lines. Both insect and plant-based expression systems have shown an increased level of expression for difficult recombinant proteins. These systems seem to alleviate the issues surrounding inclusion bodies and the presence of persistent folding chaperones which are commonly encountered with the use of bacterial cell lines (Gecchele et al., 2015). However, it should be noted that while both insect and plant-based expression systems can produce recombinant protein at a higher yield, insect cell lines are less cost-effective and plant-based systems require a long time to establish.

4.0 Objective 2: Optimization of Purification of Human GSK3β

This chapter focuses on detailing the efforts made to improve the overall amount of protein retrieved during the purification stage. Purification, in the context of this thesis, refers to the process of separating GSK3β from other proteins present in the cell lysis mixture. Purification includes the physical process of cell lysis and multiple components of column purification including column order, resin type, wash buffer components. The overall goal of the objective was to improve upon the existing purification protocol to obtain a larger yield of GSK3β that has a high purity level for use in other experiments or assays.

4.1 Results

4.1.1 Cell Lysis

4.1.1.1 Sonication Duration

Sonication is the use of sound waves to break open bacterial cells and release the cellular components from inside. Too little sonication cause cells to remain intact whereas too much sonication can potentially cause degradation of the desired proteins (Shrestha et al., 2012). One hypothesis developed to explain the low protein yield observed is a suboptimal amount of sonication resulting in pelleted or degraded protein. To address this hypothesis, a time course sonication study was conducted (Figure 4-1) with the intention of identifying a time point in which a distinct GSK3β band could be seen in the supernatant fraction and less in the pellet fraction. The presence of a clear GSK3β band in the supernatant fraction would indicate that the majority of protein in the lysate could be found in the soluble fraction and not be pelleted in the insoluble fraction.

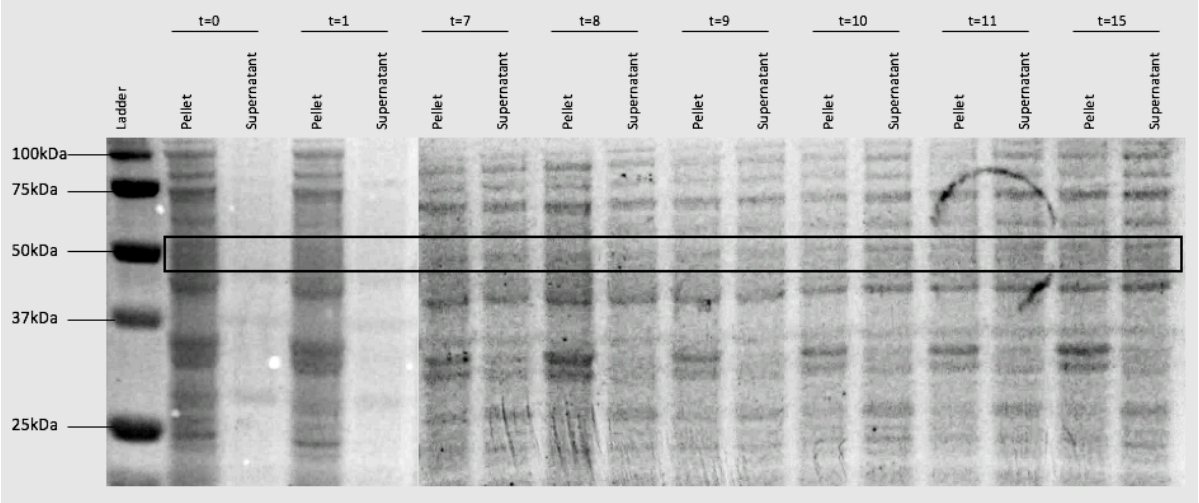

Figure 4- 1: Time course study for sonication.

Cells grown in 2xYT and induced using Ind2 were resuspended in lsL2 buffer and set up to be sonicated by a ¾" probe at 50% duty on a maximum strength output of 5 using a Branson Sonifier VC300. Samples of the lysate were collected at 1 min intervals for 15 minutes (samples from 2 min to 6 min are not shown in the figure above). Each of the samples was spun down at 15,000 RPM, and the pellet and supernatant fractions were analyzed on a 12% SDS gel. ImageJ analysis of band intensity was attempted to determine a time point where GSK3β could be seen in the supernatant fraction.

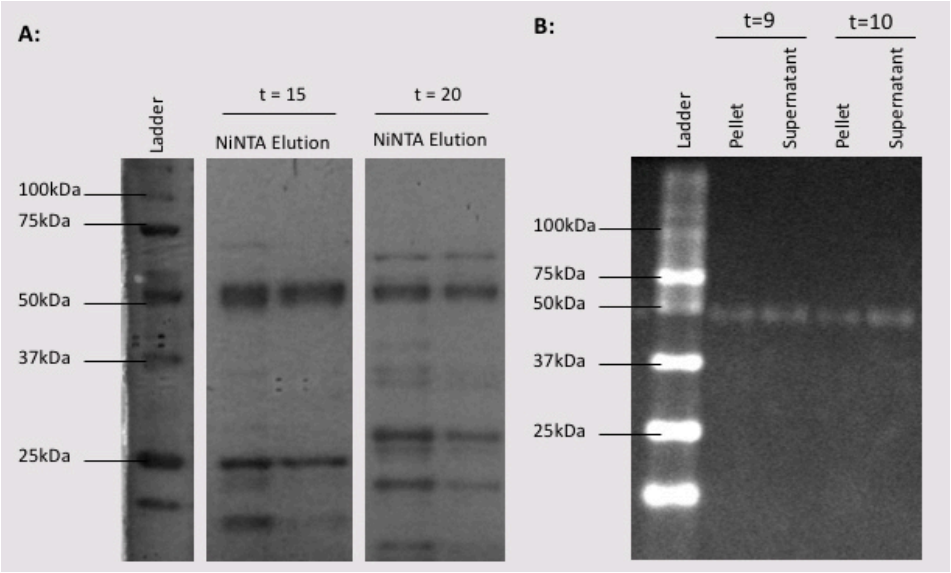

Figure 4- 2: (A) Purifiable protein after 15 and 20 min. (B) Western blot analysis of the sonication series.

(A) 50 g cell pellet that was grown in 2xYT media and induced using Ind2 were resuspended in 200 mL of lsL2 buffer and set up to be sonicated by a ¾" probe at 50% duty cycle on a maximum strength output of 5 using a Branson Sonifier VC300. Two replicates were conducted under identical circumstances expect the duration of sonication. Both samples were processed using PuriA. Samples on the left (t=15) had 15 minutes of sonication whereas samples on the right (t=20) had 20 minutes of sonication. (B) Western blot analysis of samples run during sonication series as depicted in Figure 4-1. The primary antibody was targeted against the Histidine tag at room temperature for 2 hours (See Appendix B).

Results from this series of experiments showed a faint band, suspected to be GSK3β which could begin to be identified in the supernatant fraction around 7 minutes while the intensity of the suspected GSK3β was most prominent at 15 minutes (Figure 4-1). However, it can be observed that the correlating band for GSK3β in the pellet fraction is also most prominent at 15 minutes (Figure 4-1). For the time points higher than 15 minutes, the SDS analysis does not show a distinct band correlating to GSK3β (results not shown). The whole cell lysis approach made it difficult to easily identify or confirm the presence of GSK3β at each of the time points. To confirm the presence of GSK3β in these fractions, western blot analysis was conducted (Figure 4-2 B) on the same whole cell preparations presented in Figure 4-1. Antibodies used for Western Analysis were targeted against GSK3β (data not shown) and the Histidine tag to add confidence to the confirmation of GSK3βs presence in both the supernatant and the pellet fractions. Western blot analysis was able to positively confirm the presence of GSK3β in each fraction from t=2 to t=17 but was unable to distinguish a difference in band intensity as depicted above (Figure 4-2 B).

To further investigate the difference in sonication times in more quantifiable terms of soluble protein, identical samples were compared for sonication times of 15 minutes and 20 minutes (Figure 4-2 A). Chromatogram peak height (data not shown) and ImageJ analysis from the NiNTA-purified samples, confirmed that the overall amount of retrievable GSK3β after 20 minutes of sonication is less than the amount retrieved after 15 minutes of sonication (Figure 4-2 A). It should also be noted that the comparison between the two sonication conditions showed that increased sonication above 15 minutes yields a resulting NiNTA fraction with an increased number of protein species present between 50 and 25 kDa. Also, the 60 kDa chaperon in the 20-minute sonication condition appears to be more prominent.

The results from the sonicator comparison analysis suggest that sonication times at 20 minutes or above are detrimental to the amount of protein product which remains in a purifiable state. While 15 minutes appears to be superior to 20 minutes, it can still be argued that the amount of protein retrieved is lower than expected for the number of cells processed. The western blot analysis of the timed series shows that GSK3β is present in the supernatant fraction after only 2 minutes and is most noticeable on the SDS gel at 7 minutes suggesting that sonication times less than 15 minutes may be able to retrieve even higher amounts of purifiable GSK3β. Additional

studies conducted with 10 minutes of sonication time proved to be less effective at retrieving GSK3β when compared to preparations conducted using 15-minute sonication protocols (results not shown). Overall, in the event of sonication alone as a cell lysis method 15 minutes appears to be the most beneficial when compared to 20 minutes and 10 minutes for 25-50 g of cell pellets resuspended in lysis buffer at a ratio of 4:1.

4.1.1.2 Cell Disruptor Comparison

Sonication as a cell lysis tool possesses the potential to be too aggressive on cells which may lead to aggregation of protein products. In comparison, cell disruption acts by using pressure and force to burst open cells which has the potential to be less detrimental to protein yield when used in the proper proportion (Vanderheiden et al., 1970). This series of experiments attempted to compare the effectiveness of sonication to cell disruption as they pertain to cell lysis. It is hypothesized that a higher yield of purifiable protein can be obtained when the method of cell lysis used is cell disruption instead of sonication. Since cell disruption is thought to be a milder approach, there should subsequently be less protein degradation or aggregation. This series of experiments compared the yield of two separate purifications which only varied in the type of cell lysis method utilized; sonication or cell disruption.

The NiNTA elution fraction and 100% reverse wash fractions depicted above (Figure 4-3) illustrate the main differences between the lysis methods under investigation. The NiNTA elution fractions shows what protein species are retrieved when the affinity column is the first to be introduced to the lysate. The 100% Elution Reverse Wash occurs after elution is complete, it is a subsequent 100% Elution wash in the up-flow direction. The purpose of the reverse wash is to determine if any protein species became stuck above the filter of the column and as such were unable to be washed off in the downward direction. Reverse wash analysis is an additional indication of potential protein aggregation within the lysate.

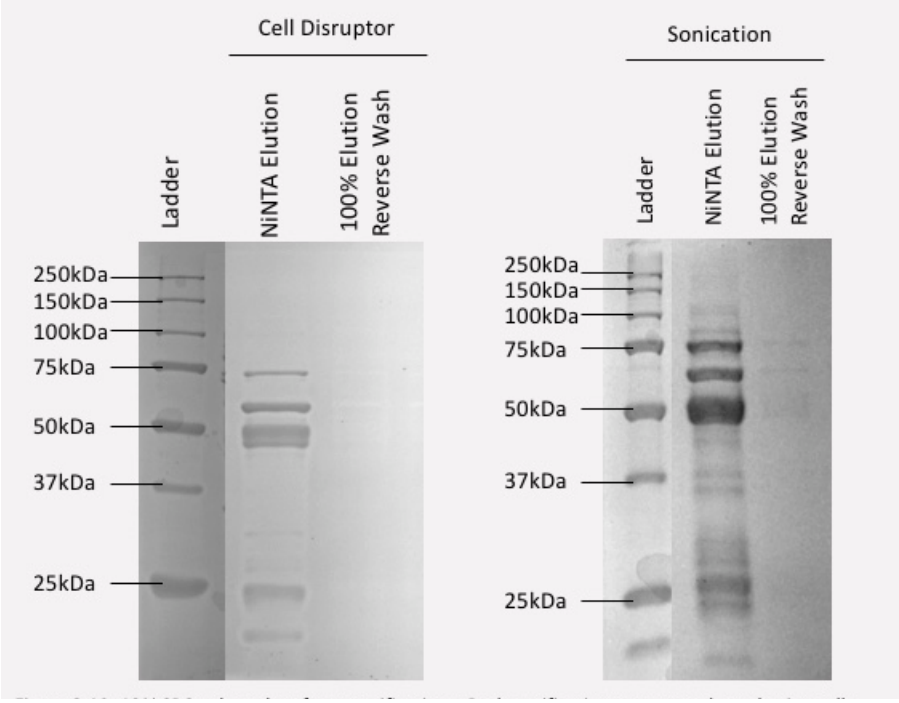

Figure 4- 3: Comparison of purifiable protein between cell lysis with cell disruption and sonication.

12% SDS gel results of two separate purifications. 10 g (cell disruptor-left) and 9 g (sonication-right) of cells grown in 2xYT and induced via Ind1 were resuspended in 15 mL of lsL3 and lysed. Lysed cells were spun down at 40,000 RPM for 60 min then purified according to PuriB. 1mL column was used and washed with 25 mL of lsNA1, then washed with 10 mL lsNA2. Elution occurred with Gradient and 10 mL elution buffer lsNB1. The gels displayed show the NiNTA elution fraction and the 100% reverse wash fraction. Cells that had undergone lysis via cell disruptor underwent three rounds of cell disruption at 25 PSI. Cells that had undergone lysis via sonication underwent sonication with a ¾" probe of the S3000 in timed increments of 2 seconds on/2 seconds off for a total process time of 3 minutes.

The cell disruptor analysis shows a clear band for GSK3β with the typical 60, 70 and 25 kDa contaminants frequently seen eluting together. The 100% elution reverse wash fraction from this analysis is clear showing no protein bands which indicates that there is little to no aggregates stuck above the filter. The sonication analysis shows GSK3β in the elution fraction with the typical 60, 70 and 25 kDa contaminants. However, protein bands at 100 and 80 kDa along with multiple bands between 37 and 25 kDa can be seen, that were not present in the elution fraction from the cell disruption analysis. The presence of these additional bands makes the elution look dirtier which is undesirable as it can be difficult to remove these bands during later stages of purification. In addition, the 100% elution reverse wash fraction from the sonication analysis shows GSK3β and the 60 and 70 kDa contaminants (Figure 4-3) suggesting that the sonication process may be causing some level of aggregation of the proteins or the protein complex in solution. Overall, both

methods of cell lysis can be utilized effectively, but cell disruption appears to cause less aggregation and produce a cleaner protein product after affinity column purification.

4.1.2 Column Purification

4.1.2.1 Purification History

Initial work by previous lab members established a protocol whereby GSK3β was expressed in a bacterial culture grown in TB media and induced via Ind2. The initial purification protocol focused on PuriA whereby the lysate was applied to cation exchange resin (SP-HP) before its application to affinity resin (NiNTA). However, the final product after the NiNTA purification could only generate a small fraction of protein with an approximate purity level of 60%. When the protein product at this stage was applied to a gel filtration column, the purity level increased to >90%, but the overall yield decreased to minimal amounts. The primary contaminants persistently seen in this fraction were three substantial bands that appeared to purify along with GSK3β repeatedly. These contaminants are generally referred to within this thesis by their weights of 60 kDa (Contaminant60), 70 kDa (Contaminant70) and 25 kDa (Contaminant25). These contaminants often remained associated with GSK3β after histidine tag cleavage and subsequent rounds of Ni-NTA purification. In some cases, the contaminants even remained associated with GSK3β throughout the process of gel filtration. This observation strongly suggests that Contaminant60 and Contaminant70 are bound directly to GSK3β in some capacity.

Further studies within the lab were able to employ Mass Spectrometry technology to confirm that Contaminant60 is the bacterial chaperone GroEL. GroEL is known to aid in folding of proteins between 20-60 kDa that contain hydrophobic regions (Joanna L. Feltham and Lila M. Gierasch, 2000). It is assumed that Contaminant70 is likely a bacterial chaperone as well. It has been documented that DnaK is a 70 kDa bacterial chaperone that tends to co-purify with recombinant proteins (Hellebust et al., 1990; Rial and Ceccarelli, 2002). Like GroEL, DnaK also has a wide range of substrates that range in size and isoelectric point making GSK3β a likely substrate (Calloni et al., 2012). These chaperones and/or contaminants could be partially removed by cation exchange chromatography if run before affinity purification with Ni-NTA (PuriA). Within the confines of this thesis these contaminants and/or chaperone bands will collectively be

referred to as contaminants. Further attempts at optimizing purification aim to address the removal of these bacterial contaminants to increase the fraction purity without sacrificing protein yield.

4.1.2.2 Optimization of Cation Exchange Resin

The original protocol utilized SP-HiTrap (SP-HP) resin for the cation exchange purification step. SP-HP is useful as it has a decent capture ability, but it was problematic due to the smaller resin bead size which created a limitation in running speeds for viscous lysates of large volume. The ÄKTA system monitors column pressure and can adjust the speed of application to avoid overpressure conditions that may damage the column bed. As a result, the flow rates experienced with the SP-HP resin were slow which increased the overall amount of time the protein was sitting in the lysate. Increased time of protein in lysate is problematic as it has a higher potential for protein degradation via proteases. To address this issue, two additional types of SP resin beads with different qualities were tested. The different varieties examined include; SP-Fast Flow (SP-FF) resin and SP-Extra Large (SP-XL). SP-FF is distinct from SP-HP as the beads have a larger diameter (90uM compared to 34uM) allowing for faster flow rates. SP-XL is similar to SP-FF in that it too has a bead with a 90uM diameter, but it is distinct from the SP-FF in that it contains extra-long surface extenders on each bead to allow for greater lysate interaction.

The amount of GSK3β produced from purification with SP-FF had a band intensity from ImageJ analysis that was 1.5X greater than the amount of GSK3β obtained from purification with SP-XL (Figure 4-4). The bacterial contaminants (Contaminant60, Contaminant70, and Contaminant25) were not seen in the elution fraction when the SP-FF column was used. In comparison, the contaminants were seen in the early stages of elution (Elution 1 for SP-XL in Figure 4-4). Both columns appeared to be equally efficient at removing large amounts of the contaminating bands, but the SP-FF column was more effective at retaining GSK3β. As a result of this series of experiments further large-scale purifications were conducted using 5 mL SP-FF Sepharose columns in place of the SP-HP columns. When tested in large-scale environments, the usage of SP-FF columns did allow for larger volumes of cell lysate to be processed at a faster rate while retaining a satisfactory proportion of GSK3β.

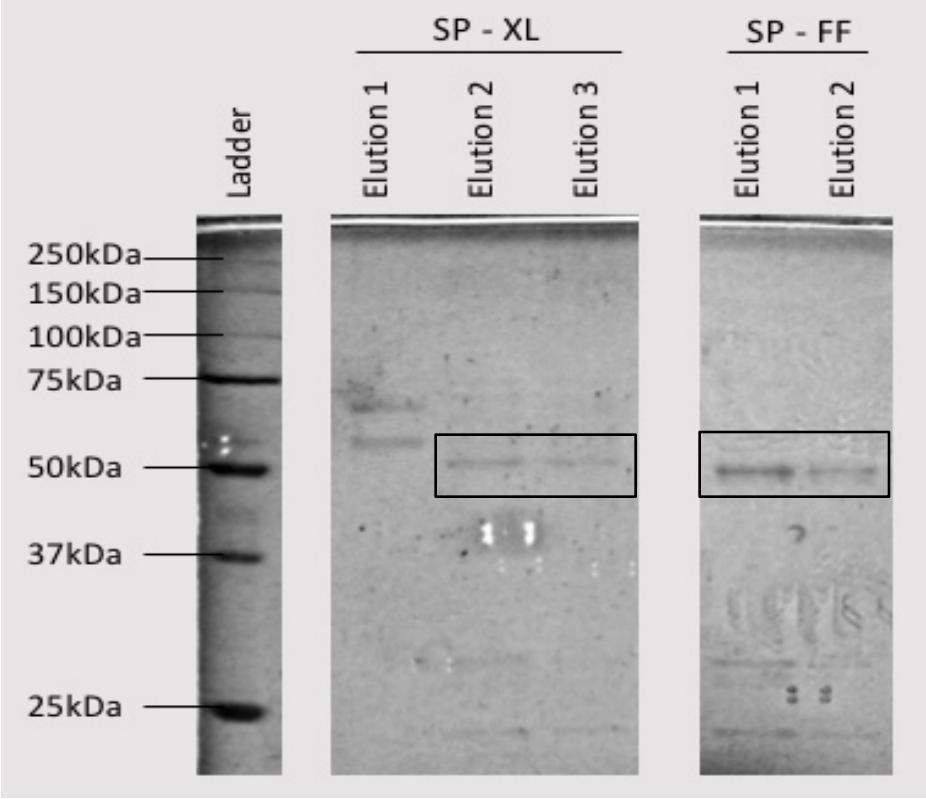

Figure 4- 4: Comparison between two types of cation exchange columsn (XL and FF).

4g of cells grown in 2xYT were resuspended in 16mL of lsL3 and lysed via sonication method. Lysed cells were spun down at 40,000 RPM for 40 mins and purified according to PuriA protocol. The lysate was bound to a 1mL column and washed with 25mL of lsNA1 buffer. The column was eluted using 10mL of lsNB1 buffer. The 12% SDS gel depicts the NiNTA elution fractions from preparation where SP-XL was used as the cation exchange column (left) and where SP-FF was used as the cation exchange column (right). Image J analysis of band intensity for GSK3β was conducted and normalized.

4.1.2.3 Optimization of Affinity Wash Conditions

Manipulation of wash conditions can be useful in altering interactions between protein species. In this way, simply changing the wash conditions has the potential to significantly increase the purity level of elution products (Bornhorst and Falke, 2000). A more effective wash buffer composition may provide the added benefit of no longer requiring the use of a cation exchange column first to disrupt protein-protein interactions. Although the PuriA protocol had been successfully removing some of the bacterial contaminants, its effectiveness was below optimal. It was speculated that using the affinity column, in combination with a selective wash buffer, before the ion exchange column could increase protein yield. The increase in yield would be on account

of greater selectivity of the NiNTA column for protein binding. A series of small-scale experiments using NiNTA resin was performed to compare wash buffers with different components hypothesized to disrupt protein-protein interactions. The goal behind this series of experiments was to obtain a wash buffer that would be able to dislodge the persistent contaminants without disrupting GSK3β binding and thus would remove the necessity of the SP column before the NiNTA column. For this series of experiments, the standard wash buffer (lsNA1) was adjusted or built upon with various components that have properties to disrupt different types of protein-protein interactions. The conditions investigated include; high salt concentration (500 mM), Tween20 (1%), Glycerol (20%), Low Salt (NaCl) (50 mM), Low pH (pH 6.3), No salt (0 mM), Ethanol (EtOH) (20%) and β-mercaptoethanol (βME) (10 mM). High salt has the advantage of reducing non-specific ionic interactions (Dumetz et al., 2007). Tween20 is a surfactant detergent which has the potential to prevent weaker non-specific interactions from occurring. Glycerol stabilizes proteins in solution and also acts to cover hydrophobic patches reducing hydrophobic interactions (Chi et al., 2003; Farnum and Zukoski, 1999). Low salt and no salt buffers will provide a low ionic interaction environment which may help certain hydrophobic species release from their bound contaminants (Dumetz et al., 2007). Ethanol in the wash buffer has also been shown to decrease the amount and strength of non-specific hydrophobic interactions (Bornhorst and Falke, 2000). βME reduces disulfide bonds and can potentially disturb protein complexes bound in this fashion. The low pH buffer was intended to disrupt the overall charge of all the proteins present in an attempt to disturb the protein-protein interactions.

The 20% EtOH, No-salt (0 mM NaCl) and Low-pH (6.31) buffer washes were unable to dislodge Contaminant60 or Contaminant70. The High-Salt (500 mM NaCl) wash had the lowest retention of GSK3β compared to any of the other buffer compositions. Tween (1%), βME (10 mM) and Glycerol (20%) were better able to dislodge Contaminant60 but were unable to dislodge Contaminant70. The Low-salt wash (50 mM NaCl) appeared to remove all of Contaminant60 and

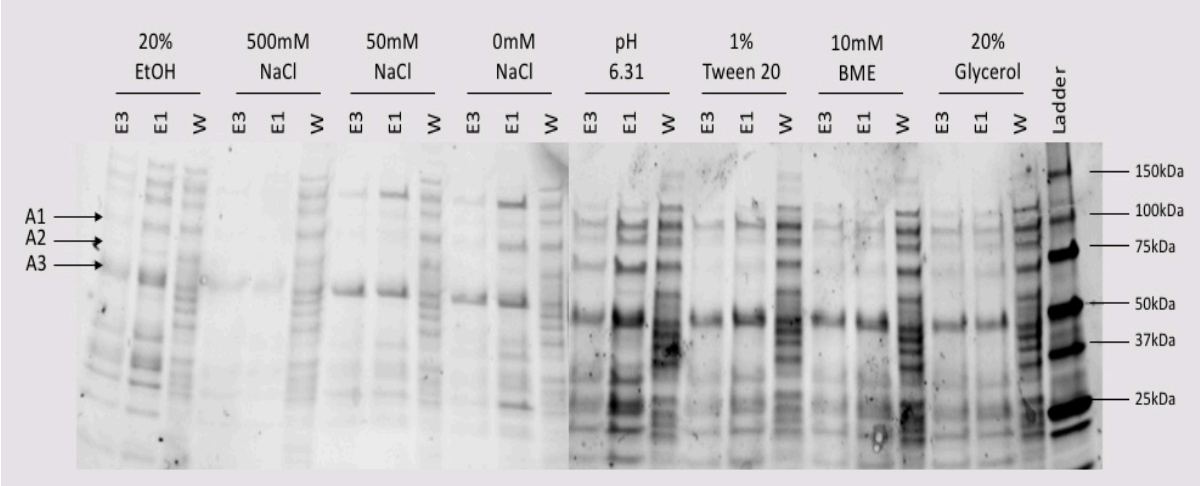

Figure 4- 5: Controlled comparison of the various wash buffers on NiNTA resin.

All pellets were from the same batch of cells. 10 g of cell pellets grown in 2xYT were resuspended in 15 mL of lsL1 buffer. Lysis was conducted via sonication (6 mins at 50% duty and output 5) and bound to 100 µL of NiNTA resin at 4°C for 40min. The resin was then washed with 2.5 mL of each respective buffer. The resin was eluted with 125 µL of ssNB1. Elution fractions (E1 and E3) and wash fraction (W) were run on a 12% SDS gel to identify the effectiveness of each wash buffer. ImageJ analysis of band intensity for GSK3β (A1), Contaminant60 (A2) and Contaminant70 (A3) was compared between conditions.

most of Contaminant70. However, the majority of the experiments were analyzed using a precast stain-free gel from BioRad (Mini-Protean TGX Stain-Free Gels). Even though Figure 4-5 showed a GSK3β band with no visible Contaminat60, subsequent analysis using an SDS gel visualized with Coomassie stain revealed that Contaminant60 was still present after washing with low-salt buffer. The Mini-Protean TGX Stain-Free gels contain a trihalo compound which reacts with tryptophan in the presence of UV light to produce a fluorescent signal. This fluorescence is what is detected and measured to generate the final gel image. This is in contrast to Coomassie staining which utilizes a dye that binds to proteins through ionic interactions between the dye and protein amine groups. It was concluded that the stain-free gels and their subsequent visualization process are not able to detect the contaminating band with the same ability as Coomassie staining. In retrospect, this conclusion may have led to a disproportionate emphasis within the initial observation that a low-salt buffer was able to dislodge Contaminant60 completely. Regardless, the low-salt wash was still noted as the most efficient of the buffer compositions in its ability to dislodge a good majority of the protein contaminants. Future purifications were conducted with an added wash step which contained a low-salt wash buffer (lsSPA2).

4.1.2.4 Column Reversal Protocol

Building upon previous observations geared towards the sequential use of affinity and ion exchange columns, it was proposed that using the NiNTA column before the SP column (PuriB) could be more effective at retrieving higher quantities of GSK3β. The theory follows that by using the NiNTA column first, more His tagged GSK3β could be retrieved and separated away from other proteins present in the lysate. Then this more concentrated fraction from the NiNTA column could be subjected to the same protein-disruption qualities provided by the SP column with less interference from other non-specifically binding proteins. This method should allow for a higher amount of GSK3β to be purified with fewer contaminants. This series of experiments sets out to examine the final elution fractions after a sample has gone through two sequential columns (SP first followed by NiNTA) compared to when the sample has gone through one single column (NiNTA with Low-salt wash).

The results show that using a single NiNTA column complemented with an additional low-salt wash produced a final elution fraction that was cleaner than when the SP column is used first. The NiNTA first fraction (Figure 4-6) clearly shows five distinct protein species; GSK3β (50kDa), Contaminant70, Contaminant60, Contaminant25 and another species located at 10kDa. The SP first fraction (Figure 4-6) clearly shows more than ten distinct protein species including the same main ones seen in the NiNTA first lane plus additional bands located at 125 kDa, 100kDa, 30kDa, and 15kDa. Concerning the effectiveness of the low-salt buffer, comparing the results from Figure 4-6 to the results depicted in Figure 3-1 it can be stated that the use of the low-salt wash significantly reduces the proportion of Contaminant60 and Contaminant70 to GSK3β after NiNTA elution. Considering that the two-column approach using SP first not only requires more steps but also produces a final elution fraction with a higher proportion of unwanted protein species, it was concluded that using NiNTA first with a low-salt wash was the superior method for purification of GSK3β.

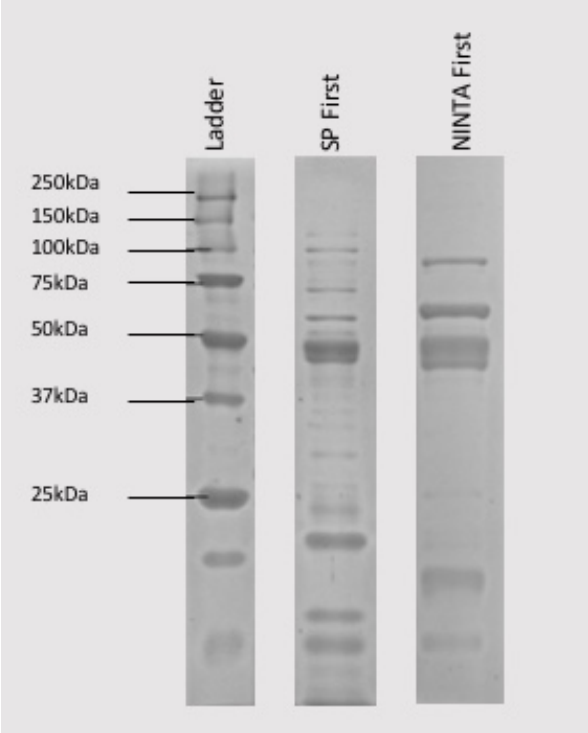

Figure 4- 6: Comparison of final elution fractions between SP column first and NINTA column alone.

12% SDS gels depicting the final elution fraction after a two-column purification (either 1 mL NiNTA column or 5 mL SP-FF column). 10 g cell pellets of cells grown in 2xYT were resuspended in 15mL of lsL3 and lysed with cell disruption (three rounds using 25 PSI). Lysed cells were spun down at 40,000 RPM for 40 mins. The supernatant was then applied to either a NiNTA column or an SP-FF column. While on the SP column the lysate was washed with 30 cv of lsSPA1 buffer and eluted with 10 cv of lsSPB1 buffer. While on the NiNTA column the lysate was washed with 20 cv of lsNA1 buffer, 10 cv lsNA2 buffer and eluted with 10 cv of lsNB1 buffer. Elutions occurred without gradient. The gel on the left shows GSK3β in the NiNTA elution when the lysate was run over an SP column first. The gel on the right shows GSK3β after a single column NiNTA purification utilizing the low-salt wash (lsNA2).

4.1.2.5 SP Column with Low-salt Wash

The elution fractions from the NiNTA column (Figure 4-6) were then subjected to ion-exchange chromatography. The chromatogram results from the SP gradient elution showed overlapping peaks (Figure 4-7) within the elution fractions. It was hypothesized that these overlapping peaks were two distinct species eluting from the column at separate times. Corresponding gel analysis of the contents of the fractions showed the presence of Contaminant10 eluting with GSK3β in the second fraction but not the others (Figure 4-8). It was postulated that a wash buffer containing a lower concentration of salt might be useful in eluting or dislodging Contaminant10 or the entire GSK3β-Contaminant10 complex apart from GSK3β alone. It was in turn, investigated if a Low-salt wash for the ion exchange column could potentially increase the overall product purity level and remove Contaminant10 entirely. The wash buffer (lsSPA1) used

for the ion exchange column contains no salt (0 mM NaCl), elution is accomplished with lsSPB1 which contains a 1 M NaCl concentration. The change in buffer composition from low salt to high salt is how proteins are eluted. Proteins that bind less tightly to the resin (i.e., less positive charge) will elute at a lower concentration of salt and vice versa. The rationale behind using a Low-salt wash for the cation exchange column was an attempt to determine if the Contaminant10 binds less tightly to the resin and if so if it can be eluted separately from GSK3β with a buffer containing 50 mM NaCl.

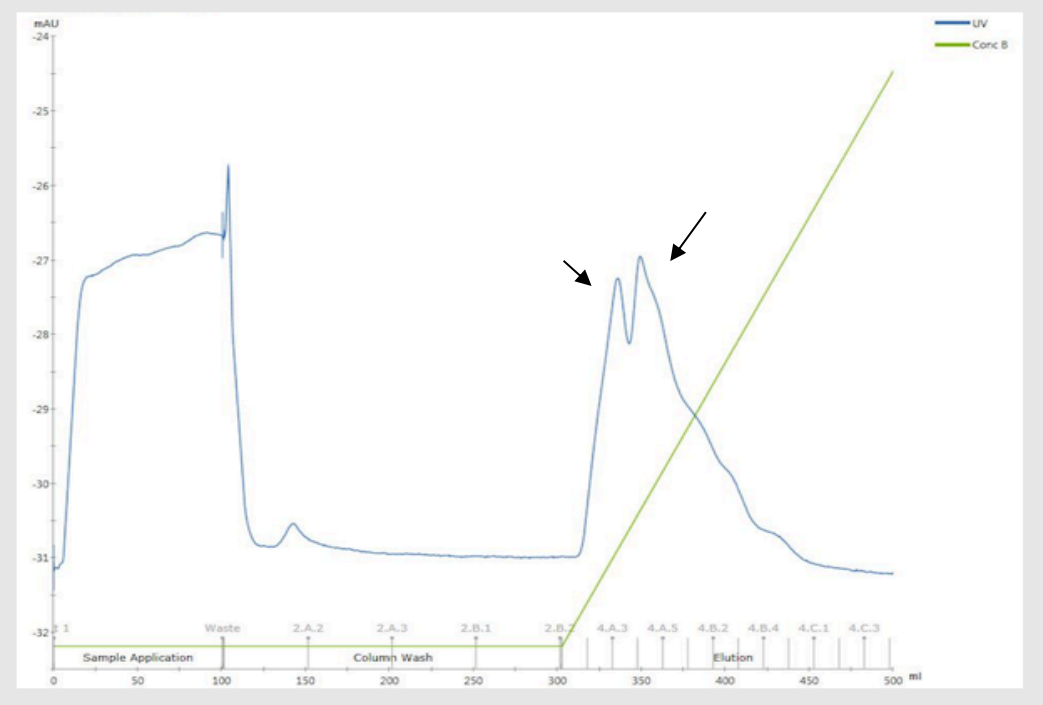

Figure 4- 7: Chromatogram of Flow Through, Wash and Elution phases of an ion exchange column.

Chromatogram shows the purification of 10 g cell pellet grown in 2xYT using Ind1 over 10 mL SP-FF column. The measured response is in mAu. Blue line depicts UV response. Green line is the concentration of elution buffer. Two peaks of interest indicated with arrows.

The use of a buffer containing 50 mM NaCl to wash the cation exchange column proved to be ineffective (Figure 4-8). Contaminant10 remained present in the elution fraction after washing with a Low-salt buffer (indicated with the box in Figure-4-8). In addition to the persistence of this contaminating species, the Low-salt buffer decreased GSK3β's ability to be retained on the column resulting in a lower overall yield of the desired product. The Low-salt wash did not influence the retention of Contaminant60 either. Since 50 mM of NaCl in the wash buffer is

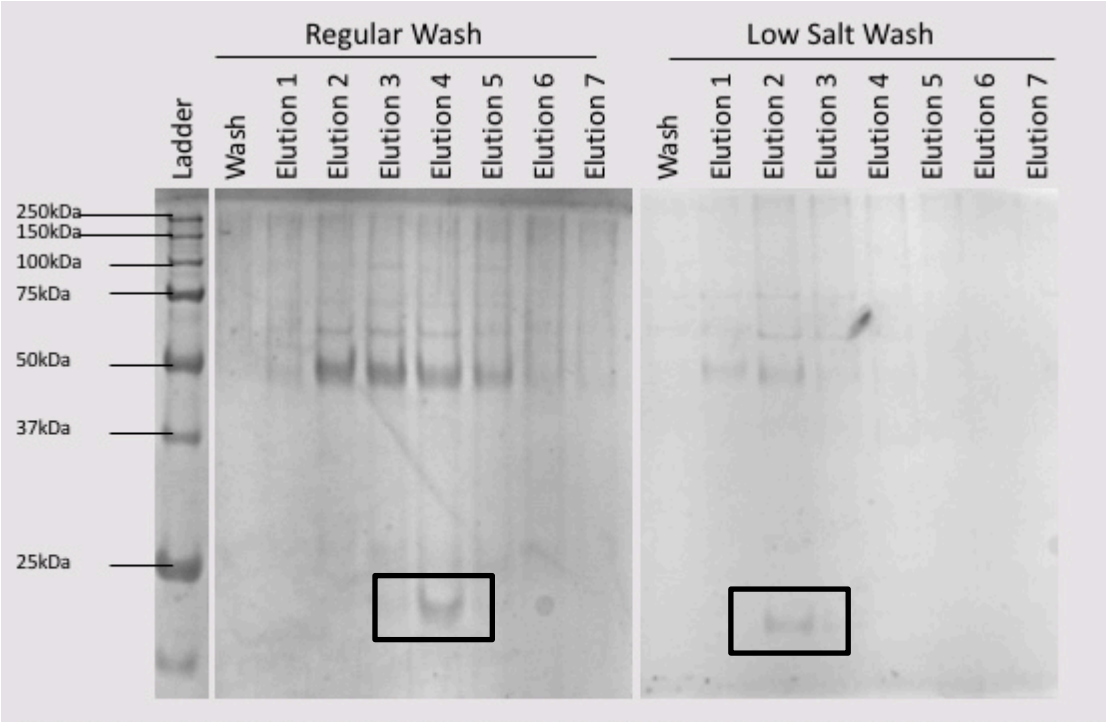

Figure 4- 8: Comparison of the wash and elution fractions between regular wash and a low salt wash.

12% SDS gel depicting the final elution fraction after a two-column purification. 10 g cell pellets of cells grown in 2xYT were resuspended in 15 mL of lsL3 and lysed with cell disruption (3 rounds of 25 PSI). Lysed cells were spun down at 40,000 RPM for 40 mins then purified according to PuriB. The Regular Wash gel depicts a standard elution series when the SP column is washed with a buffer containing no salt (lsSPA1). Low Salt Wash depicts an elution series where the SP column is washed with a buffer containing 50 mM NaCl (lsSPA2).

enough to begin the elution process of GSK3β and fails at removing the lower contaminating bands, further investigation into the potential use of a Low-salt buffer for this column was not pursued. A gradient elution was not attempted since Contaminant25 is consistently seen in the second elution fraction and is interpreted as being more strongly bound than the species in the first elution fraction, therefore, it was predicted that GSK3β might be lost in too great of an amount to justify using a gradient elution.

4.1.2.6 Anion Exchange Column for Binding of Contaminant60

Mass spectrometry was used by another member within the lab to determine that the persistent Contaminant60 is the common bacterial chaperone GroEL. GroEL is a 60 kDa folding chaperone found in many bacterial cell lines that are utilized for protein overexpression. It works in conjuncture with a 10 kDa folding partner termed GroES and requires ATP and Mg^{2+} to ensure the proper folding of native proteins (Hayer-Hartl et al., 2016; Lin and Rye, 2006). The isoelectric

point for GroEL was determined from the literature to be 4.5. The isoelectric point for GSK3β is 8.9. The pH of the buffer used for all column chromatography experiments is 7.2. In these conditions, GSK3β should have an overall net positive charge and GroEL should have an overall net negative charge. Anion exchange resin is coated with positively charged groups which serve to bind negatively charged species in contrast to the reverse scenario for cation exchange resin. Considering the fact that the two proteins have opposite overall charges but still purify together with the cation exchange column, it is reasonable to assume that the two proteins are in complex together despite having very different isoelectric points. Therefore, the rationale behind this series of experiments attempted to use the positively charged anion exchange resin to determine if it was more useful in disrupting the GSK3β-GroEL complex than the cation exchange resin.

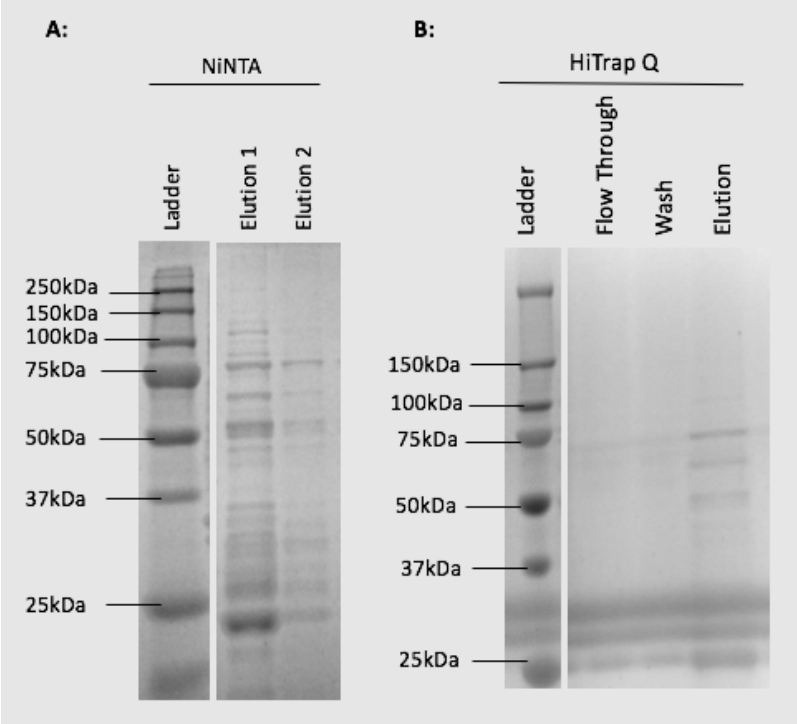

Figure 4- 9: Results of the HiTrapQ column to dislodge contaminants.

20 g cell pellets of cells grown in 2xYT and induced via Ind1 were resuspended in 30 mL of lysis buffer lsL5 and lysed via cell disruption (2 rounds at 25 PSI). Lysed cells were spun down at 40,000 RPM for 40 mins. The lysate was applied to 2 mL NiNTA column. The bound lysate was washed with 40 cv of the lsNA1 buffer, 10 cv of lsNA2 buffer and eluted with 10 cv of lsLB1 buffer without a gradient. First two elution fractions are depicted (A). The elution fractions were pooled then applied to a 1mL HiTrapQ column where they were washed with 40 cv of lsSPA1 buffer and eluted with 10 cv of the lsSPB1 buffer. The Flow-Through, Wash, and Elution fractions from the Hi-TrapQ column are depicted on the right (B).

In this series of experiments the lysate containing GSK3β was first applied to the NiNTA column then pooled and applied to the HiTrapQ column along with the protocol outlined in PuriB. If the anion exchange resin were able to disrupt the GSK3β-GroEL complex, then GSK3β would have been present in the Flow Through or Wash fractions as it would not have bound to the resin on its own in its inherent positively charged state. However, Figure 4-9 B shows GSK3β eluting in the elution fraction along with GroEL (Contaminant60) and Contaminant70 in the same fashion that was seen when the cation exchange column was used. Even though GSK3β did not wash through the column as expected and instead came off during the elution, ImageJ analysis of the band intensity in the HiTrapQ elution indicates that the overall amount of GSK3β is less than the overall amount of GSK3β in the elution fraction after NiNTA. This indicates additional protein loss at some step during this process that is not commonly seen when the cation exchange column is used. This observations adds further evidence against supplementing the HiTrapQ column in place of the SP-FF column. There was a possibility that some GSK3β was dislodged from the complex as intended and remained in the wash fraction at a concentration too dilute to detect on a gel which might have served to explain the lower GSK3β yield in the elution fraction. Additional experiments conducted further processing and examination of the wash and flow through fractions were able to confirm that there was no GSK3β present in either fraction (results not shown). This series of experiments determined that the use of an anion exchange column in place of a cation exchange column is ineffective at separating GSK3β from GroEL in any greater capacity than the SP cation exchange column.

4.1.3 Gel Filtration Optimization

4.1.3.1 Gel Filtration without Prior TEV Cleavage

Objective 3 required His-GSK3β for compatible use with a Ni^{+} coated SPR chip to accomplish the binding studies. His-GSK3β obtained from the NiNTA column after purification via PuriB was of adequate concentration but of low purity. It was hypothesized that applying the NiNTA elution fraction to a size exclusion column (Gel Filtration) might serve to increase the purity level of GSK3β. Considering that the size exclusion column separates protein species based on the size of their complexes in solution, then any proteins in the solution that was in an active complex would elute together as one distinctive peak. However, since the SDS gel is denaturing,

the sampled peak would present as multiple bands representing the number of proteins in a complex. In this manner, any species of GSK3β in the solution that elute at 15 mL, the corresponding volume of proteins 50 kDa in size for the Superdex 200 10/300 GL, should be relatively pure and any GSK3β species eluting elsewhere in the volume could be assumed to be in complex with other proteins in solution.

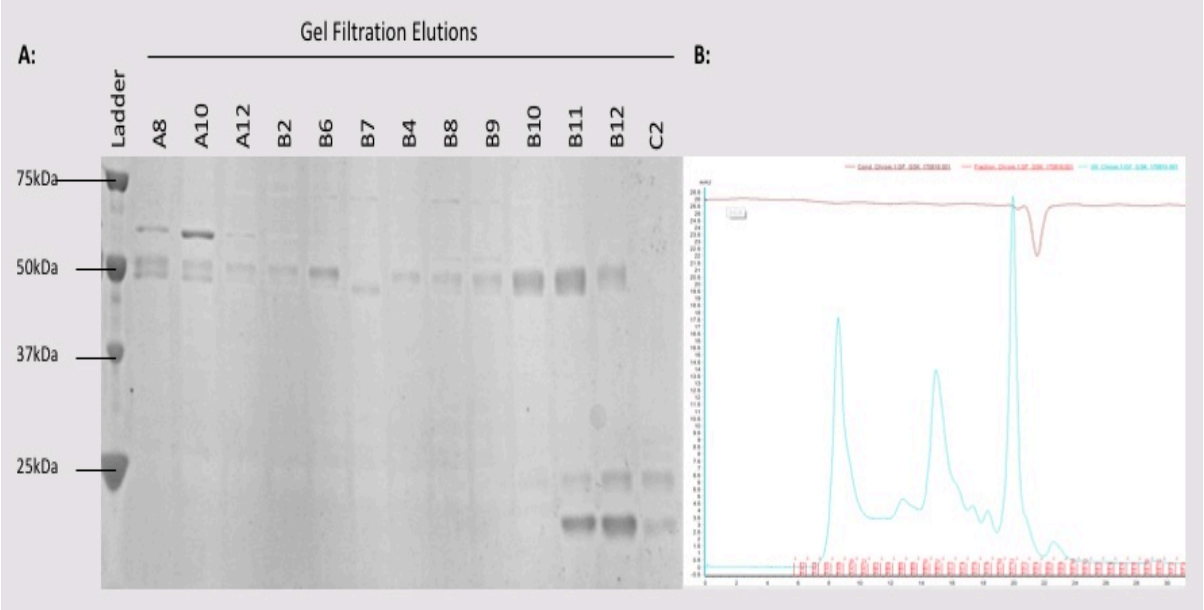

Figure 4- 10: Gel filtration elution's and chromatogram showing separation of GSK3β species.

10 g cell pellet of cells grown in 2xYT were resuspended in 15 mL of lsL3. Cells were lysed via cell disruption (25 PSIx2) and spun down at 40,000 RPM for 60 mins. The lysate was applied to a 1 mL NiNTA column (washed with 20cv of lsNA1 buffer followed by 10 cv of lsNA2 buffer and eluted with 10 cv of lsNB1 buffer. The elution fractions were then applied to a 5 mL SP-FF column (washed with 30cv of lsSPA1 buffer and eluted with 10cv of lsSPB1 buffer) as outlined in PuriB. SP elutions were pooled and concentrated down to 1.1mg/mL. 450 µL of the concentrated protein was injected onto the Superdex300 Gel Filtration column and eluted with lsGF1 over 1.5 cv at 0.5 mL/min. The resulting 12% SDS gel (A) shows the array of protein species correlated to where they eluted on the gel filtration chromatogram (B).

Results from this series of experiments were able to show that GSK3β could be separated into groups relating to what other protein species were complex with it (Figure 4-10). The earlier fractions (A8-A12) show GSK3β is eluting with Contaminant60 in the void volume segment. For this specific column, the void volume is contained within the peak from 6-13 mL on the chromatogram which correlates to all fractions up to and including B6. The presence of these proteins within the void volume suggests that they are in an aggregated form as they passed through the column quicker than expected signifying their complexed size is larger than the SDS gel

indicates in their individual sizes to be. The middle fractions (B7-B9) contained GSK3β and a small amount of Contaminant70. The later fractions (B10-B12) contained the majority of GSK3β with Contaminant25 and Contaminant10. The very last fraction depicted on the gel (C2), shows the two lower contaminants eluting on their own. Fractions B10-B12 correlate with the volume on the chromatogram where monomeric GSK3β is anticipated to elute based on its size. Future attempts to replicate these results showed the same trend with GSK3β + Contaminant60 eluting first and GSK3β + Contaminant25 and Contaminant10 eluting last with each fraction in the middle containing a small amount of Contaminant70 and none of the fractions with GSK3β on its own (results not shown). Conclusions from these experiments determined that low levels His-GSK3β with a purity above 80% can be obtained using this method. Despite the small amount of protein obtained, the product is still usable for downstream SPR and enzyme activity studies.

4.1.3.2 Replace HEPES Buffer with MES Based Buffer

The paper by Aoki *et al*. 2000, that this protocol was initially adapted from utilizes an MES buffer (pH 6.5) containing a lower salt concentration (175 mM) for the gel filtration stage. It was theorized that the conditions created by this buffer could be useful in encouraging Contaminant25 and Contaminant10 to separate from GSK3β. The conditions of the buffer might also have the ability to disrupt the interactions between GSK3β and Contaminant60/Contaminant70. The MES buffer runs at a pH of 6.5 compared with the HEPES buffer which runs at a pH of 7.4. In the case of GSK3β with a pI of 8.1, the lower pH of the MES buffer will increase the overall surface charge of the protein which could potentially disrupt some protein-protein interactions. The rationale for the lower salt concentration most likely is related to the author's optimal conditions determined for their construct. Most notably the desire to attempt purification using this buffer was to replicate the success of the authors who published the protocol.

The results from this experiment can be directly compared to the results depicted in Figure 4-10 as the initial preparation of the cells/lysate through the first two columns was shared. The final elution product after NiNTA was concentrated down to 1 mL at 1.1 mg/mL. 450 µL of this product was applied to the gel filtration column run with lsGF1 (Figure 4-10) while the remaining 450 µL of this same product was applied to the gel filtration column and run with lsGF2 (Figure 4-11). The results from this experiment illustrate that our construct of GSK3β appears to be

unstable in the MES buffer with 175 mM of NaCl (lsGF2) as the resulting gel shows no visible GSK3β bands (Figure 4-11). Contaminant60 can still be identified eluting in the void volume (Fraction A12) along with Contaminant10 which can still be detected eluting in the later fractions (Fraction B12). The chromatogram of the purification conducted with the MES buffer (Figure 4-11 / B) showed peaks that were smaller in height and area when compared to the sample counterpart conducted using HEPES buffer (Figure 4-10 / B). It can also be noted that the peak array for the MES buffer chromatogram consists of 5 distinct peaks, but only the first two within the predicted GSK3β elution range is depicted on the SDS gel. Extensive cleaning of the column with NaOH directly after this experiment showed large peaks eluting suggesting the possibility that aggregated protein had become stuck on the column during the purification process. Conclusions from this series of experiments imply that the use of MES buffer with a low salt concentration may contribute to the aggregation of this particular construct of GSK3β.

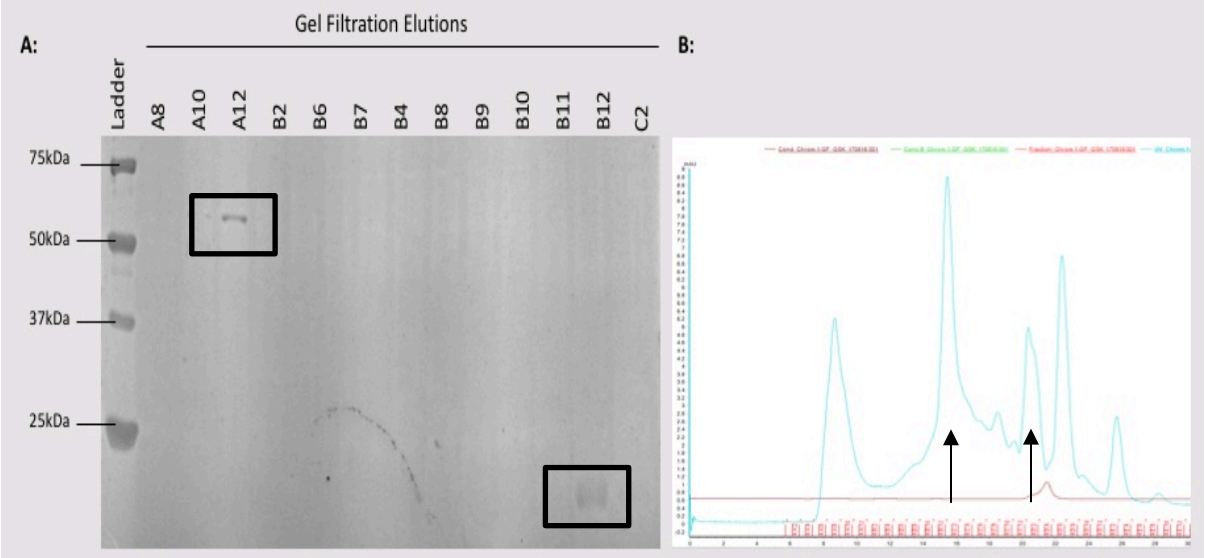

Figure 4- 11: Gel filtration elution's and chromatogram results with MES based buffer in place of a HEPES buffer.

10 g cell pellet of cells grown in 2xYT were resuspended in 15 mL of lsL3. Cells were lysed via cell disruption (25 PSIx2) and spun down at 40,000 RPM for 60 mins. The lysate was applied to a 1 mL NiNTA column (washed with 20 cv of lsNA1 buffer followed by 10 cv of lsNA2 buffer and eluted with 10 cv of lsNB1 buffer. The elution fractions were then applied to a 5 mL SP-FF column (washed with 30 cv of lsSPA1 buffer and eluted with 10 cv of lsSPB1 buffer) as outlined in PuriB. SP elutions were pooled and concentrated down to 1.1 mg/mL. 450 µL of the concentrated protein was injected onto the Superdex300 Gel Filtration column and eluted with lsGF2 over 1.5 column volumes at 0.5 mL/min. The resulting 12% SDS gel (A) shows the array of protein species correlated to where they eluted on the gel filtration chromatogram (B).

4.1.3.3 Addition of EDTA to Gel Filtration Buffer

In order to address the GSK3β/Contaminant60 and GSK3β/Contaminant25/Contaminant10 bands observed in the early and late fractions of gel filtration (Figure 4-10), it was theorized that the addition of EDTA to the gel filtration buffer could potentially decrease GSK3β aggregation (A.Levi et al., 1974). NiNTA columns can leech Ni^{+} ions into solution causing the Histidine tags present on the recombinant proteins to cluster around these leeched ions leading to increased aggregation. EDTA is useful to combat this phenomenon since it is a chemical capable of chelating metal ions including Ni^{+}. The addition of EDTA could potentially reduce the effect of the Ni^{+} ions which may lead to a decreased amount of protein aggregation. This series of experiments attempted to determine if the addition of EDTA to the gel filtration buffer could produce a fraction of GSK3β free from other protein contaminants.

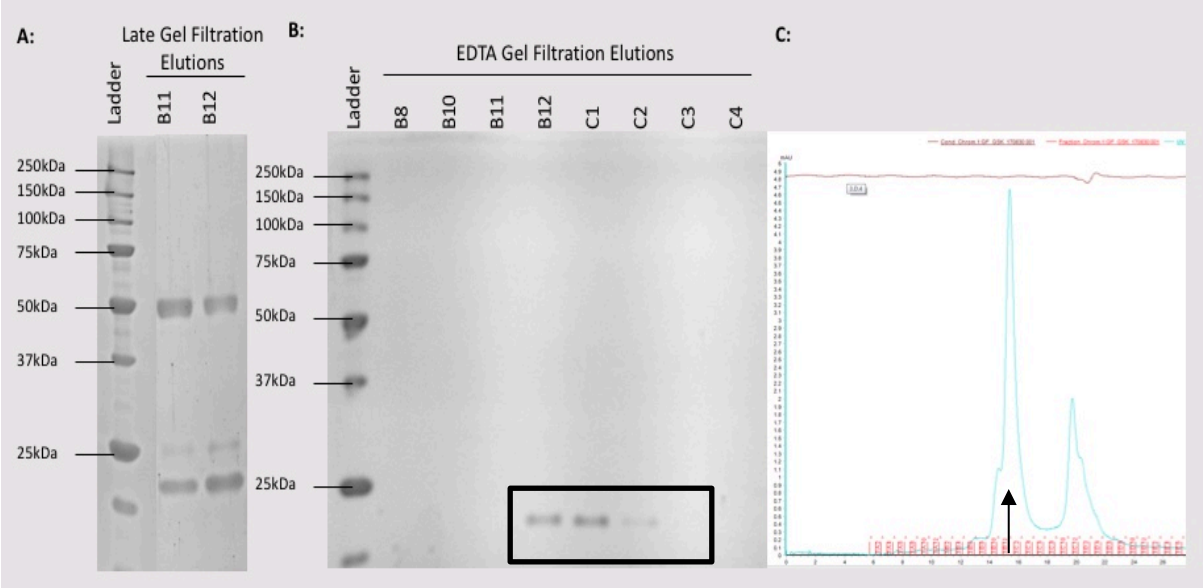

Figure 4- 12: Gel filtration elution's and chromatogram results with EDTA added to the running buffer.

10 g cell pellet of cells grown in 2xYT were resuspended in 15 mL of lsL3. Cells were lysed via cell disruption and spun down at 40,000 RPM for 60 mins. The lysate was applied to a 1 mL NiNTA column (washed with 20 cv of lsNA1 buffer followed by 10 cv of lsNA2 buffer and eluted with 10 cv of lsNB1 buffer. The elution fractions were then applied to a 5 mL SP-FF column (washed with 25 cv of lsSPA1 buffer and eluted with 15 cv of the lsSPB1 buffer. SP elutions were pooled and concentrated down to 0.96 mg/mL. 450 µL of the concentrated protein was injected onto the Superdex 200 10/300 GL gel filtration column and run with lsGF1. The later elution fractions from this gel filtration containing GSK3β and Contaminant25/Contaminant10 (A) were pooled and run over a gel filtration column using lsGF3 (B). The chromatogram for the gel filtration using lsGF3 shows two distinct peaks (C).

The results from this series of experiments aimed to show the potential of EDTA to separate Contaminant25 and Contaminant10 that elute with GSK3β in the later fractions of gel filtration

(Figure 4-12 / A). The resulting chromatogram (Figure 4-12 / C) displayed two distinct peaks at 14.5 mL and 20 mL respectively. The peak at 14.5 mL would usually indicate monomeric GSK3β in solution; however, the corresponding SDS gel (Figure 4-12 / B) showed little to no GSK3β protein in any of the fractions. The only protein easily visible on the gel is Contaminant10 which, despite its small size, elutes at 14.5 mL. Since no actual GSK3β bands can be seen on the gel from this experiment, it can be inferred that the addition of EDTA to the gel filtration buffer may not be helpful in separating the lower band contaminants from GSK3β and that the addition of EDTA may be detrimental to protein yield. It is possible that this construct of GSK3β does not respond well to buffer changes which do not occur gradually and in response to this the protein is aggregating and remaining stuck to the column. However, further investigation into this theory using a more concentrated protein sample would be valuable in order to draw any firm conclusions.

4.2 Discussion

4.2.1 Cell Lysis Protocols

The results described above demonstrate that the overuse of sonication is detrimental to the process of collecting large amounts of protein in its folded form. It is highly probable that this is due to over sonication causing aggregation of the protein products (Stathopulos et al., 2008). Sonication uses sound waves, and a side effect of this increased friction is the production of heat. Certain protein species, including GSK3β, are sensitive to increased temperatures and tend to denature or aggregate as a result. Even though the sonication process is done with the cells physically resting on ice, it still has the potential to create heat within the system since the cells closest to the probe will be more directly affected than the cells lining the outside of the tube which is closest to the ice. The process of sonication creates a force which pushes the solution down and out. This creates a system that primarily serves to mix itself which should act to keep the cells from overheating but is not always efficient. It is possible that there was not a long enough break in between bursts of sound waves. A more extended rest would have given the energy particles created more time to disperse before incurring additional rounds of sonication. It is also possible that the force of sonication can sometimes shear proteins or cause them to break apart. A clear

indication for aggregation is the loss of protein product identified by a decrease in band intensity via SDS analysis and Coomassie staining. A sign of protein sheering or degradation is a rise in the number of protein species present in solution. Both of these conditions can be observed in Figure 4-2 / A and were described above.

Cell disruption is a process which utilizes high pressure to break cells open. Cell disruption works by first compressing cells through a small orifice at high velocity, followed by their rapid expansion which disrupts the bacterial cell membrane (Burden, 2008). The process can be more effective at keeping proteins folded and in a soluble state compared to sonication. In addition to being a gentler process, it is also thought to be more desirable as the entire process occurs in a temperature-controlled unit which resists overheating more effectively than placing cells on ice. The pressure (PSI) used to act on the cells can be adjusted to suit different bacteria and can even be used to selectively disrupt for DNA, cytoplasmic protein, inclusion bodies, and membrane proteins. Like with the process of sonication, overuse of cell disruption can also result in the breakdown of protein products. Within the confines of the work conducted in this thesis, it was determined that two or three rounds at 25 PSI was suitable for high levels of protein retrieval and that this level of cell disruption was more beneficial than sonication alone.

There are additional methods for cell lysis that have yet to be attempted for GSK3β grown in *E. coli* at a large scale. These methods include thermal lysis, manual grinding, lysozyme, use of a bead mill, and chemical cell disruption (Burden, 2008). Thermal lysis is a method where cells are frozen and thawed repeatedly, this process induces the formation of ice crystals which disrupt the cell membrane and in doing so, breaks cells open. Freeze-thaw can potentially be less abrasive on cell components, but it requires more time and can lead to possible protein degradation from the continual heating and cooling process (Johnson and Hecht Michael, 1994). Manual grinding is the use of mortar and pestle to physically grind the cells into dust disrupting the cell membrane in a physical way (Johnson and Hecht Michael, 1994). Manual grinding can be useful in that it is inexpensive and straightforward, but it is more difficult to control or regulate and carries a higher risk for cross-contamination. Lysozyme is an enzyme which reacts with peptidoglycan and breaks the glyosidic bonds of polysaccharides (Valerie A. Proctor et al., 1988). It is advantageous in that it is specific for bacterial cell lysis but can be problematic with sensitive proteins as its use requires cells to be in a solution of pH 6-7 at 35 degrees C for a prolonged period. This temperature and

pH could be problematic for GSK3β. Bead mill is a process whereby cells in solution are agitated by small beads of glass, ceramic or steel which are mixed with the cells at high speeds (Burden, 2008; Shrestha et al., 2012). This process is efficient in its guaranteed ability to lyse all cells in suspension, however because it disintegrates cell membranes downstream purification can become more difficult. Finally, chemical lysis is the use of alkaline solutions or detergents to lyse cell membranes (Burden, 2008). Although these solutions can be gentler on the cell membranes themselves, it becomes more challenging to maintain proteins in their native form in the presence of harsh detergents. An appropriate lysis method is essential to determine when working with a protein such as GSK3β which does not have a significant initial overexpression rate and tends to aggregate in non-optimal conditions. It is possible that cell disruption is the best method but further investigation into alternative methods might prove to be beneficial.

4.2.2 Column Purification Protocols

4.2.2.1 Cation Exchange Resin and Flow Rate Optimization

Optimization of the resin beads was initially investigated as a potential solution for increasing the overall rate at which lysate could be processed. Faster processing allowed for the upscaling of purifications while simultaneously decreasing the potential degradation from prolonged exposure to enzymes in the lysate. It was determined that SP-FF resin was the best suited since it could run the lysate faster than SP-HP on account of the larger bead size. Larger bead sizes cause greater gaps between beads which in turn results in less resistance to higher flow rates. Even though the SP-XL column also consisted of the same sized beads as SP-FF, it was not as favorable as it appeared to retrieve less GSK3β. Nevertheless, it was interesting that the SP-XL column showed an elution fraction which seemed to contain only Contaminant60 and Contaminant70 (Figure 4-4, SP-XL, Elution 1). The SP-XL resin contains the same size beads as SP-FF resin, but it also has long extender regions. These extender regions are long chains of dextran coupled to the 6% highly cross-linked agarose matrix. Their intended purpose is to increase the surface area of the SP charged groups to the lysate which in turn would increase the loading capacity. Knowing this information, it is possible that the extender regions might play a role in physically dislodging Contaminant60 and Contaminant70 from GSK3β. Even more interesting is that the contaminants are prone to eluting first a whole fraction before GSK3β elutes. Perhaps the

contaminants are resting on the extender regions and are less tightly associated might explain why they are first to come off. Despite this useful characteristic, the resin was unable to retain high levels of GSK3β and as such was not pursued. However, it is possible that the two columns could somehow be used in tandem to utilize the retention capability of SP-FF with the contaminant dislodging capability of SP-XL. Continued investigations into that line of thinking might be useful in the future.

4.2.2.2 Affinity Wash Buffer with Column Order Reversal

To further examine the desire to rid the protein preparation of Contaminant60 and Contaminant70, affinity column wash buffers with varying properties were explored. Proteins in solution may interact with each other on account of electrostatic and van der Waals forces, hydration effects, disulfide bonds, salt bridging and ion binding (Dumetz et al., 2007). The main components in each of the wash buffers tested include; high salt concentration (500 mM), Tween20 (1%), Glycerol (20%), Low Salt (50 mM), Low pH (pH 6.3), No salt (0 mM), Ethanol (20%) and BME (10 mM). The purpose of testing different wash buffer components were described in detail within the results section.

Of all the different wash varieties tested the low salt wash appeared to be the most useful. Even though the low salt wash was unable to dislodge 100% of the protein contaminants, it was still successful in its ability to dislodge a majority of the contaminants. The results from this strongly suggest that the majority of the contaminants seen after NiNTA purification are associated with GSK3β in some way. The logical assumption is that these contaminants are either in a complex or aggregated. It remains difficult to distinguish if all the contaminants are bound in this manner or if only a subset are. It is likely that while some of the proteins can be washed off with the low salt wash, the others may remain bound to GSK3β by alternative means and thus be unaffected by the low salt wash. The investigation of other component washes to be used in combination with a low salt wash might increase the amount of Contaminant60 and Contaminant70 being dislodged from GSK3β or the column. The initial intention to investigate wash buffers for the NiNTA affinity column originally stemmed from the desire to remove the need for the lysate to pass over the ion exchange column before being introduced to the affinity column. The results here suggest that the use of an ion exchange step might still be the best way

to begin the process of purification as it seems to have the ability to dislodge the protein-protein interactions at a greater rate than relying on an affinity wash buffer alone. However, the low salt wash should be adapted into the NiNTA column purification step to increase the purity of the overall protein yield.

To further address the usefulness of the low salt wash for the NiNTA purification and the apparent requirement of an ion exchange step, a series of experiments was designed based upon the reversal of the previously established column order. This meant running the NiNTA column before the SP column with the overall goal being to purify GSK3β that still retains its His tag. The purity of the product after this step is much higher than when the columns are run in the opposite order. This is likely because more GSK3β is retained when the affinity column is used first since the attraction between the His tag and the NiNTA resin is more specific than the attraction between opposite charges in the cation exchange column. It is also possible that when the SP column was run first, it was becoming overloaded by the wide variety of protein species in the lysate and thus either failing to separate GSK3β effectively from its contaminants or merely failing to bind GSK3β all together. Overall it can be stated that the use of NiNTA before SP is more beneficial for retrieving higher yields of His tagged protein. However, this column reversal is not as useful for when the desired product is to be without its His tag. This is due to the incompatibility of the buffer components with downstream steps. For example, the next step after the first two columns is to incubate the eluted products with TEV protease. This is problematic when the SP column is second because TEV protease has low activity and tends to aggregate in the presence of high salt and the SP elutions are in a buffer containing 1 M NaCl. Attempts to cleave the tag with the protein in this buffer resulted in protein or enzyme precipitation. To fix the incompatibility issue would require diluting out the salt which runs the risk of GSK3β loss from being over-diluted. Alternatively, the protein preparation could undergo dialysis to reduce the salt. Lastly, the preparation could start with a greater amount of cell pellet to accommodate for the additional protein loss.

4.2.2.3 SP Column with Low Salt Wash

A low salt wash for the cation exchange column was investigated after a notable indication of overlapping peaks was observed in the chromatogram (Figure 4-7). It was hypothesized that a low salt wash at this step could dislodge the Contaminant10 seen eluting with GSK3β if the two

proteins were associated via electrostatic interactions. However, the use of a low salt wash for the cation exchange column proved to be ineffective. Ion exchange elution works with less specificity than affinity elution as it relies on the varying strength of different ionic interactions. Increasing the salt concentration in the wash buffer will provide additional ions to compete with binding to the column displacing the protein interactions already associated with the column. Since ions in solution non-specifically associate with ions on the column, it becomes increasingly difficult to use varying concentrations of salt to elute protein species selectively. This series of experiments serves to support this theory by showing that even a small amount of salt in the buffer is enough to dislodge GSK3β from the column in the wash fraction. Concerning the elution of Contaminant10 along with GSK3β in a distinct fraction strongly suggests that a small subset of GSK3β in solution is bound by Contaminant10 and this binding alters the surface charge of the complex thereby causing it to elute in a separate fraction. Further attempts to optimize the wash buffer for the SP cation exchange column would not be advised in order to minimize unnecessary GSK3β loss.

4.2.2.4 Anion Exchange Column for Binding of 60kD contaminant

Anion exchange differs from cation exchange in that it contains positively charged resin beads instead of negatively charged resin beads. The experiment attempted to use a column of opposite charge to separate GSK3β from its contaminants based on their difference in surface charge. However, the use of the anion exchange column was overall ineffective at separating Contaminant60, suspected to be GroEL, from GSK3β. The ineffectiveness of this column was likely because the initial theory was developed based on the assumption that GSK3β and Contaminant60 were only co-purifying together and not complexed together. The results showed that GSK3β still eluted in the elution fraction despite its assumed positive surface charge. The results show that GSK3β and Contaminant60 will bind equally well to a negatively charged resin (cation exchange column) or a positively charged resin (anion exchange column) despite GSK3β having a surface charge opposite that of Contaminant60 (GroEL) in a buffer of pH 7.4. From these results, it could be suggested that GSK3β might possibly be in a complex with Contaminant60, and that the complex has an overall surface charge that binds equally well to anion resin as cation resin. GroEL works by forming a barrel-like structure that surrounds its target protein and uses the

hydrolysis of ATP to complete the reaction that releases the target from the barrel in its fully folded state (Lin and Rye, 2006). If the two are purifying as one complex then that fraction of retrieved GSK3β is not likely to be functional in an unobstructed and active state. In order to increase GSK3β purity and activity, it would be beneficial to design a protocol that would specifically dislodge the GroEL from GSK3β. Some suggestions for future researchers to attempt include the use of a wash buffer containing ATP and Mg^{2+}. Both ATP and Mg^{2+} are necessary for the completion of the GroEL folding and release reaction (Hayer-Hartl et al., 2016; Lin and Rye, 2006). The addition of these components to subsequent wash buffers could potentially encourage the GroEL attached to GSK3β to complete its reaction, release the protein and ultimately yield a higher portion of folded active GSK3β for downstream use.

4.2.2.5 Gel Filtration Optimization without Prior TEV Cleavage

The remainder of the purification work focused primarily on optimizing the process of gel filtration so that it could be used to produce fractions of His-GSK3β with greater than 80% purity for downstream use in enzyme kinetic and activity assays. The positive aspect of the protocol is that small amounts of relatively pure His tagged protein can be obtained. This is beneficial for enzymatic studies which only require nanomolar amounts of protein for completing the analysis and where the presence of the His tag is useful instead of a hindrance. In contrast, the negative aspect of this protocol is that it fails to retrieve large amounts of protein at a concentration high enough to attempt structural analysis. However, it remains possible that the protocol could be further optimized to bring it to a point where enough protein could be purified for structural studies. Concerning structural studies, the presence of this His tag might be a hindrance as it is currently unknown if the tag could potentially interfere with crystal formation. Despite its inadequacy for use in purifying the protein for structural analysis, the gel filtration after two-column protocol has the potential to be optimized further to increase the amount of retrievable His-GSK3β.

The published paper, from which this protocol was initially adopted, utilized an MES buffer with a lower pH in place of HEPES (Aoki et al., 2000). However, attempts to replicate the experiment using the buffer proved detrimental to protein retrieval as demonstrated in Figure 4-11. It can be hypothesized that the protein, in the presence of the MES buffer, was lost due to the low concentration of salt. The specific GSK3β construct utilized in this thesis prefers to be in a

solution containing 300 mM – 500 mM NaCl and it is possible that the low concentration of salt caused some degree of aggregation. Future attempts at optimization could include the use of the MES buffer with a salt concentration between 300-500 mM. Another possibility is that the construct did not favor the slightly acidic environment with the pH being below 7.0. Some recombinant proteins are intolerant of acidic environments and are prone to denaturation. Additionally, the protonation state of the Histidine tag is altered at or below a pH level of 6.5. The change in protonation could potentially cause aggregation of the Histidine tagged product. The most likely explanation for the resulting protein loss is that the combination of the two conditions (low pH and low salt) caused the protein to aggregate during this experimental. After the preparation was completed an extensive clean on the gel filtration column was conducted, and large peaks were observed eluting from the column during reverse flow cleaning. This observation confirms that the protein was more than likely aggerated and becoming stuck on the column at or above the filter. This scenario explains why no protein was observed in the actual elution, but a clear peak was observed when the column was run using reverse flow. A more comprehensive pH optimization series of experiments would be beneficial in the future to address if the issue indeed is related to the change in pH or the low salt concentration. For this thesis, no subsequent work utilized MES buffer or low salt running buffers.

Regarding the potential use of EDTA in the gel filtration buffer to act as a chelator of any leeched Ni^{+} ions, the results were mostly negative. The lack of GSK3β bands on the SDS gel strongly suggests that the protein became aggregated, and similar to the MES buffer results, remained stuck at or above the filter of the gel filtration column. Since EDTA works to chelate metal ions, one assumption is that the Histidine tags present on the proteins were even more strongly drawn together due to the concentrated collection of Ni^{+} ions and formed aggregated clumps as a result. The only prominent bands that had an intensity bright enough to be visible on the SDS gel was Contaminant10 which eluted at the 15 mL mark. This observation is similar to the results seen in other experiments where the contaminants are eluting in the same region without the visible presence of GSK3β. It does not follow that the smaller proteins would elute at the same volume as a protein five times its size unless it is an entirely different protein species that forms an oligomer in solution. It could also be possible that this is a truncation product of GSK3β forming an aggregate or oligomer. This would explain why it is eluting off the gel filtration column as if

its size was 50 kDa but running on an SDS gel as if its size was 10 kDa. The main argument against this suggestion is that the presence of TCEP in the buffer should cause any dimers/oligomers to take their monomeric form if they were held together by disulfide bonds. However, it is possible that the oligomers are forming due to other forces or favorable interactions. Investigations into the identity of Contaminant10 are essential for the purification process as the band appears to associate tightly with GSK3β through the many column steps and even elutes at the same volume during gel filtration. Alternate studies, including Mass Spectrometry, could focus on detecting the identity of this band so that more effective and targeted attempts to remove it could be explored.

Any further work put forth to optimize gel filtration after a two-column purification without TEV cleavage of the His tag should include experimenting with reducing the speed of the gel filtration column. It is possible that by reducing the speed and allowing more time for the separation of protein species, the yield of pure protein could increase slightly higher. However, considering the three main peaks that consistently elute from the gel filtration column, it does not seem apparent that this protocol would ever serve to separate all of the GSK3β in solution from all other protein species.

4.3 Summary

The purification of this construct is currently at a stage where it is useful at producing His tagged GSK3β at levels adequate for enzymatic characterization analysis such as ADP-GLO and SPR. However, the purification protocol has a few significant hurdles concerning its ability to produce cleaved GSK3β at levels useful for crystallization and other characterization studies requiring concentrated and highly pure protein. The overall purification protocol was able to utilize 10 g of cell pellets lysed using a cell disruptor (two rounds at 25 PSI) bound first to a NiNTA column and washed with a buffer containing 50 mM NaCl before being applied to an ion exchange column. The elutions from the ion exchange column were concentrated down an applied to a gel filtration column where approximately 0.2 mg of protein at a purity level of 80% could be obtained. One of the most prominent issues experienced throughout purification is the presence of the Contaminant60, Contaminant70, Contaminant25, and Contaminant10. These contaminants appear to be in complexes with GSK3β. The gel filtration elution fractions show that not all of the GSK3β in solution are complexed with the same combination of contaminants and thus elute at different places accordingly. This could potentially suggest that these contaminants are becoming associated

with GSK3β at different stages of the overexpression or purification process. For example, it is possible that the GSK3β complexed with Contaminant60 seen eluting mostly in the void volume could be aggregated protein which formed as a result of overexpression and was purified in that form. It is conceivable that the GSK3β seen eluting with Contaminant25 and Contaminant10 later on in the elution phase is GSK3β which has become associated with these contaminants during the process of purification or even during the concentration stages where the protein is prepared for the gel filtration column. At this point, it is difficult to distinguish what complexed species emerged as a result of which stage. This ambiguity ultimately increases the difficulty in correcting the issue or removing the contaminants. Some suggestions were described above, and it can be stated that the purification protocol, albeit operational, requires more work in order to be of a desirable efficiency.

5.0 Objective 3: Investigation of the Inhibition Mechanism of DISC1-44mer Against GSK3β using Biochemical and Biophysical Approaches

This chapter focuses on detailing the enzymatic relationships between GSK3β, a short fragment of DISC1 (DISC1-44mer) and a short fragment of FRAT (FRATtide). Both protein fragments are known to bind and inhibit GSK3β. It is known that FRAT binds to GSK3β at a site that overlaps with Axin binding and has been theorized to inhibit GSK3β activity towards select substrates (β-catenin) by obstructing Axins access to GSK3β (Bax et al., 2001; Fraser et al., 2002; Li, 1999). FRATs inhibition does not interfere with GSK3βs activity towards other substrates such as GSP2 (Culbert et al., 2001). The method of inhibition and the binding site for DISC1-44mer is still largely unknown. This chapter attempts to address the hypothesis and use surface plasmon resonance (SPR) studies in combination with enzyme inhibition kinetic studies (ADP-GLO) to determine if DISC1-44mer and FRATtide compete for the same binding site on GSK3β. This information will allow additional insight into how DISC1-44mer influences GSK3β inhibition and if this mechanism is similar to FRATs unique mechanism for GSK3β inhibition. For the series of SPR experiments, a double-tagged GSK3β product (His-GSK3β-His) was used in order to decrease the amount of protein drifting off the surface of the SPR chip. For the ADP-GLO experiments, a cleaved GSK3β product without a histidine tag (GSK3β) was used.

5.1 SPR Results

5.1.1 SPR Calculations

For the SPR experiments the model chosen was a One to One model which assumes that one enzyme will interact with one molecule of analyte in solution. The equation used to calculate the fitted curve for a one to one model is;

$dY/dt = (K_a * c - K_d) * Y$ ……..(5.1.1)

where Y is the recorded signal (RU) observed after injection and c is the concentration of sample (M) in the bulk liquid. The equation described is a differential equation to which the measured data is fitted. The association rate (K_a) describes the rate at which the analyte-ligand complex is formed and is directly proportional to the concentration of analyte in solution ([A]) and the concentration of enzyme bound to the surface ([B]). The dissociation rate (K_d) describes the rate at which the analyte-ligand complex is being disassembled and is proportional to the concentration of the analyte-ligand complex ([AB]). The affinity constant (KD) represents the strength of the attraction between analyte and ligand at equilibrium. KD is accurately described as the concentration of analyte at half the enzyme concentration bound during equilibrium. The association and dissociation constants are described in more detail in Table 5-1. For the purposes of SRP studies, the concentration of analyte is measured in M and determined by the user. This concentration is essentially the concentration of analyte in solution and is maintained by the system throughout the duration of the injection. The enzyme-ligand complex (AB) is extrapolated from the data directly as the observed response (RU) following analyte injection. Lastly, the concentration of available unbound enzyme is determined by subtracting the observed response (RU) following the analyte injection from the R_{max}. The R_{max} is a measure of the maximum amount of enzyme bound to the surface and is calculated by multiplying the molecular weight (MW) of the analyte (g/mol) with the response observed from the initial capture of the enzyme (RU) and dividing the result by the MW of the enzyme (Table 5-2). In relation to the net rate equation in Table 5-1, the overall rate (d[AB]/dt) is (d[R]/dt) where R is the response observed after analyte injection. The [A] is the concentration of analyte in the injection, the [B] is taken from the $R_{max} - R$ and, the [AB] is R. The affinity kinetics described can be measured in one of two ways; as steady state parameters while the enzyme and analyte are at equilibrium or by measuring the on and off rates of the enzyme and calculating k_d/k_a.

Table 5- 1: Affinity and kinetics equations and units' derivations.

At equilibrium:	$A + B \underset{k_d}{\overset{k_a}{\rightleftharpoons}} AB$
Association (k_a) $M^{-1}s^{-1}$	$\frac{d[AB]}{dt} = k_a \cdot [A] \cdot [B]$
Dissociation (k_d) s^{-1}	$\frac{-d[AB]}{dt} = k_d \cdot [AB]$
Enzyme/Analyte (M)	[A] [B]
Net Rate Equation (Ms^{-1})	$\frac{d[AB]}{dt} = \left[k_a \cdot [A] \cdot [B]\right] - \left[k_d \cdot [AB]\right]$

Table 5- 2: Rmax equation and units' derivation.

$$R_{max} = \frac{MW_{analyte} * R_{enzyme}}{MW_{enzyme}}$$

$$RU = \frac{(g/mol) * (RU)}{(g/mol)}$$

5.1.2 Binding Kinetics and Affinity of DISC1-44mer

SPR technology was utilized to determine the binding kinetics and affinity constants for DISC1-44mer. Binding kinetics for mDISC1-44mer with hGSK3β had been previously determined in the literature, replication using hGSK3β with hDISC1-44mer was required to confirm binding and determine the kinetics. Kinetics and affinity measurements are essential to increase the understanding regarding the rate and strength of the interaction between the peptide and the protein.

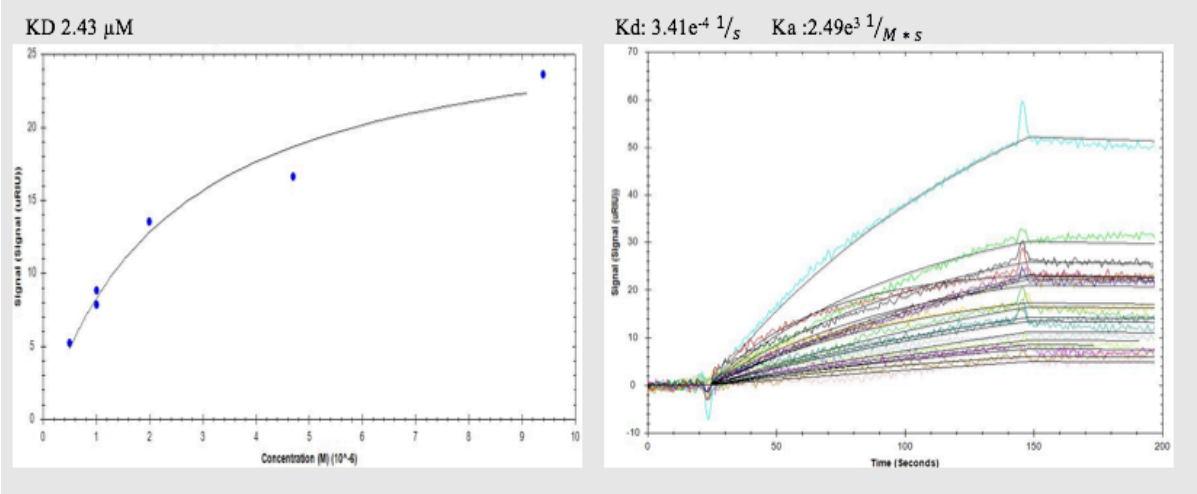

Figure 5- 1: Affinity (Panel A) and Kinetics (Panel B) graphs of GSK3β binding associations with DISC1-44mer.

Individual binding replicates were conducted with the peptide at varying concentrations. His-GSK3β-His was captured on an SPR NINTA chip, and the peptide was analyzed at a 250 µL injection at 50 µL/min over 2 minutes followed by a 2-minute dissociation. All data points were collected separately with regeneration of the surface in-between runs. All data was collectively pooled to fit into one affinity or kinetics curve represented above. From the data KD, K_a and K_a for DISC1-44mer were determined. Number of replicates is 1. Kinetics Chi^2 =0.80. Affinity Chi^2 = 1.69.

DISC1-44mer successfully shows binding to the His-GSK3β-His construct on an SPR chip at room temperature in the RB1 buffer (Figure 5-1). KD is a measure of affinity between the peptide and the enzyme, which for DISC1-44mer with GSK3β is 2.43 µM as determined by affinity calculations (Figure 5-1 / Panel A). DISC1-44mer has a slow on rate of $2.49e^{3}$ $(M*s)^{-1}$ (K_a) and a slow off-rate of $3.41e^{-4}$ s^{-1} (K_d) (Figure 5-1 / Panel B). The data was collected as a result of separate full replicates meaning; His-GSK3β-His was captured on the SPR surface, a single concentration of DISC1-44mer was flown over the top, the kinetics were determined, and the surface was regenerated so that another capture of GSK3β could occur and be tested with a new concentration of DISC1-44mer. The data was collected in this fashion because DISC1-44mers slow off-rate made it difficult to ensure that all the ligand had been removed from the bound protein before an additional injection occurred. The individual data sets were compiled together using TraceDrawer™ software to yield the graphs and data in Figure 5-1.

5.1.3 Binding Kinetics and Affinity of FRATtide

SPR technology was utilized to determine binding kinetics and affinity for FRATtide with His-GSK3β-His. Binding kinetics for this peptide fragment has not yet been determined in the

literature. This kinetic data was required to determine the ability of this peptide to bind to His-GSK3β-His and to define the apparent strength of the interaction. Kinetics and affinity measurements are critical to increasing understanding of how the peptide fragment interacts with the double His tagged construct of GSK3β.

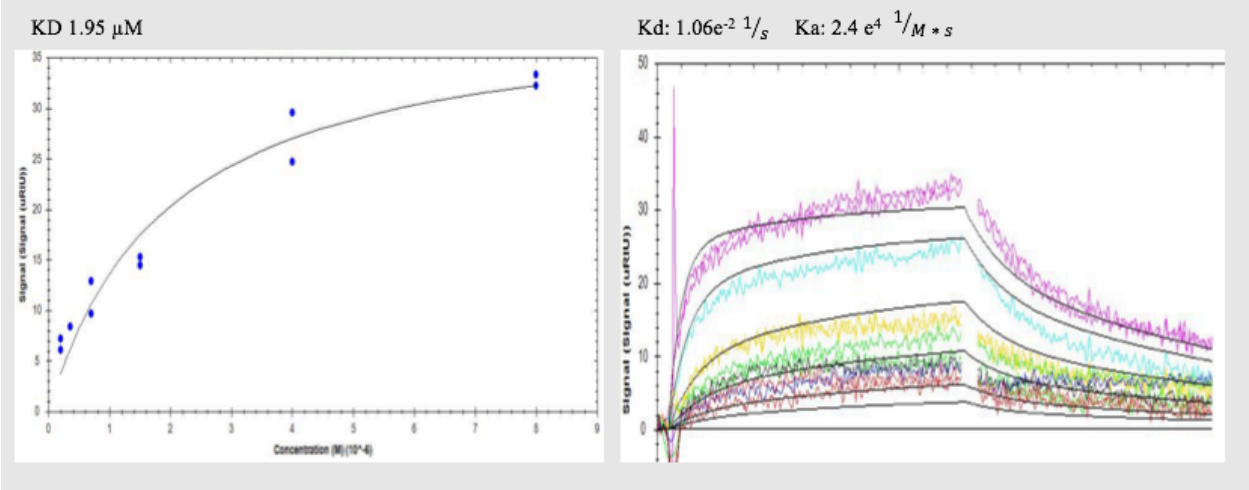

Figure 5- 2: Affinity (Panel A) and kinetics (Panel B) graphs of GSK3β binding associations with FRATtide.

Individual binding replicates were conducted with the peptide at varying concentrations. His-GSK3β-His was captured on an SPR NiNTA chip and peptide was analyzed at 250 µL injection at 50 µL/min over 2 minutes followed by a 2-minute dissociation. Some data points were obtained from the sequential injection of FRATtide at different concentrations without intermittent regeneration. Some data points were collected separately with regeneration of the surface in-between runs. From the data KD, K_d and K_a for FRATtide were determined. The fitted curve was determined using a one to one two State model to incorporate the conformational change of GSK3β that occurs as a result of FRATtide binding. Number of replicates = 1. Kinetics Chi^2 = 8.3. Affinity Chi^2 = 6.32.

FRATtide successfully shows binding with the His-GSK3β-His construct on an SPR chip at room temperature in the RB1 buffer (Figure 5-2). The KD, affinity measure between peptide and enzyme, for FRATtide with GSK3β, is 1.95 µM as determined by affinity calculations (Figure 5-2 / Panel A). FRATtide has a relatively fast on rate of $2.4e^4$ $(M*s)^{-1}$ (ka) and a moderately fast off rate of $1.06e^{-2}$ s^{-1} (Kd) (Figure 5-2 / Panel B). Due to its fast on and off rate, regeneration in between replicates, as was done for DISC1-44mer, was not necessary. However, in order to create a reliable replicate to the DISC1-44mer data, the FRATtide data was also compiled with replicates occurring over separate runs which included regeneration of the SPR surface in-between. This was conducted in the same manner as described for DISC1-44mer where His-GSK3β-His was captured on the SPR surface, a single concentration of FRATtide was flown over the top, the kinetics were

determined, and the surface was regenerated so that another capture could occur with a new concentration of FRATtide. This data was compiled with data collected from a continuous run which analyzed multiple concentrations of FRATtide sequentially flow over captured His-GSK3β-His, without intermittent regeneration. It should be noted that the KD generated from this sequential run with no intermittent regeneration was 1.85 μM (data not shown) which is not considerably different from the KD calculated from the pooled data. As a result, data sets were merged using TraceDrawer™ software to yield the plots in Figure 5-2 so that they would be more comparable, in terms of methodology, to the DISC1-44mer data.

5.1.4 Binding of DISC1-44mer and FRATtide

In an attempt to use SPR studies to determine if DISC1-44mer and FRATtide share the same binding site, combined and sequential binding studies were conducted. The initial investigation focused on the use of combined binding studies. The experiment aimed to determine the presence of a notable difference in KD from equilibrium when the analyte solution contained FRATtide and DISC1-44mer together as compared to when the analyte solution contained FRATtide or DISC1-44mer individually.

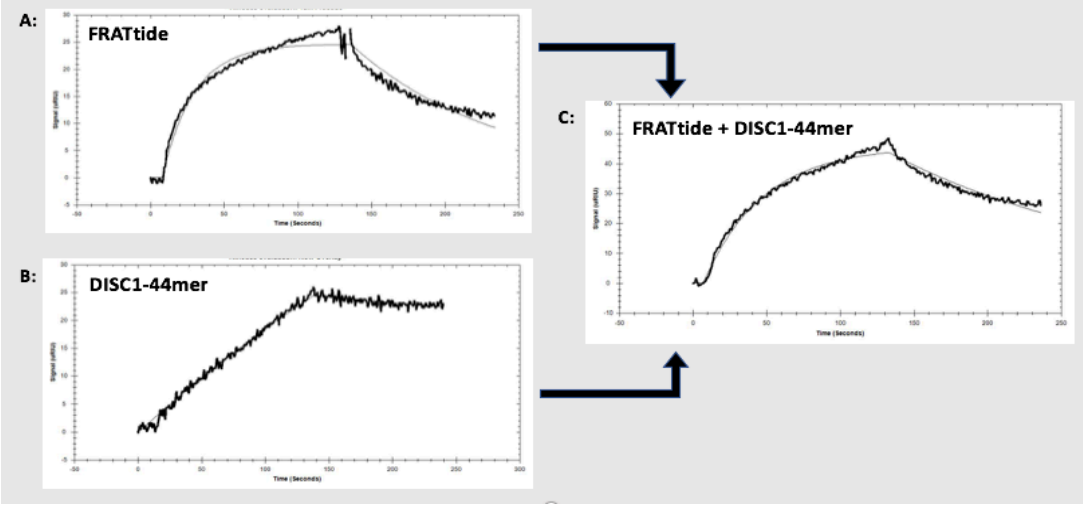

Figure 5- 3: Combined Binding Studies Data of DISC1-44mer, FRATtide and DISC1-44mer with FRATtide.

Kinetics curve for His-GSK3β-His at a capture level of 2781 RU with 4 μM FRATtide with a signal response of 28 uRIU (Panel A). Kinetics curve for His-GSK3β-His at a capture level of 2210 with 2.3 μM of DISC1-44mer with a signal response is 25 uRIU (Panel B). Kinetics curve for His-GSK3β-His at a capture level of 2781 RU with 2.3 μM of DISC1-44mer mixed with 4 μM of FRATtide and a signal response is 49 uRIU (Panel C).

His-GSK3β-His was captured on to the SPR chip, and an analyte solution containing 4 μM of FRATtide was introduced (Figure 5-3 / Panel A). The results from this condition were compared to the results of His-GSK3β-His when 2.3 μM of DISC1-44mer was introduced (Figure 5-3 / Panel B). For both the FRATtide and DISC1-44mer conditions the capture level of His-GSK3β-His was above 2200 RU. For the FRATtide only condition, the R_{max} was 162.46 RU. For the DISC1-44mer condition, the R_{max} was 202.37 RU. The observed R_{max} is much smaller than the theoretical R_{max} for both single analyte conditions which indicates that the analyte concentration is not sufficient to occupy all of the available enzyme binding sites. The KD from the mixed condition is not useful in determining any insight into peptide binding as originally hypothesized. This is largely due to the fact that the DISC1-44mer condition does not conclusively reach saturation. As a result, the KD from the combined condition is not useful for any form of interpretation. Since the data from the combined binding study did not provide evidence into the possible presence of binding competition and is limited in its ability to produce steady state equilibrium for DISC1-44mer, further investigation using this method of analysis was not continued. However, the initial question regarding binding sites required added examination which included the sequential binding studies outlined below.

The sequential method of investigation for this series of experiments encompassed capturing His-GSK3β-His on the SPR surface then injecting DISC1-44mer and FRATtide one after the other. The theory follows that if DISC1-44mer and FRATtide bind GSK3β at the same site, then the injection of DISC1-44mer should occupy all of the available binding sites leaving no opportunity for FRATtide to bind. In this scenario, the secondary injection of FRATtide should show no response on the resulting sensorgram.

His-GSK3β-His was captured on the SPR surface, and DISC1-44mer at 4 μM was introduced, the response was approximately 11.1 RU (Figure 5-4 / Panel A). The SPR system automatically shifted to the sequential 4 μM FRATtide injection, and the response was approximately 13.1 RU (Figure 5-4 / Panel B). Dissociation over 3 minutes showed the response decrease by approximately 13 RU (Figure 5-4 / Panel C). The data suggest that both peptides are binding the enzyme at the same time since the expectation for Panel B in the event of a shared binding site was a flat line representing no association. The main issue regarding the data concerns

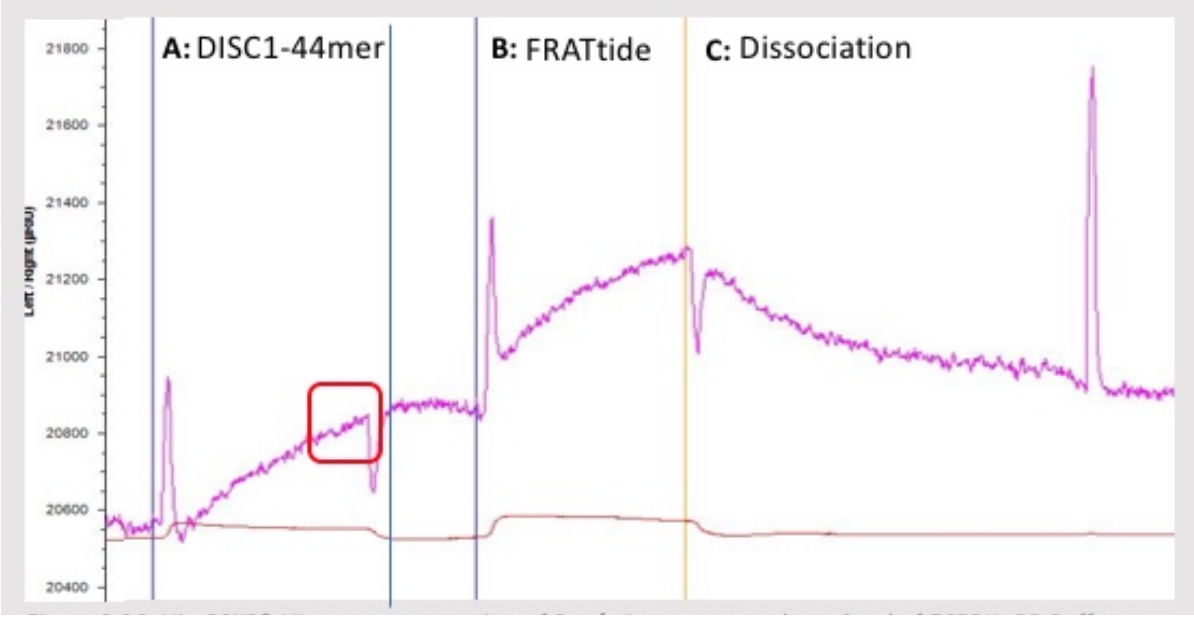

Figure 5- 4 Initial attempts to use sequential binding studies to determine possible peptide competitive binding.

His-GSK3β-His at a concentration of 3 μg/mL was captured at a level of 765 RU. RB buffer was run over the captured construct until the drift rate was 2.59 RU/min. A series of blanks was injected. DISC1-44mer peptide (4 μM) dissolved in RB1 underwent a 25 μL injection at 50 μL/min over 2 minutes (Panel A). Immediately after, FRATtide (4 μM) dissolved in RB1 underwent a 250 μL injection at 50 μL/min over 2 minutes (Panel B). The construct was then allowed to undergo dissociation over 3 minutes (Panel C).

the un-apparent saturation of His-GSK3β-His with DISC1-44mer before FRATtide injection (Figure 5-4 / Panel A Red Box). Since the experiment does not indicate if DISC1-44mer has occupied all of the available binding sites provided by the captured His-GSK3β-His, then it can be argued that FRATtide in Panel B is binding to any open or unclaimed sites.

To address this issue, DISC1-44mer and GSK3β were incubated together at room temperature for 20 minutes, then the complex of DISC1-44mer/GSK3β was captured onto the SPR chip as a single unit. After capturing the complex, DISC1-44mer and FRATtide were injected sequentially in the same fashion described in the previous series of experiments. The theory behind this experimental design considers DISC1-44mers slow association rate and allows the peptide and enzyme sufficient time to form a complex in solution before capture. Since SPR methods includes the constant flow of solution over the chip and the analyte concentration is maintained by fixed injection rates, it is possible that DISC1-44mer does not have enough time to bind GSK3β before it is flown past. Allowing a period for incubation before capture serves to rectify this potential issue. The subsequent secondary injection and response of DISC1-44mer will serve to

illustrate if any DISC1-44mer open binding sites remain, and thereby confirm saturation, before the injection of FRATtide.

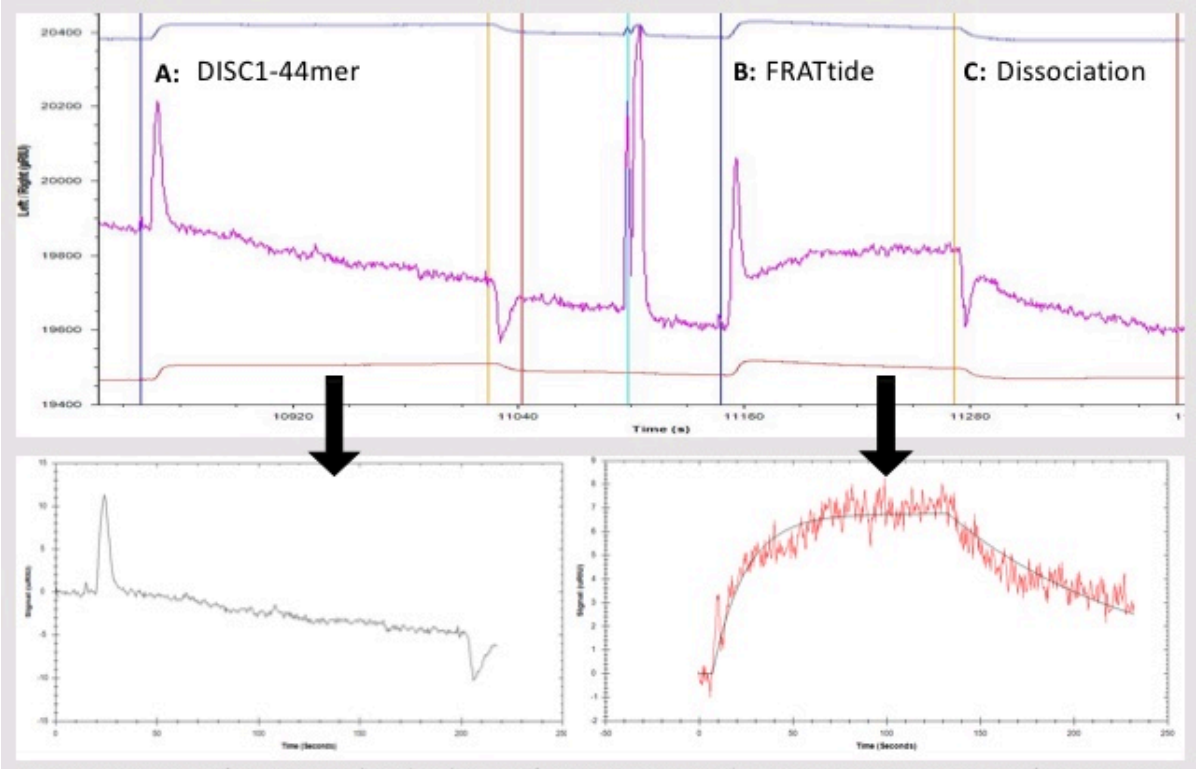

Figure 5- 5: Sequential binding studies using incubation of protein and analyte prior to capture.

His-GSK3β-His was incubated with 4 μM of the DISC1-44mer peptide in RB1 at room temperature for 20 minutes then captured onto a NiNTA chip at a capture level of 553 RU. RB1 was passed over the surface until the drift was 2.23 RU/min. DISC1-44mer peptide (4 μM) dissolved in RB1 underwent a 250 μL injection at 50 μL/min over 3 minutes and allowed to dissociate for 20 seconds (Panel A). Immediately after, FRATtide (4 μM) dissolved in RB1 underwent a 250 μL injection at 50 μL/min over 2 minutes with a response of 7.1 RU (Panel B) followed by a 2-minute dissociation (Panel C). The top graph represents the real-time response while the bottom graphs represent the data post-processing with TraceDrawer software.

His-GSK3β-His was allowed to complex with DISC1-44mer in solution at room temperature to ensure the association had time to occur. The His-GSK3β-His/DISC1-44mer complex was captured onto the SPR surface with a capture response of 553 RU and a R_{max} of 29.59 RU. Following the capture, DISC1-44mer at 4 μM was injected on top of the complex, and the resulting sensorgram showed no increase in response units (Figure 5-5 / Panel A). This flat line strongly suggests that all DISC1-44mer binding sites on GSK3β are saturated. Immediate injection of FRATtide at 4 μM following DISC1-44mer injection showed a clear response of approximately 7.1 RU (Figure 5-5 / Panel B). Dissociation shows FRATtide coming off of the construct as expected (Figure 5-5 / Panel C). The response observed for FRATtide after the injection of DISC1-

44mer was comparable to the response observed when FRATtide was injected alone without the prior injection of DISC1-44mer (data not shown).

5.2 ADP-GLO Results

5.2.1 Determination of Optimal GSK3β concentration and Substrate K_m

The determination of K_M for GSP2 and ATP is a necessary step in the process of studying enzyme inhibition as it allows for the basic characterization of proper enzyme concentrations for planning competition studies. The K_M of both substrates was determined via a luminescence response to an ATP dependent reaction assay (ADP-GLO). The ADP-GLO kit determines enzyme activity by first depleting unused ATP in a reaction then converting the ADP present in the reaction mixture back into ATP. Finally, the ATP undergoes an additional reaction which gives off a luminescent signal that is detected and interpreted directly as enzyme activity. Firstly, an optimal GSK3β concentration was determined via GSK3β enzyme activity assays. The ideal concentration was chosen from the middle of the produced curve. The concentration produced activity that gave an adequate reading without falling in the range of enzyme maximum activity (Figure 5-6). The experimental protocol for K_M determination utilized the conventional technique of maintaining the concentration of one substrate while varying the concentration of the other substrate. Plotting the luminescent response against varying concentration allows the data to undergo Michaelis-Menten type analysis in order to determine the substrates apparent K_M. GSP2 is a primed peptide fragment of the glycogen synthase protein which is a common GSK3β substrate.

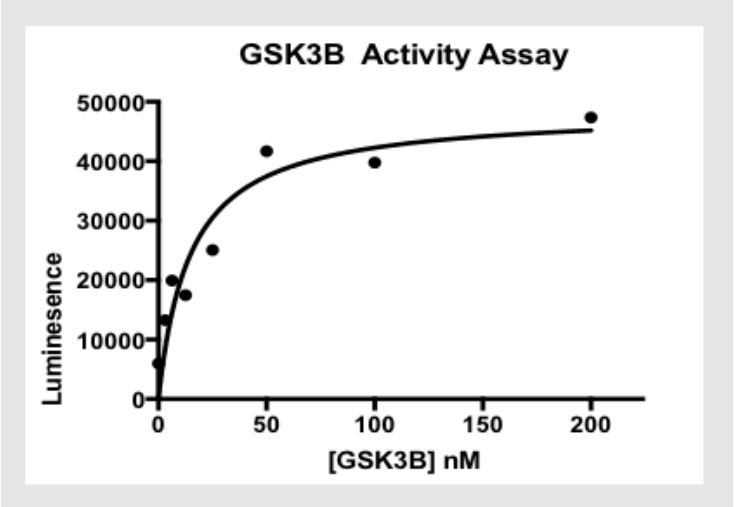

Figure 5- 6: GSK3β activity assay.

Two-fold series dilution of GSK3β from 3.125 nM to 200 nM was tested for luminescence readings when incubated with 9 μM GSP5, 15uM ATP and RxnB1 over one hour. Experiment was preliminary in nature to determine an adequate concentration of enzyme to use in order to obtain good luminescence readings in the 20000-30000 range. Number of replicates is 1. R^2= 0.71. Standard error = 6.57.

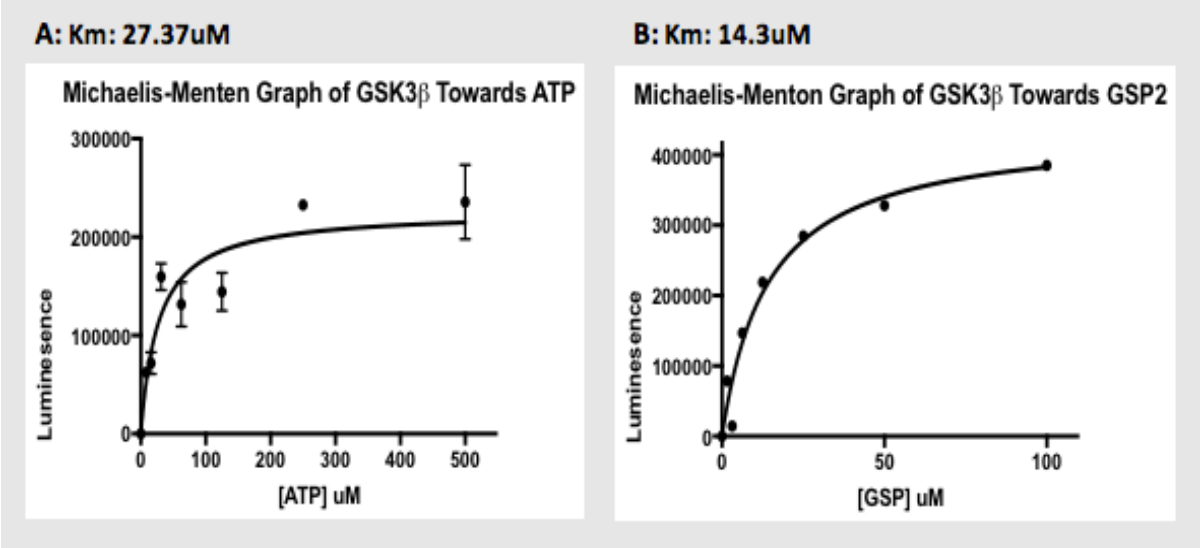

Figure 5- 7: ADP-GLO studies to determine K_M of ATP and GSP2 as substrates of GSK3β.

Michaelis-Menton type kinetics was determined with varying concentrations of ATP while holding the concentration of GSP2 constant at a concentration of 35 μM n=2. R^2=0.85. Standard error = 8.82 μM (Panel A). Michaelis-Menton type analysis was determined with varying concentrations of GSP2 while holding the concentration of ATP constant and at a concentration of 150 μM n= 1. R^2=0.93. Standard error = 3.50 μM (Panel B).

The activity assay (Figure 5-6) showed that 25 nM of GSK3β yielded an optimal luminescence reading between 20000 and 30000 units and falls in the middle of the curve in a

region that is apart from GSK3β's maximum activity. Therefore, a 25 nM concentration of GSK3β was used for all subsequent experiments. The determined K_M for ATP is 27.37 μM (Figure 5-7 / Panel A). The determined K_M for GSP2 is 14.3 μM (Figure 5-7 / Panel B). ATP has a comparatively higher K_M compared to GSP2 (substrate) which indicates a moderately lower affinity for GSK3β. The determination of K_M for ATP was conducted from replicate data. The determination of K_M for GSP2 was conducted from a single set of data. The information collected from this series of experiments was useful in the design of future experiments. Therefore, the inhibition assays were conducted using 25 nM of GSK3β, and more than double the K_M of ATP (27.37 μM) and half the K_M of GSP2 (14.3 μM).

5.2.2 Inhibition Activity Assay

An inhibition activity assay was designed to ascertain if DISC1-44mer and FRATtide were competing for binding at the same site on GSK3β. From the literature, it is known that FRATtide binds to GSK3β without causing inhibition towards GSP2 *in vitro* but is able to cause inhibition *in vivo*. From lab experience, it is known that binding of DISC1-44mer to GSK3β does cause inhibition towards GSP2 *in vitro*. To ensure enough DISC1-44mer and FRATide were added to affect GSK3β activity, a concentration ~10x their corresponding KD as determined by SPR was used. This assay was conducted by examining enzyme activity of GSK3β (25 nM) in the presence of DISC1-44mer (25 μM), FRATtide (25 μM) and DISC1-44mer (25 μM) + FRATtide (25 μM) together. All experiments were conducted in the presence of GSP2 (9 μM) and ATP (100 μM). The hypothesis behind this experiment follows: if DISC1-44mer and FRATtide compete for the same binding site, then the result should show reduced activity in the condition where both peptides are incubated together. The theory follows that the GSK3β enzyme units bound to DISC1-44mer in solution will have no activity while the GSK3β units bound to FRATtide will retain activity. Therefore, the overall result for the mixed condition should show a partially reduced enzyme activity.

The experiment revealed that GSK3β activity in the presence of FRATtide was comparable to GSK3β alone in the absence of any peptides (Figure 5-8), which is expected as FRATtide does not inhibit GSK3β activity towards GSP2 *in vitro*. As was previously discussed in the introduction, FRAT acts to inhibit GSK3β by blocking the enzymes access to Axin and this effect is

predominantly seen in vivo towards the substrates β-catenin and Tau only (Culbert et al., 2001; Fraser et al., 2002; Li, 1999). The results demonstrated that GSK3β activity was inhibited almost entirely towards GSP2 in the presence of DISC1-44mer. GSK3β activity towards GSP2 in the presence of DISC1-44mer and FRATtide together revealed fully functional enzyme activity at a level comparable to GSK3β activity alone. The experiment was replicated to confirm the presence of the observed trend (results not shown).

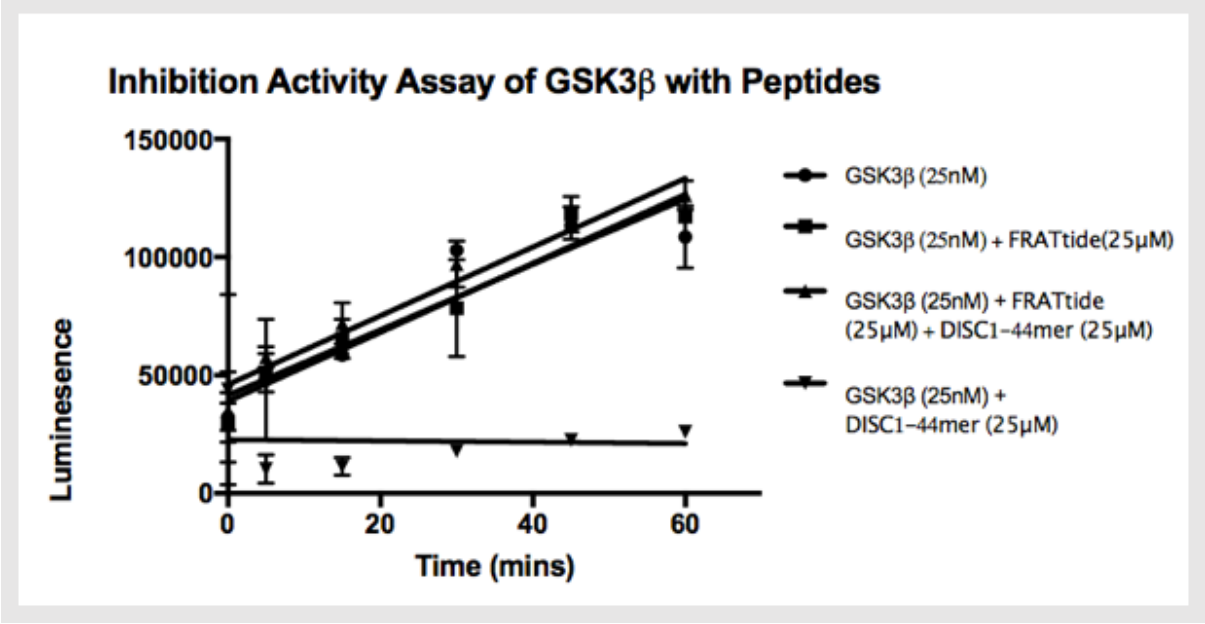

Figure 5- 8: ADP-GLO luminescent assay to compare GSK3β activity in the presence of peptides.

Each condition contains GSK3β (25 nM), GSP2 (9 μM) and ATP (100 μM) in RxnB1. Each condition contains a combination of FRATtide (25 μM), DISC1-44mer (25 μM), both or none. The peptides were used at concentrations at least 10X the KD as determined from the SPR studies. All conditions were incubated at room temperature for 60 mins and samples were taken at 0, 5, 15, 30, 45 and 60 mins. Number of replicates is 1. R^2 for GSK3β = 0.79. R^2 for GSK3β and FRATtide = 0.89. R^2 for GSK3β, FRATtide and DISC1-44mer = 0.93.

5.3 Discussion

5.3.1 Potential Model for DISC1-44mer and FRATtide Binding

One potential model to explain the binding patterns of DISC1-44mer and FRATtide to GSK3β is outlined in Figure 5-9. Since the sequential SPR data strongly suggests that both peptides can bind simultaneously to GSK3β (Figure 5-5), it can be reasoned that their primary binding sites are not identical or overlapping in a manner that hinders either peptides binding ability. In contrast,

the kinetics data from the ADP-GLO study shows that incubating both peptides with GSK3β prevents the predominantly inhibitory effects of DISC1-44mer (Figure 5-8). The data taken together lends evidence for a model of DISC1-44mer and FRATtide binding where the binding sites are likely overlapping to some extent. Mao and colleges (2009) were able to show that of the 44 amino acids present in the DISC1 peptide, only the 15 amino acids in the middle were required

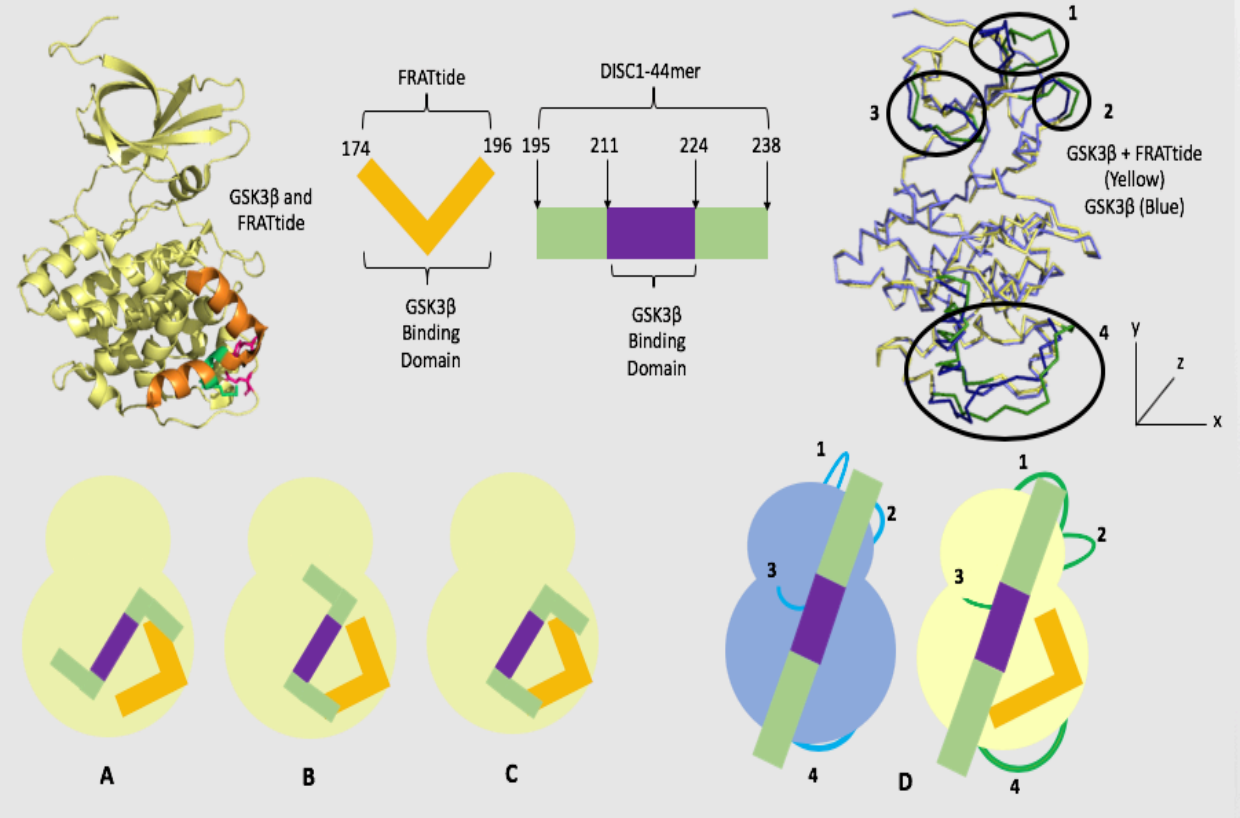

Figure 5- 9: Model depicting probable binding sites of DISC1-44mer and FRATtide to GSK3β.

Top left is the crystal structure of FRATtide (orange) bound to GSK3β (yellow) which occurs in the C terminal region away from the active site. Scenarios A-C depicts a possible binding site for DISC1-44mer which would allow for the middle 15-mer region responsible for binding to be unobstructed. Scenario A shows FRATtide physically blocking the C terminal region of DISC1-44mer, Scenario B shows FRATtide physically blocking the N terminal region of DISC1-44mer and Scenario C shows FRATtide physically blocking both the C and N terminals of DISC1-44mer simultaneously. The top right crystal structure shows GSK3β alone (blue) overlayed with GSK3β bound to FRATtide (yellow/orange) and highlights the four major regions of GSK3β that change in response to FRATtide binding. Scenario D illustrates a possible binding mechanism of DISC1-44mer to GSK3β without FRATtide (blue). In this illustration, DISC1-44mer interacts with regions 2-4 on GSK3β but not region 1. GSK3β bound to both DISC144mer and FRATtide (yellow) shows how regions 1-4 shift and how these shifts might change the way DISC1-44mer interacts with GSK3β regions 1-4. GSK3β with FRATtide is from PDB file 1GNG (Yellow). GSK3β alone is from PDB file 1H8F.

for binding (Figure 1-5 / Green and purple rectangle) (Mao et al., 2009). However, the 15-mer segment on its own was not sufficient to cause inhibition of GSK3β. Their findings reiterate that

the region of DISC1-44mer necessary for binding (15-mer) is distinct from the region necessary for inhibition. It is yet unknown if the inhibitory effect of the DISC1-44mer peptide resides in the N-terminal end between amino acids 195-211, the C-terminal end between amino acids 224-238, or some combination of the regions collectively. Therefore, the model depicted in Figure 5-9 represents a variety of possible scenarios (A-C) whereby FRATtide binding blocks either the N terminus, C-terminus or both termini of the DISC1-44mer without interfering with the middle 15-mer segment known to be necessary for binding. Scenarios A-C assume that the N- and C-terminal regions are flexible or contain a hinge section. This is a basic model which suggests how the two peptides might be able to bind simultaneously and create an outcome that has FRATtide physically blocking DISC1-44mers ability to inhibit GSK3β.

Scenario D depicted in Figure 5-9 illustrates a possible situation where FRATtide binding causes conformational changes in GSK3β in such a way that prevents DISC1-44mer from forming inhibitory interactions with GSK3β. The crystal structure on the right shows GSK3β alone (blue) superimposed on GSK3β bound to FRATtide (yellow). The superimposed structure shows four distinct regions where the FRATtide bound structure differs from the GSK3β alone structure (dark green/dark blue). These regions include residues 118-128 (1), residues 87-93 (2), residues 62-67 (3) and residues 261-276 (4). With FRATtide bound to GSK3β, region 1 is pushed along the XZ plane and turned into the Z axis, region 2 is shifted backward in three-dimensional space in the YZ plane, region 3 is shifted forwards in the ZX plane and region 4, which includes the helix and the loop, is moved upwards along the YZ plane towards the N-terminal β-strand domain of the enzyme. Scenario D illustrated in Figure 5-9 supposes that DISC1-44mer interacts with specific regions of GSK3β which are no longer in reach or properly exposed when FRATtide is bound. This illustration is just one of multiple ways that DISC1-44mer interaction with GSK3β could be altered with the added binding of FRATtide. It is possible that DISC1-44mer is only interacting with one of these four regions or any combination of these regions. Region 2 is the C loop of GSK3β which is known to be involved in inhibition mechanisms by sitting down on top of inhibitors and blocking the active site. Perhaps its subsequent backward shift in response to FRATtide binding puts the C loop out of reach for DISC1-44mer eliminating its ability to cause inhibition. At this point, it is difficult to make assumptions regarding which of the regions described above, if any, are involved with DISC1-44mer binding and inhibition. It is also difficult

to determine if DISC1-44mer is physically blocked from inhibition (Figure 5-9 / A-C) or deterred by the shifting of GSK3β surface residues (Figure 5-9 / D). However, it is reasonably likely that DISC1-44mer and FRATtide are interacting with GSK3β in one of the models depicted in Figure 5-9. One way to confirm this model includes extended mutagenesis studies. Each of the regions described above (1-4) could be mutated individually or in select combinations in separate constructs by replacing the amino acids in that region with alanine residues. The new mutated constructs would need to be subjected to enzyme activity studies both in the presence and absence of DISC1-44mer. Each mutated construct would need to retain full enzyme activity on its own before incubation with DISC1-44mer to ensure that the introduced mutations did not interfere with the enzymes native function. If DISC1-44mer fails to inhibit any of the mutated constructs it would lend evidence to the role that particular region plays in the DISC1-44mer-GSK3β inhibition interaction.

It is essential to consider the SPR data and ADP-GLO data together when attempting to develop a model as the SPR sequential binding data and the ADP-GLO kinetic data on their own could be interpreted to support different conclusions. The novelty of this combined model is that it lends evidence to the likelihood that DISC1-44mer is acting in a non-competitive allosteric fashion. Experiments conducted by our collaborators showed that DISC1-44mer acts as an inhibitor which is non-competitive for ATP binding. One potential question raised by the model is the possibility that DISC1-44mer binding or inhibition might be reversed or negated after the addition of FRATtide. This possibility is drawn from the experiments of FRATtide and DISC1-44mer incubated together with full enzyme activity. For example, if DISC1-44mer is bound to GSK3β causing inhibition, FRATtide (with a separate binding site) could be introduced, and its binding would shift regions of GSK3β interacting with DISC1-44mer potentially ceasing the inhibitory effect. The data from this thesis does not serve to answer this particular query but poses it as a potential question for future experiments. To determine if DISC1-44mer inhibition is reversible double titration enzyme assay with DISC1-44mer and FRATtide could be conducted. If FRATtide was able to reverse DISC1-44mer inhibition the resulting graph would show an increase in GSK3β activity with increasing FRATtide concentration. The prospect that FRATtide can hinder DISC1-44mers inhibition creates a scenario where enzyme activity could potentially be

more strictly controlled or finetuned. In this case, varying concentrations or doses of FRATtide and DISC1-44mer could allow for a type of enzyme activity switch.

5.3.2 Other Possible Explanations

Other possible explanations could serve to describe the observed data. One potential scenario is that DISC1-44mer and FRATtide are binding to each other (Figure 5-10 / A). It could be possible that the exposed surface residues of DISC1-44mer, or the regions of the peptide not directly interacting with GSK3β, are a complementary match for the binding residues on FRATtide. It would follow that what is being observed in the SPR sequential binding data (Figure 5-5) is FRATtide associating and dissociating from DISC1-44mer instead of from GSK3β itself. In regard

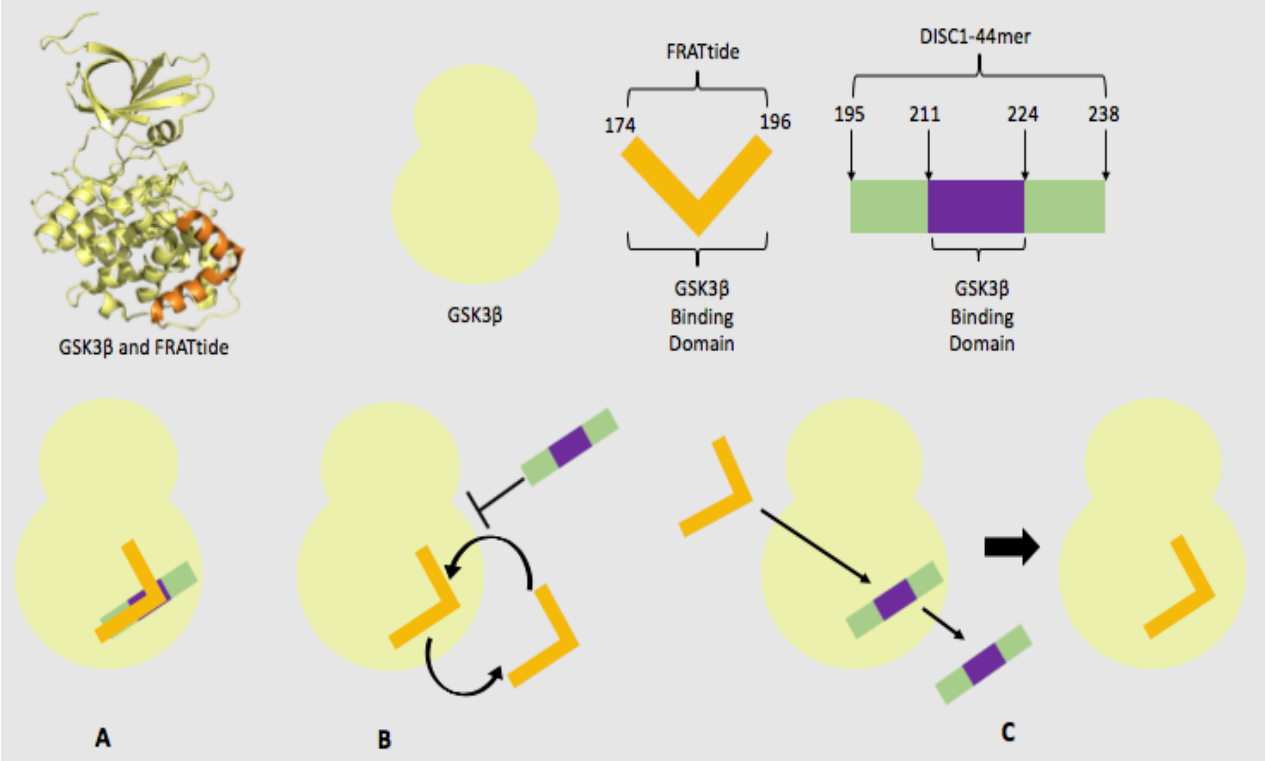

Figure 5- 10: Model to represent the other explanations that could apply to the data.

Scenario A shows FRATtide binding to DISC1-44mer directly instead of binding to GSK3β. Scenario B depicts FRATtide, and DISC1-44mer sharing a binding site but FRATtide associates and dissociates with GSK3β at a rate too fast thus not allowing DISC1-44mer the opportunity to bind. Scenario C depicts DISC1-44mer being ejected by FRATtide from a shared binding site.

to the results observed in the ADP-GLO studies, it could be theorized that FRATtide has higher affinity for DISC1-44mer than GSK3β and as such FRATtide is sequestering DISC1-44mer away

from the enzyme. In this case the full enzyme activity is explained by the lack of any peptide binding (Figure 5-8). Out of the three possible scenarios proposed in Figure 5-10 this is the most probable. One assay which could potentially help determine if Scenario A (Figure 5-10) is occurring would be to produce a His-tagged DISC1-44mer fragment and capture it onto the NiNTA surface of the SPR chip. Once captured, FRATtide would be injected across the chip, and the resulting response measured. If FRATtide showed any affinity for the DISC1-44mer fragment without the presence of GSK3β, then an association curve would be produced. However, if there were no association response, then it would be highly unlikely that Scenario A (Figure 5-10) would be an appropriate explanation of the observations. Alternatively, a sample of FRATtide and DISC1-44mer could be run on a native gel to determine if the peptides were associating in solution. Of course, it could still be a possibility that FRATtide only binds specifically to DISC1-44mer while it is bound to GSK3β in which case a native gel of a sample containing GSK3β, FRATtide and DISC1-44mer would address this possibility more accurately.

It could also be argued that FRATtide and DISC1-44mer share a binding site, but since FRATtide has a faster association rate for GSK3β than DISC1-44mer ($2.4e^{4}$ $M^{-1}s^{-1}$ for FRATtide compared to $2.49e^{4}$ $M^{-1}s^{-1}$ for DISC1-44mer), its non-inhibitory effect is the one predominantly seen in the activity assay (Figure 5-8). This theory assumes that since FRATtide has a faster association rate, it will bind GSK3β more quickly than DISC1-44mer (Figure 5-10 / B) thereby monopolizing the shared binding site. In this suggested scenario, FRATtide would associate then dissociate then re-associate with GSK3β thereby continually occupying the binding site and preventing DISC1-44mer the opportunity to bind. While this model is plausible and accounts for the non-inhibition seen in the ADP-GLO studies, it does not account for the observations recorded by the SPR data. For example, if FRATtide were monopolizing a shared binding site the addition of FRATtide after DISC1-44mer saturation would not have had such a clear response (Figure 5-4 and Figure 5-5). Not only was the response obvious, but it was characteristic in shape, size, and kinetics to FRATtide's standard response to GSK3β alone without the presence of DISC1-44mer. Given the lack of support from the SPR data, Scenario B in Figure 5-10 is also possible but not probable.

A third possibility that could serve to explain the data presented in this chapter is that FRATtide is ejecting or replacing bound DISC1-44mer peptide (Figure 5-10 / C) in a competitive

fashion. This scenario explains the enzyme activity (ADP-GLO) data as it suggests that any GSK3β enzymes inhibited by DISC1-44mer would be freed from this inhibition when FRATtide replaced the DISC1-44mer peptide. However, Scenario C (Figure 5-10) is not well supported by the SPR data. If FRATtide were actually ejecting DISC1-44mer from a shared binding site, the injection of FRATtide would cause a decrease in overall mass on the surface of the NiNTA chip, and the response curve would show a decline (Figure 5-4). This is especially true considering DISC1-44mer is larger than FRATtide and as such the mass being lost would be higher than the mass gained. Similar to Scenarios B (Figure 5-10), Scenario C is also possible but not probable as it is only supported by the ADP-GLO data and not the SPR data. Additional work to further address the possibility of Scenario C could include a three-tier version of the sequential SPR experiment. This experiment would occur similarly to the original sequential binding (Figure 5-5) except immediately after FRATtide injection and dissociation, DISC1-44mer would be injected a second time. If FRATtide was actively acting to eject DISC1-44mer then the binding spot would be open and available after FRATtide dissociation and a clear response would be observed for the second DISC1-44mer injection. This three-tire sequential SPR experiment would clearly indicate if FRATtide is acting in a manner which dislodges or removes DISC1-44mer lending more evidence to the theory that the two peptides share the same binding site.

5.3.3 Final Determination of Binding Sites

As described above, mutagenesis studies would be helpful in narrowing down the final determination of binding sites. The first step would include designing a construct with one of the four regions in Figure 5-9/D mutated by replacing the amino acid residues with alanine residues. The largest region indicated in Figure 5-9/D is 15 amino acid residues while the smallest region is 5 amino acid residues. It would be sensible to use site directed mutagenesis to mutate the entirety of each of the regions to alanine residues. Site directed mutagenesis works by denaturing the whole plasmid, annealing a primer containing the desired mutation and extending. The original/parental strand is methylated and thus digested using the enzyme, Dpn1. The nicked DNA is then ligated and transformed into competent cells. In the event that none of the four regions mutated alone negate DISC1-44mer inhibition then mutation constructs can be designed with different combinations of the four regions mutated at the same time. This process can continue until a region, or combination of regions, that prevents DISC1-44mer inhibition is identified. Once the broad

region is known, smaller segments of mutations within those regions can be done to further narrow down the specific residues necessary for DISC1-44mer inhibition. This type of mutagenesis experiment relies on enzyme activity assays and as such, controls must be set to ensure that the induced mutations on their own do not cause the protein to fold improperly or otherwise be inactive. If mutagenesis is unable to produce active mutated enzymes or otherwise unable to identify DISC1-44mer binding regions, an alternative way to determine what is happening involves crystallography studies. Crystallography studies on GSK3β with DISC1-44mer, GSK3β with FRATtide and GSK3β with both DISC1-44mer and FRATtide together would be most optimal. Solving of these three structure complexes would allow for definitive determination of binding sites. It is the most accurate way to compare and contrast binding patterns and would ultimately determine if the two peptides compete for binding or have small overlapping binding regions. The hurdles towards obtaining a crystal structure thus far include the yield and purity of the GSK3β product which was thoroughly addressed in Chapters 3 and 4.

In summary, the data most accurately reflects the model outlined in Figure 5-9 whereby DISC1-44mer and FRATtide have binding sites that are close to one another and overlap in a region of DISC1-44mer responsible for GSK3β inhibition or that FRATtide binding shifts the surface residues required for DISC1-44mer inhibition to occur. This model is supported by both the SPR data and the enzyme activity (ADP-GLO) data. In order to confirm this model, a crystal structure or mutagenesis studies would be necessary. The additional assays suggested in the section proposed to address the other possible scenarios would help lend evidence to prove or disprove other possible explanations thereby strengthening the most likely model.

6.0 Conclusions & Future Work

More investigation into the observed phenomenon of FRATtide's ability to restrict DISC1-44mer's inhibition of GSK3β is necessary to draw any concrete conclusions regarding what is occurring at the molecular level. However, the data from the SPR studies married with the data from the ADP-GLO studies strongly suggest that DISC1-44mer and FRATtide appear to have mostly different binding sites. It remains possible that the peptide binding sites may overlap in the regions that obstruct DISC1-44mer inhibition without interfering with DISC1-44mer binding. The data indicate that both peptides are binding simultaneously and in a manner that does not allow for DISC1-44mer to cause inhibition. The data can be interpreted to mean that either small fractions of the binding sites overlap (Figure 5-8 / Scenario A, B or C) or that in order to cause inhibition DISC1-44mer needs to interact with at least one of the regions of GSK3β that becomes shifted as a result of FRATtide binding (Figure 5-8 / Scenario D). This conclusion is supported by the SPR data which exhibited FRATtide's ability to bind GSK3β after DISC1-44mer was already in place. Although this sequential binding data does not address the kinetic ability of the enzyme at this point, it does indicate that the binding of DISC1-44mer does not interfere with the binding of FRATtide. The overall conclusion is also supported by the ADP-GLO results which revealed that GSK3β activity in the presence of DISC1-44mer is inhibited compared to the full GSK3β activity observed in the presence of FRATtide. This simple observation alone is minor evidence that the peptides probably do not share a common inhibition strategy. Finally, the overall conclusion is supported by the ADP-GLO studies which show normal GSK3β activity towards GSP2 in the presence of both peptides. Both of the proposed models consider the ability of the peptides to bind separately but simultaneously while allowing for differing outcomes in enzyme activity. The thesis elaborated the original hypothesis that DISC1-44mer and FRATtide compete for the same binding site on GSK3β by suggesting instead that the peptides may likely contain binding sites that partially overlap. Further investigations involving mutagenesis or structural studies need to be completed in order to confirm the suggestions posed by this work.

This project is a small subset of a large puzzle involving DISC1's interaction with GSK3β and how that interaction causes inhibition in a seemingly specific and targeted manner. The work as a whole is impactful to the scientific community as it provides a baseline interaction that can be targeted for drug therapy in the potential treatment of mental health disorders. Suggestions for experiments to improve each objective were described in detail within the discussion section of each chapter. The first two objectives of overexpression and purification have been brought to the point of functionality but would benefit from further optimization so that their execution can be done in a more streamlined fashion with a higher overall yield of a protein product containing fewer contaminants. The third objective of enzyme studies could benefit from additional SPR and ADP-GLO studies which may help eliminate some of the possible scenarios outlined in Figure 5-10. Future work for this project as a whole should mainly focus on enzymatic, mutagenic and crystallographic studies of GSK3β complexed with DISC1-44mer to identify where the peptide binds and what, if any, structural changes occur which may cause enzyme inhibition. Furthermore, future work should include crystallographic studies of GSK3β complexed with FRATtide and DISC1-44mer together to visualize the binding locations of both peptides. Crystallization of this complex will allow an accurate representation to compliment the kinetic data provided in this thesis regarding FRATtide's apparent ability to obstruct DISC1-44mers inhibitory effect.

The potential of confirming DISC1-44mers binding location is an essential piece of knowledge both for better understanding the activity of GSK3β's binding partners and for identifying what factors of DISC1 binding causes its inhibition to be limited towards specific substrates. The potential for confirming FRATtide's ability to obstruct DISC1-44mer's inhibition is valuable to the niche as well because it would provide a greater understanding of DISC1-44mer inhibition and add potential avenues for inhibition manipulation. Furthermore, it would also be useful to identify the scope of specificity for DISC1-44mer inhibition via GSK3β. Identifying which GSK3β substrates are affected as a result of DISC1-44mer inhibition could broaden the scope of the utility for DISC1-44mer as a potential drug target and help increase the knowledge base surrounding DISC1 and the pathways it is involved in.

References

A.Levi, P.Calissano, S.Alemà, and S.Alemà (1974). Anomalous behaviour of EDTA during gel filtration: Studies on the possible contamination of the S100 protein. Analytical Biochemistry *62*, 301–304.

Aoki, M., Mariko Iwamoto-Sugai, Ikuko Sugiura, Chizuko Sasaki, and Tsukasa Hasegawa (2000). Expression, purification and crystallization of human tau-protein kinase I/glycogen synthase kinase-3b. Acta Cryst *11*, 1464–1465.

Bax, B., Carter, P.S., Lewis, C., Guy, A.R., Bridges, A., Tanner, R., Pettman, G., Mannix, C., Culbert, A.A., Brown, M.J.B., et al. (2001). The Structure of Phosphorylated GSK-3β Complexed with a Peptide, FRATtide, that Inhibits β-Catenin Phosphorylation. Structure *9*, 1143–1152.

Bax, B., Carter, P.S., Lewis, C., Guy, A.R., Bridges, A., Tanner, R., Pettman, G., Mannix, C., Culbert, A.A., Brown, M.J.B., et al. The Structure of Phosphorylated GSK-3β Complexed with a Peptide, FRATtide, that Inhibits β-Catenin Phosphorylation. 10.

Beaulieu, J.-M. (2007). Not only lithium: regulation of glycogen synthase kinase-3 by antipsychotics and serotonergic drugs. The International Journal of Neuropsychopharmacology *10*, 3.

Bechard, M., Trost, R., Singh, A.M., and Dalton, S. (2012). Frat Is a Phosphatidylinositol 3-Kinase/Akt-Regulated Determinant of Glycogen Synthase Kinase 3 Subcellular Localization in Pluripotent Cells. Molecular and Cellular Biology *32*, 288–296.

Beurel, E., Grieco, S.F., and Jope, R.S. (2015). Glycogen synthase kinase-3 (GSK3): Regulation, actions, and diseases. Pharmacology & Therapeutics *148*, 114–131.

Blackwood, D.H.R., Fordyce, A., Walker, M.T., St. Clair, D.M., Porteous, D.J., and Muir, W.J. (2001). Schizophrenia and Affective Disorders—Cosegregation with a Translocation at Chromosome 1q42 That Directly Disrupts Brain-Expressed Genes: Clinical and P300 Findings in a Family. The American Journal of Human Genetics *69*, 428–433.

Bornhorst, J.A., and Falke, J.J. (2000). Purification of proteins using polyhistidine affinity tags. In Methods in Enzymology, (Elsevier), pp. 245–254.

Burden, D.W. (2008). Guide to the Homogenization of Biological Samples. Random Primers *7*, 1–14.

Calloni, G., Chen, T., Schermann, S.M., Chang, H., Genevaux, P., Agostini, F., Tartaglia, G.G., Hayer-Hartl, M., and Hartl, F.U. (2012). DnaK Functions as a Central Hub in the E. coli Chaperone Network. Cell Reports *1*, 251–264.

Chen, J., Wang, M., Waheed Khan, R.A., He, K., Wang, Q., Li, Z., Shen, J., Song, Z., Li, W., Wen, Z., et al. (2015). The GSK3B gene confers risk for both major depressive disorder and schizophrenia in the Han Chinese population. Journal of Affective Disorders *185*, 149–155.

Chhetri, G., Kalita, P., and Tripathi, T. (2015). An efficient protocol to enhance recombinant protein expression using ethanol in Escherichia coli. MethodsX *2*, 385–391.

Chi, E.Y., Krishnan, S., Kendrick, B.S., Chang, B.S., Carpenter, J.F., and Randolph, T.W. (2003). Roles of conformational stability and colloidal stability in the aggregation of recombinant human granulocyte colony-stimulating factor. Protein Science *12*, 903–913.

Cole, A., Frame, S., and Cohen, P. (2004). Further evidence that the tyrosine phosphorylation of glycogen synthase kinase-3 (GSK3) in mammalian cells is an autophosphorylation event. Biochemical Journal *377*, 249–255.

Cross, D.A.E., Alessi, D.R., Cohen, P., Andjelkovich, M., and Hemmings, B.A. (1995). Inhibition of glycogen synthase kinase-3 by insulin mediated by protein kinase B. Nature *378*, 785–789.

Culbert, A.A., Brown, M.J., Frame, S., Hagen, T., Cross, D.A.E., Bax, B., and Reith, A.D. (2001). GSK-3 inhibition by adenoviral FRAT1 overexpression is neuroprotective and induces Tau dephosphorylation and β-catenin stabilisation without elevation of glycogen synthase activity. FEBS Letters *507*, 288–294.

Dajani, R., Fraser, E., Roe, S.M., Yeo, M., Good, V.M., Thompson, V., Dale, T.C., and Pearl, L.H. (2003). Structural basis for recruitment of glycogen synthase kinase 3β to the axin±APC scaffold complex. Embo J *22*, 494–501.

Dajani, R., Fraser, E., Roe, S.M., Young, N., Good, V., Dale, T.C., and Pearl, L.H. Crystal Structure of Glycogen Synthase Kinase 3β: Structural Basis for Phosphate-Primed Substrate Specificity and Autoinhibition. Cell 105, 721-732 12.

Ding, V.W., Chen, R.-H., and McCormick, F. (2000). Differential Regulation of Glycogen Synthase Kinase 3β by Insulin and Wnt Signaling. Journal of Biological Chemistry *275*, 32475–32481.

Doble, B.W. (2003). GSK-3: tricks of the trade for a multi-tasking kinase. Journal of Cell Science *116*, 1175–1186.

Donnelly, M.I., Stevens, P.W., Stols, L., Xiaoyin Su, S., Tollaksen, S., Giometti, C., and Joachimiak, A. (2001). Expression of a Highly Toxic Protein, Bax, in Escherichia coli by Attachment of a Leader Peptide Derived from the GroES Cochaperone. Protein Expression and Purification *22*, 422–429.

Duan, X., Chang, J.H., Ge, S., Faulkner, R.L., Kim, J.Y., Kitabatake, Y., Liu, X., Yang, C.-H., Jordan, J.D., Ma, D.K., et al. (2007). Disrupted-In-Schizophrenia 1 Regulates Integration of Newly Generated Neurons in the Adult Brain. Cell *130*, 1146–1158.

Dumetz, A.C., Snellinger-O'Brien, A.M., Kaler, E.W., and Lenhoff, A.M. (2007). Patterns of protein-protein interactions in salt solutions and implications for protein crystallization. Protein Science *16*, 1867–1877.

Eastman, Q., and Grosschedl, R. (1999). Regulation of LEF-1/TCF transcription factors by Wnt and other signals. Current Opinion in Cell Biology *11*, 233–241.

Emamian, E.S., Hall, D., Birnbaum, M.J., Karayiorgou, M., and Gogos, J.A. (2004). Convergent evidence for impaired AKT1-GSK3β signaling in schizophrenia. Nature Genetics *36*, 131–137.

Farnum, M., and Zukoski, C. (1999). Effect of Glycerol on the Interactions and Solubility of Bovine Pancreatic Trypsin Inhibitor. Biophysical Journal *76*, 2716–2726.

Fink, A.L. (2005). Natively unfolded proteins. Current Opinion in Structural Biology *15*, 35–41.

Frame, S., Cohen, P., and Biondi, R.M. (2001). A Common Phosphate Binding Site Explains the Unique Substrate Specificity of GSK3 and Its Inactivation by Phosphorylation. Molecular Cell *7*, 1321–1327.

Fraser, E., Young, N., Dajani, R., Franca-Koh, J., Ryves, J., Williams, R.S.B., Yeo, M., Webster, M.-T., Richardson, C., Smalley, M.J., et al. (2002). Identification of the Axin and Frat Binding Region of Glycogen Synthase Kinase-3. Journal of Biological Chemistry *277*, 2176–2185.

Freemantle, S.J., Portland, H.B., Ewings, K., Dmitrovsky, F., DiPetrillo, K., Spinella, M.J., and Dmitrovsky, E. (2002). Characterization and tissue-specific expression of human GSK-3-binding proteins FRAT1 and FRAT2. Gene *291*, 17–27.

Gao, C., and Chen, Y.-G. (2010). Dishevelled: The hub of Wnt signaling. Cellular Signalling *22*, 717–727.

Gecchele, E., Merlin, M., Brozzetti, A., Falorni, A., Pezzotti, M., and Avesani, L. (2015). A Comparative Analysis of Recombinant Protein Expression in Different Biofactories: Bacteria, Insect Cells and Plant Systems. Journal of Visualized Experiments 2–8.

Grossman, T.H., Kawasaki, E.S., Punreddy, S.R., and Osburne, M.S. (1998). Spontaneous cAMP-dependent derepression of gene expression in stationary phase plays a role in recombinant expression instability. Gene *209*, 95–103.

Gubellini, F., Verdon, G., Karpowich, N.K., Luff, J.D., Boël, G., Gauthier, N., Handelman, S.K., Ades, S.E., and Hunt, J.F. (2011). Physiological Response to Membrane Protein Overexpression in E. coli. Molecular & Cellular Proteomics *10*, 1–17.

Haar, E., Coll, J.T., Austen, D.A., Hsiao, H.-M., Swenson, L., and Jain, J. (2001). Structure of GSK3B reveals a primed phosphorylation mechanism. Nature Structural Biology *8*, 593–596.

Hagen, T., Cross, D.A.E., Culbert, A.A., West, A., Frame, S., Morrice, N., and Reith, A.D. (2006). FRAT1, a Substrate-specific Regulator of Glycogen Synthase Kinase-3 Activity, Is a Cellular Substrate of Protein Kinase A. Journal of Biological Chemistry *281*, 35021–35029.

Hayashi-Takagi, A., Takaki, M., Graziane, N., Seshadri, S., Murdoch, H., Dunlop, A.J., Makino, Y., Seshadri, A.J., Ishizuka, K., Srivastava, D.P., et al. (2010). Disrupted-in-Schizophrenia 1 (DISC1) regulates spines of the glutamate synapse via Rac1. Nature Neuroscience *13*, 327–332.

Hayer-Hartl, M., Bracher, A., and Hartl, F.U. (2016). The GroEL–GroES Chaperonin Machine: A Nano-Cage for Protein Folding. Trends in Biochemical Sciences *41*, 62–76.

He, X. (2004). LDL receptor-related proteins 5 and 6 in Wnt/ -catenin signaling: Arrows point the way. Development *131*, 1663–1677.

Hedgepeth, C.M., Deardorff, M.A., Rankin, K., and Klein, P.S. (1999). Regulation of Glycogen Synthase Kinase 3␣ and Downstream Wnt Signaling by Axin. Mol Cel BioL. *19*, 7147–7157.

Hellebust, H., Uhlén, M., and Enfors, S.O. (1990). Interaction between heat shock protein DnaK and recombinant staphylococcal protein A. Journal of Bacteriology *172*, 5030–5034.

Hikida, T., Jaaro-Peled, H., Seshadri, S., Oishi, K., Hookway, C., Kong, S., Wu, D., Xue, R., Andrade, M., Tankou, S., et al. (2007). Dominant-negative DISC1 transgenic mice display schizophrenia-associated phenotypes detected by measures translatable to humans. Proceedings of the National Academy of Sciences *104*, 14501–14506.

Hodgkinson, C.A., Goldman, D., Jaeger, J., Persaud, S., Kane, J.M., Lipsky, R.H., and Malhotra, A.K. (2004). Disrupted in Schizophrenia 1 (DISC1): Association with Schizophrenia, Schizoaffective Disorder, and Bipolar Disorder. The American Journal of Human Genetics *75*, 862–872.

Hsu, W., Zeng, L., and Costantini, F. (1999). Identification of a Domain of Axin That Binds to the Serine/Threonine Protein Phosphatase 2A and a Self-binding Domain. Journal of Biological Chemistry *274*, 3439–3445.

Hughes, K., Nikolakaki, E., Plyte, S.E., Totty, N.F., and Woodgett, J.R. (1993). Modulation of the glycogen synthase kinase-3 family by tyrosine phosphorylation. Embo J *12*, 803–808.

Hur, E.-M., and Zhou, F.-Q. (2010). GSK3 signalling in neural development. Nature Reviews Neuroscience *11*, 539–551.

Joanna L. Feltham, and Lila M. Gierasch (2000). GroEL-Substrate Interactions: Molding the fold, or folding the mold? Cell *100*, 193–196.

Johnson, B., and Hecht Michael (1994). Recombinant Proteins Can Be Isolated from E. coli Cells by Repeated Cycles of Freezing and Thawing. Nature *12*, 1357–1360.

Johnstone, M., Thomson, P.A., Hall, J., McIntosh, A.M., Lawrie, S.M., and Porteous, D.J. (2011). DISC1 in Schizophrenia: Genetic Mouse Models and Human Genomic Imaging. Schizophrenia Bulletin *37*, 14–20.

Kamiya, A., Kubo, K., Tomoda, T., Takaki, M., Youn, R., Ozeki, Y., Sawamura, N., Park, U., Kudo, C., Okawa, M., et al. (2005). A schizophrenia-associated mutation of DISC1 perturbs cerebral cortex development. Nature Cell Biology *7*, 1167–1178.

Karege, F., Perroud, N., Burkhardt, S., Fernandez, R., Ballmann, E., La Harpe, R., and Malafosse, A. (2012). Protein levels of β-catenin and activation state of glycogen synthase kinase-3β in major depression. A study with postmortem prefrontal cortex. Journal of Affective Disorders *136*, 185–188.

Kilpinen, H., Ylisaukko-oja, T., Hennah, W., Palo, O.M., Varilo, T., Vanhala, R., Nieminen-von Wendt, T., von Wendt, L., Paunio, T., and Peltonen, L. (2008). Association of DISC1 with autism and Asperger syndrome. Molecular Psychiatry *13*, 187–196.

Kim, J.Y., Liu, C.Y., Zhang, F., Duan, X., Wen, Z., Song, J., Feighery, E., Lu, B., Rujescu, D., St Clair, D., et al. (2012). Interplay between DISC1 and GABA Signaling Regulates Neurogenesis in Mice and Risk for Schizophrenia. Cell *148*, 1051–1064.

Klein, P.S., and Melton, D.A. (1996). A molecular mechanism for the effect of lithium on development. Proceedings of the National Academy of Sciences *93*, 8455–8459.

Kleinridders, A., Ferris, H.A., Cai, W., and Kahn, C.R. (2014). Insulin Action in Brain Regulates Systemic Metabolism and Brain Function. Diabetes *63*, 2232–2243.

Kram, K.E., and Finkel, S.E. (2014). Culture Volume and Vessel Affect Long-Term Survival, Mutation Frequency, and Oxidative Stress of Escherichia coli. Applied and Environmental Microbiology *80*, 1732–1738.

Kram, K.E., and Finkel, S.E. (2015). Rich Medium Composition Affects Escherichia coli Survival, Glycation, and Mutation Frequency during Long-Term Batch Culture. Applied and Environmental Microbiology *81*, 4442–4450.

Krishnankutty, A., Kimura, T., Saito, T., Aoyagi, K., Asada, A., Takahashi, S.-I., Ando, K., Ohara-Imaizumi, M., Ishiguro, K., and Hisanaga, S. (2017). In vivo regulation of glycogen synthase kinase 3β activity in neurons and brains. Scientific Reports *7*, 1–15.

Li, L. (1999a). Axin and Frat1 interact with Dvl and GSK, bridging Dvl to GSK in Wnt-mediated regulation of LEF-1. The EMBO Journal *18*, 4233–4240.

Li, L. (1999b). Axin and Frat1 interact with Dvl and GSK, bridging Dvl to GSK in Wnt-mediated regulation of LEF-1. The EMBO Journal *18*, 4233–4240.

Lin, Z., and Rye, H.S. (2006). GroEL-Mediated Protein Folding: Making the Impossible, Possible. Critical Reviews in Biochemistry and Molecular Biology *41*, 211–239.

Lipska, B.K., Peters, T., Hyde, T.M., Halim, N., Horowitz, C., Mitkus, S., Weickert, C.S., Matsumoto, M., Sawa, A., Straub, R.E., et al. (2006). Expression of DISC1 binding partners is reduced in schizophrenia and associated with DISC1 SNPs. Human Molecular Genetics *15*, 1245–1258.

Liu, C., Li, Y., Semenov, M., Han, C., Baeg, G.-H., Tan, Y., Zhang, Z., Lin, X., and He, X. (2002). Control of ␣-Catenin Phosphorylation/Degradation by a Dual-Kinase Mechanism. Cell *108*, 837–847.

Lochhead, P.A., Kinstrie, R., Sibbet, G., Rawjee, T., Morrice, N., and Cleghon, V. (2006). A Chaperone-Dependent GSK3β Transitional Intermediate Mediates Activation-Loop Autophosphorylation. Molecular Cell *24*, 627–633.

Logan, C.Y., and Nusse, R. (2004). THE WNT SIGNALING PATHWAY IN DEVELOPMENT AND DISEASE. Annual Review of Cell and Developmental Biology *20*, 781–810.

Ma, L., Liu, Y., Ky, B., Shughrue, P.J., Austin, C.P., and Morris, J.A. (2002). Cloning and Characterization of Disc1, the Mouse Ortholog of DISC1 (Disrupted-in-Schizophrenia 1). Genomics *80*, 662–672.

MacDonald, B.T., Tamai, K., and He, X. (2009). Wnt/β-Catenin Signaling: Components, Mechanisms, and Diseases. Developmental Cell *17*, 9–26.

Magavi, S.S., Leavitt, B.R., and Macklis, J.D. (2000). Induction of neurogenesis in the neocortex of adult mice. Nature *405*, 951–955.

Mannava, A.G., and Tolwinski, N.S. (2015). Membrane Bound GSK-3 Activates Wnt Signaling through Disheveled and Arrow. PLOS ONE *10*.

Mao, Y., Ge, X., Frank, C.L., Madison, J.M., Koehler, A.N., Doud, M.K., Tassa, C., Berry, E.M., Soda, T., Singh, K.K., et al. (2009). Disrupted in Schizophrenia 1 Regulates Neuronal Progenitor Proliferation via Modulation of GSK3β/β-Catenin Signaling. Cell *136*, 1017–1031.

Maqbool, M., Mobashir, M., and Hoda, N. (2016). Pivotal role of glycogen synthase kinase-3: A therapeutic target for Alzheimer's disease. European Journal of Medicinal Chemistry *107*, 63–81.

Martin, S.A., Souder, D.C., Miller, K.N., Clark, J.P., Sagar, A.K., Eliceiri, K.W., Puglielli, L., Beasley, T.M., and Anderson, R.M. (2018). GSK3β Regulates Brain Energy Metabolism. Cell Reports *23*, 1922–1931.

McManus, E.J., Sakamoto, K., Armit, L.J., Ronaldson, L., Shpiro, N., Marquez, R., and Alessi, D.R. (2005). Role that phosphorylation of GSK3 plays in insulin and Wnt signalling defined by knockin analysis. The EMBO Journal *24*, 1571–1583.

Meares, G.P., and Jope, R.S. (2007). Resolution of the Nuclear Localization Mechanism of Glycogen Synthase Kinase-3 : FUNCTIONAL EFFECTS IN APOPTOSIS. J Biol Chem *282*, 16989–17001.

Millar, J.K., Wilson-Annan, J., Anderson, S., Christie, S., Taylor, M.S., Semple, C., Devon, R.S., St. Clair, D.M., Muir, W.J., Blackwood, D.H.R., et al. (2000). Disruption of two novel genes by a translocation co-segregating with schizophrenia. Human Molecular Genetics *9*, 1415–1423.

Miller, J.R., Hocking, A.M., Brown, J.D., and Moon, R.T. (1999). Mechanism and function of signal transduction by the Wnt/β-catenin and Wnt/Ca2+ pathways. Oncogene *18*, 7860–7872.

Miyoshi, K., Honda, A., Baba, K., Taniguchi, M., Oono, K., Fujita, T., Kuroda, S., Katayama, T., and Tohyama, M. (2003). Disrupted-In-Schizophrenia 1, a candidate gene for schizophrenia, participates in neurite outgrowth. Molecular Psychiatry *8*, 685–694.

Morris, J.A. (2003). DISC1 (Disrupted-In-Schizophrenia 1) is a centrosome-associated protein that interacts with MAP1A, MIPT3, ATF4/5 and NUDEL: regulation and loss of interaction with mutation. Human Molecular Genetics *12*, 1591–1608.

Muneer, A. (2017). Wnt and GSK3 Signaling Pathways in Bipolar Disorder: Clinical and Therapeutic Implications. Clinical Psychopharmacology and Neuroscience *15*, 100–114.

Nakata, K., Lipska, B.K., Hyde, T.M., Ye, T., Newburn, E.N., Morita, Y., Vakkalanka, R., Barenboim, M., Sei, Y., Weinberger, D.R., et al. (2009). DISC1 splice variants are upregulated in schizophrenia and associated with risk polymorphisms. Proceedings of the National Academy of Sciences *106*, 15873–15878.

Niwa, M., Kamiya, A., Murai, R., Kubo, K., Gruber, A.J., Tomita, K., Lu, L., Tomisato, S., Jaaro-Peled, H., Seshadri, S., et al. (2010). Knockdown of DISC1 by In Utero Gene Transfer Disturbs Postnatal Dopaminergic Maturation in the Frontal Cortex and Leads to Adult Behavioral Deficits. Neuron *65*, 480–489.

Park, C.-H., Lee, B.-H., Ahn, S.-G., Yoon, J.-H., and Oh, S.-H. (2013). Serine 9 and Tyrosine 216 Phosphorylation of GSK-3β Differentially Regulates Autophagy in Acquired Cadmium Resistance. Toxicological Sciences *135*, 380–389.

Patel, P., and Woodgett, J.R. (2017). Glycogen Synthase Kinase 3. In Current Topics in Developmental Biology, (Elsevier), pp. 277–302.

Piatti, V.C., Ewell, L.A., and Leutgeb, J.K. (2013). Neurogenesis in the dentate gyrus: carrying the message or dictating the tone. Frontiers in Neuroscience *7*.

Rial, D.V., and Ceccarelli, E.A. (2002). Removal of DnaK contamination during fusion protein purifications. Protein Expression and Purification *25*, 503–507.

Saltiel, A.R., and Kahn, C.R. (2001). Insulin signalling and the regulation of glucose and lipid metabolism. Nature *414*, 799–806.

Shaw, M., Cohen, P., and Alessi, D.R. (1997). Further evidence that the inhibition of glycogen synthase kinase-3 by IGF-1 is mediated by PDKl/PKB-induced phosphorylation of Ser-9 and not by dephosphorylation of Tyr-216. FEBS Letters *416*, 307–311.

Shrestha, P., Holland, T.M., and Bundy, B.C. (2012). Streamlined extract preparation for Escherichia Y coli-based cell-free protein synthesis by sonication L or bead vortex mixing. Biotechniques *53*, 163–174.

Snyder, E.Y., Deitcher, D.L., Walsh, C., Arnold-Aldea, S., Hartwieg, E.A., and Cepko, C.L. (1992). Multipotent neural cell lines can engraft and participate in development of mouse cerebellum. Cell *68*, 33–51.

Soares, D.C., Carlyle, B.C., Bradshaw, N.J., and Porteous, D.J. (2011). DISC1: Structure, Function, and Therapeutic Potential for Major Mental Illness. ACS Chemical Neuroscience *2*, 609–632.

Stamos, J.L., Chu, M.L.-H., Enos, M.D., Shah, N., and Weis, W.I. (2014). Structural basis of GSK-3 inhibition by N-terminal phosphorylation and by the Wnt receptor LRP6. ELife *3*, 1–22.

Stathopulos, P.B., Scholz, G.A., Hwang, Y.-M., Rumfeldt, J.A.O., Lepock, J.R., and Meiering, E.M. (2008). Sonication of proteins causes formation of aggregates that resemble amyloid. Protein Science *13*, 3017–3027.

Taylor, M.S., Devon, R.S., Millar, J.K., and Porteous, D.J. (2003). Evolutionary constraints on the Disrupted in Schizophrenia locus. Genomics *81*, 67–77.

Temple, S. (1989). Division and differentiation of isolated CNS blast cells in microculture. Nature *340*, 471–473.

Thomas, G.M., Frame, S., Goedert, M., Nathke, I., Polakis, P., and Cohen, P. (1999). A GSK3-binding peptide from FRAT1 selectively inhibits the GSK3-catalysed phosphorylation of Axin and L-catenin. FEBS Letters 5. 15-17.

Tong, Y., Park, S., Wu, D., Harris, T.E., Moskaluk, C.A., Brautigan, D.L., and Fu, Z. (2018). Modulation of GSK3β autoinhibition by Thr-7 and Thr-8. FEBS Letters *592*, 537–546.

Valerie A. Proctor, F. E. Cunningham, and Daniel Y. C. Fung (1988). he chemistry of lysozyme and its use as a food preservative and a pharmaceutical. C R C Critical Reviews in Food Science and Nutrition *26*, 359–395.

Vanderheiden, G.J., Fairchild, A.C., and Jago, G.R. (1970). Construction of a Laboratory Press for Use with the French Pressure Cell. Applied and Environmental Microbiology *19*, 875–877.

Willert, K., Shibamoto, S., and Nusse, R. (1999). Wnt-induced dephosphorylation of Axin releases β-catenin from the Axin complex. Genes & Development *13*, 1768–1773.

Woodgett JR (1991). cDNA cloning and properties of glycogen synthase kinase-3. Methods Enzymol *200*, 564–577.

Wu, D., and Pan, W. (2010). GSK3: a multifaceted kinase in Wnt signaling. Trends in Biochemical Sciences *35*, 161–168.

Yalla, K., Elliott, C., Day, J.P., Findlay, J., Barratt, S., Hughes, Z.A., Wilson, L., Whiteley, E., Popiolek, M., Li, Y., et al. (2018). FBXW7 regulates DISC1 stability via the ubiquitin-proteosome system. Molecular Psychiatry *23*, 1278–1286.

Yerabham, A.S.K., Weiergräber, O.H., Bradshaw, N.J., and Korth, C. (2013). Revisiting Disrupted-in-Schizophrenia 1 as a scaffold protein. Biological Chemistry *394*.

Yost, C., Farr, G.H., Pierce, S.B., Ferkey, D.M., Chen, M.M., and Kimelman, D. (1998). GBP, an Inhibitor of GSK-3, Is Implicated in Xenopus Development and Oncogenesis. Cell *93*, 1031–1041.

Appendix A

Total Reagent List

Acrylamide (Fisher # 01065-500)

Ampicillin (VWR # CA97061-442)

APS (Sigma #A3678-100G)

ATP (Thermo Scientific # FERR0441)

B-Per Bacterial Extraction (VWR #CAPI90084)

Bacto-Agar (Anachemia # 02116-300)

Bacto-Tryptone (Fisher # BP1421-2)

EDTA (Fisher # PR-V4231)

Glycerol (Fisher # BP2291)

HEPES (Fisher # BP3101)

Imidazole (Fisher # BP30550)

KH_2PO_4 (Fluka # 60220)

K_2HPO_4 (Fisher BP363-1)

Magnesium Chloride (VWR # W1917603

$NiSO_4$ (Sigma-Aldrich # 7786-81-4)

Pierce Protease Inibitor (Thermo Fisher# 88666)

Precision Plus Protein Unstained Standard (Biorad # 161-0363)

Sodium Chloride (VWR # CA71008-564)

Sodium Hydroxide (Alfa Aesar # AAA1603736)

TCEP HCl (Fisher-Pierce # PI20491)

TEMED (Sigma # T9281-100ML)

Tris Base (Fisher # BP1521)

Tryptone (Fisher # BP14212)

Tween 20 (VWR # CA97062-332)

Yeast Extract (Fisher #BP14222)

Appendix B

Western Blot Methods

Protein samples were run on a 12% SDS-PAGE gel at 120 V for 90 mins. A n Immobilon-FL pore size 0.45 μm membrane (Millipore Cat# IPFL00010) was activated with methanol for 30 sec, rinsed with water and then equilibrated with transfer buffer (25 mM Tris, 192 mM glycine, 20% methanol, pH 8.3) along with the sponge, gel and blotting paper. The membrane was placed in-between the blotting paper and the sponges, then assemble into the western blot apparatus. The transfer was run at 350 mAmp for 60 min. Once the transfer was complete the membrane was rinsed with 1X PBST (3.2 mM Na_2HPO_4, 1.3 mM KCl, 135 mM NaCl, 0.05% Tween 20, pH 7.4) then placed in blocking solution (1X PBST + 5% dry milk powder) for 1 hour. Once the membrane was sufficiently incubated in blocking solution it was rinsed with PBST and incubated with the primary antibody (Anti-GSK3β at a dilution of 1:6000 in blocking solution) overnight at 4°C. Following overnight incubation, the membrane was washed with PBST and incubated with the secondary antibody (Anti-mouse dylight 680 at a dilution of 1:10000 in blocking solution) at room temperature for 1 hour. Following the secondary antibody incubation, the membrane was washed with PBST and protein bands were detected using a gel imager system.